EUROPEAN COMMISSION

Community Research

SEVENTH FRAMEWORK PROGRAMME

CARBOWASTE

Treatment and Disposal of Irradiated Graphite and Other Carbonaceous Waste

Epoxy-Based Coatings with Reduced Gas Permeation: Formulation and Properties

Deliverable Number: T-6.2.2

Author(s): **Louis Johann van Rooyen**
Necsa, RSA

Date of first issue of this report: 25/03/2012

Start date of project : **01/04/2008** Duration : **60 Months**

Project co-funded by the European Commission under the Seventh Framework Programme (2007 to 2011) of the European Atomic Energy Community (EURATOM) for nuclear research and training activities		
Dissemination Level		
PU	Public	
RE	Restricted to the partners of the CARBOWASTE project	
CO	Confidential, only for specific distribution list defined on this document	**X**

Distribution list

Person and organisation name and/or group	Comments
WP6 partners	
Executive Board	
Coordinator	
European Commission	

CARBOWASTE		
Work package: 6 **Task: :** 6.2	**CARBOWASTE document no:** CARBOWASTE-1203-T-6.2.2	**Document type:** T=Technical Report
Issued by: Necsa, RSA **Internal no.:** CW1203-T-6-2-2-a		**Document status:** Final

Document title

Epoxy-Based Coatings with Reduced Gas Permeation: Formulation and Properties

Executive summary

The gas permeability of composite epoxy resins formulated with graphene platelets and glass flakes was investigated. The purpose of researching the gas permeability of the composite resins was to develop a possible coating system that could prevent or limit the release of radioactive gases like tritium from irradiated graphite waste which may accumulate in underground repositories. Helium was used as a substitute gas to simulate the diffusive properties of tritium gas.

The samples were prepared as doctor blade sheets, moulded discs, and multilayer sheets using mechanical and ultrasonic mixing techniques. Organic solvents were used with some samples to aid the dispersion of the graphene platelets. The helium permeability was measured with a specially designed permeation cell attached to a helium leak detector.

The incorporation of the fillers did reduce the helium permeability of the epoxy resin with increasing weight fractions. The glass flakes performed better than the graphene nanoplatelets by reducing the helium leak rate by almost three orders of magnitude. The results were fitted according to Fick's law of diffusion and the amount of tritium that might leak into a hypothetical repository was successfully simulated.

Revisions

Rev.	Date	Short description	Author	Internal Review	Task Leader	WP Leader
00	Dd/mm/yyyy	Issue	Name, Organisation	Name, Organisation *Signature*	Name, Organisation *Signature*	Name, Organisation *Signature*
01	01/02/2012	First issue	Van Rooyen Necsa	Meyer Necsa		Grambow Subatech
02	09/03/2012	Final Issue	Van Rooyen Necsa	Meyer Necsa		Grambow Subatech

EPOXY-BASED COATINGS WITH REDUCED GAS PERMEATION: FORMULATION AND PROPERTIES

by

LOUIS JOHANN VAN ROOYEN

Submitted in partial fulfillment of the requirements for the degree

MAGISTER TECHNOLOGIAE: POLYMER TECHNOLOGY

in the

Department of Mechanical Engineering

FACULTY OF ENGINEERING AND THE BUILT ENVIRONMENT

TSHWANE UNIVERSITY OF TECHNOLOGY

Supervisor: Prof OC Vorster

Co-Supervisor: Prof J Karger-Kocsis

February 2012

DECLARATION BY CANDIDATE

"I hereby declare that the dissertation submitted for the degree M Tech: Polymer Technology, at the Tshwane University of Technology, is my own original work and has not previously been submitted to any other institution of higher education. I further declare that all sources cited or quoted are indicated and acknowledged by means of a comprehensive list of references".

LJ van Rooyen

Date

Copyright © Tshwane University of Technology 2012

This dissertation is dedicated to my wife, Charlotte, thank you for all your love, support, patience and companionship over the past few years and I pray for many more (Psalm 128).

Also, my parents, your love and support have always been a major influence in my life. Thank you for working so hard to give me an education which we can only see the fruits of now.

ACKNOWLEDGEMENTS

This is my humble effort to thank all the individuals, groups and institutions who have helped me along this journey to complete my research and the writing up of my dissertation.

Firstly, I am greatly indebted and thankful to my supervisors, Professor Olof Vorster and Professor József Karger-Kocsis, whose approachability, input and guidance was essential in me completing my work. Even with their busy schedules, they managed to give great attention and assistance to any research obstacle I was faced with. I really appreciate the effort with the high resolution FESEM analysis of the graphene samples. It was a great honour and very humbling to work with men of your standard.

Dr. David Kock and Dr. Hertzog Bisset whose understanding of physical chemistry and membrane science helped me immensely to model the helium permeability of the composite coatings and to predict the tritium concentrations.

I am greatly indebted to my two scientific editors, Dr. Oosthuizen and Mr. JC Thompson. Dr. Hester Oosthuizen for her long hours of proof reading all my drafts leading up to the final document. Your attention to detail picked up a lot of errors that most people would've missed and your suggestions to improve my work were vital. Mr. Cliff Thompson for his continual encouragement and faith in my work, even when everything seemed to go wrong. Thank you for pushing me beyond what I thought I was capable of and I owe you a lot of cups of cappuccino because of that.

I am also grateful to the following personnel from Necsa and Applied Chemistry:

- Dr. Willie Meyer from Nuclear Waste Research and the Carbowaste project advisory committee, who suggested the idea for the project and funded the materials.
- Mr. Driekus van der Westhuizen for the help with setting up the computer interface to log the permeation data and for the opportunity to further my studies.
- Dr. Ettienne Snyders and Mr. Ryno van der Merwe from the Nuclear Materials group for the use of their Scanning Electron Microscope and analysis.
- Dr. PAB Carstens for the use of his books on diffusion which also improved my understanding of other morphological effects on the diffusion of gases through polymers.
- Mr. Lindani Ngidi for the use of his Buchi rotovap setup.
- Mr. Willie Groenewald from vacuum services, for the use of his helium leak detector.
- Mr. Frik Beeslaar for supplying the safe regulatory limits of exposure to radioactive gases.

I also would like to thank the following institutions, The Department of Science and Technology (South Africa) and the Carbowaste project (European Union) for funding the research, and Necsa for funding me to further my studies at the TUT.

Last, but not least, my Heavenly Father for the mercy and Grace that He has bestowed upon my life on the road to sanctification. To you be the glory and honour, forever.

ABSTRACT

The gas permeability of composite epoxy resins formulated with graphene platelets and glass flakes was investigated. The purpose of researching the gas permeability of the composite resins was to develop a possible coating system that could prevent or limit the release of radioactive gases like tritium from irradiated graphite waste which may accumulate in underground repositories. Helium was used as a substitute gas to simulate the diffusive properties of tritium gas.

The samples were prepared as doctor blade sheets, moulded discs, and multilayer sheets using mechanical and ultrasonic mixing techniques. Organic solvents were used with some samples to aid the dispersion of the graphene platelets. The helium permeability was measured with a specially designed permeation cell attached to a helium leak detector.

The incorporation of the fillers did reduce the helium permeability of the epoxy resin with increasing weight fractions. The glass flakes performed better than the graphene nanoplatelets by reducing the helium leak rate by almost three orders of magnitude. The results were fitted according to Fick's law of diffusion and the amount of tritium that might leak into a hypothetical repository was successfully simulated.

TABLE OF CONTENTS

PAGE

ACKNOWLEDGEMENTS ..... *iv*

ABSTRACT ..... *vi*

TABLE OF CONTENTS ..... *vii*

LIST OF FIGURES ..... *xi*

LIST OF TABLES ..... *xiv*

1 INTRODUCTION 1

1.1 FOCUS OF THE RESEARCH 1

1.2 PROBLEM STATEMENT 2

1.3 OBJECTIVES 3

2 LITERATURE REVIEW 5

2.1 IRRADIATED GRAPHITE WASTE 5

2.1.1 Carbowaste project initiative 5

2.1.2 Decommissioning of reactors and irradiated graphite waste 7

2.1.3 Radionuclide generation in graphite waste and gaseous release 9

2.2 POLYMER RESINS AS GAS BARRIER MATERIAL FOR RADIONUCLIDE GASES 10

2.2.1 Immobilisation of graphite waste 10

2.2.2 Polymer resins and the effect of irradiation 11

2.2.3 Epoxy resin 13

2.2.4 Additives to improve gas barrier properties 15

2.3 METHODS OF MEASURING GAS PERMEABILITY OF POLYMER MEMBRANES 18

3 METHODOLOGY 21

3.1 MATERIALS 21

3.2 TECHNIQUES FOR PREPARING THE COMPOSITE SHEETS 23

3.2.1 Doctor blade technique 23

3.2.2 Composite disc castings and use of solvents 24

3.2.3 Multilayer sheets 24

3.3 GRAPHENE/EPOXY NANOCOMPOSITE FORMULATION 24

3.3.1 Mixing methods 24

3.3.2 Doctor blade graphene/epoxy composite sheets 25

3.3.3 Graphene/epoxy composite moulded disc 27

3.3.4 Stacked layers of graphene/epoxy nano-composite 28

3.4 GLASS FLAKE/EPOXY COMPOSITE FORMULATION 28

3.4.1 Introduction 28

3.4.2 Formulation of doctor blade glass flake/epoxy composite sheets 29

3.4.3 Formulation of glass flake moulded discs 30

3.4.4 Formulation of stacked multiple layer glass flake/epoxy composite sheet 31

3.5 HELIUM PERMEATION MEASUREMENT 31

3.6 CHARACTERISATION OF THE COMPOSITE COATINGS 35

3.6.1 Microscopic examination of composite coating morphology 35

3.6.2 Adhesion to graphite surface 37

4 PERMEABILITY OF COMPOSITE COATING 39

4.1 INTRODUCTION 39

4.2 FICKIAN MODEL DEVELOPMENT AND THEORETICAL CONSIDERATIONS 41

4.3 MODEL APPLICATION 44

4.4 TRITIUM MASS TRANSPORT 48

4.5 TRITIUM RELEASE SCENARIOS AND CALCULATION.....49

5 RESULTS & DISCUSSION 52

5.1 EXPERIMENTAL AND CHARACTERISATION OVERVIEW 52

5.2 EPOXY COMPOSITE PREPARATION & SAMPLE MORPHOLOGY 53

5.2.1 Doctor blade sheets..... 53

5.2.2 Moulded discs..... 60

5.2.3 Multilayer sheets..... 68

5.3 HELIUM LEAK RATE MEASUREMENTS.....72

5.3.1 Doctor blade sheets..... 72

5.3.2 Moulded discs..... 79

5.3.3 Multilayer samples..... 83

5.3.4 Fit according to Fick's law 85

5.4 TRITIUM RELEASE PREDICTIONS.....97

5.4.1 Threshold determination..... 97

5.4.2 Scenario predictions of radioactivity concentrations 101

5.5 ADHESION TO GRAPHITE.....109

6 CONCLUSION 114

6.1 SUMMARY OF OBJECTIVES 114

6.2 EFFECT OF MIXING TECHNIQUES AND SAMPLE FABRICATION ON THE DISPERSION OF THE FILLERS 115

6.3 EFFECT OF THE FILLERS ON THE HELIUM BARRIER PROPERTIES 116

6.4 FIT TO FICK'S LAW AND PREDICTION OF THE POTENTIAL RELEASE OF TRITIUM GAS.....117

6.5 ADHESIVE PROPERTIES OF EPOXY RESIN TO GRAPHITE.....117

6.6 EVALUATION OF THE GRAPHENE AND GLASS FLAKE EPOXY RESIN COMPOSITES.....118

6.7 RECOMMENDATIONS FOR FUTURE WORK.....118

REFERENCES.....120

ANNEXURE A: MODEL FIT OF REFERENCE SAMPLES.....131

ANNEXURE B: MODEL FIT OF DOCTOR BLADE SHEET SAMPLES.....133

ANNEXURE C: MODEL FIT OF MOULDED DISC SAMPLES.....144

ANNEXURE D: MODEL FIT OF MULTILAYER SHEETS.....151

LIST OF FIGURES

PAGE

FIGURE 2.1 DIAGRAM OF THE A) MAGNOX AND B) RBMK REACTORS 6

FIGURE 2.2 THE ADDITION OF BISPHENOL A WITH EPICHLOROHYDRIN TO CREATE EPOXY PRE-POLYMER 13

FIGURE 2.3 THE REACTION OF A DIAMINE WITH THE EPOXY PRE-POLYMER RESIN 14

FIGURE 2.4 CROSS-LINKED STRUCTURE OF EPOXY RESIN 15

FIGURE 2.5 DIAGRAM OF A HYPOTHETICAL COMPOSITE MEMBRANE DISPLAYING THE TORTUOUS PATH CREATED BY EXFOLIATED AND ORIENTATED PLATELET FILLERS 16

FIGURE 3.1 SEM IMAGES OF (A) THE GLASS FLAKES AND (B) THE DIMENSIONS 22

FIGURE 3.2 SEM IMAGES OF THE (A) GRAPHENE NANOPLATELETS AND (B) THE DIMENSIONS 22

FIGURE 3.3 DIAGRAM DISPLAYING THE COMPONENTS OF THE DOCTOR BLADE 23

FIGURE 3.4 PHOTOGRAPH OF PERMEATION CELL 32

FIGURE 3.5 PERMEATION CELL WITH DISC SAMPLE POSITIONED BETWEEN THE O-RINGS 32

FIGURE 3.6 HELIUM PERMEATION EXPERIMENTAL SETUP 33

FIGURE 3.7 PHOTOGRAPH DISPLAYING THE INTERNAL COMPONENTS OF THE HELIUM LEAK DETECTOR 34

FIGURE 3.8 DIAGRAM OF THE FEI QUANTA 200 3D SEM 37

FIGURE 3.9 CROSS-HATCH ADHESION TEST 38

FIGURE 4.1 DIAGRAM DEMONSTRATING HOW THE CONCENTRATION CHANGES AS MOLECULES TRAVEL THROUGH A MEMBRANE OF AN UNKNOWN THICKNESS 41

FIGURE 4.2 LISTED BOUNDARY CONDITIONS 43

FIGURE 4.3 LINEAR PLOT OF MEASURED DATA AND LINEAR TRENDLINE 46

FIGURE 4.4 EXAMPLE DEMONSTRATING GOOD FICKIAN MODEL FIT OF MEASURED LEAK RATE FLUX. 47

FIGURE 4.5 SCHEMATIC OF SCENARIO 1 AND SCENARIO 2 WITH GIVEN DIMENSIONS OF THE HYPOTHETICAL REPOSITORIES 51

FIGURE 5.1 MICROSCOPIC IMAGES (40X) OF THE GRAPHENE FILLED DOCTOR BLADE SHEETS (CROSS SECTION) PREPARED WITH THE BLENDER AT A) 1 WT%, B) 2 WT%, AND C) 3 WT% 57

FIGURE 5.2 MICROSCOPIC IMAGES OF A) 10 AND B) 20 WT% GLASS FLAKE FILLED DOCTOR BLADE SHEETS (CROSS SECTION) 57

FIGURE 5.3 SEM MICROGRAPH OF 1 WT% GRAPHENE FILLED DOCTOR BLADE SHEET PREPARED WITH BLENDER (CROSS SECTION) 58

FIGURE 5.4 SEM IMAGE OF 10 WT% GLAS FLAKE FILLED DOCTOR BLADE SHEET (CROSS SECTION) 59

FIGURE 5.5 SEM IMAGE OF 20 WT% GLASS FLAKE FILLED DOCTOR BLADE SHEET (CROSS SECTION) 59

FIGURE 5.6 MICROSCOPIC IMAGES OF THE A) 4 AND B) 6 WT% GRAPHENE FILLED SAMPLES PREPARED WITH DMF 61

FIGURE 5.7 VOID FORMATION FROM ENTRAPPED SOLVENT (DCM) IN 6 WT% GRAPHENE MOULDED DISC 62

FIGURE 5.8 SEM IMAGE OF THE 10 WT% GRAPHENE FILLED DISC PREPARED WITH DMF62

FIGURE 5.9 SEM IMAGE OF 4 WT% GRAPHENE SAMPLE SHOWING THE FORMATION OF VOIDS FROM ENTRAPPED SOLVENT 63

FIGURE 5.10 SEM IMAGE OF DISC SAMPLE DISPLAYING AGGLOMERATED REGIONS OF GRAPHENE PLATELETS 64

FIGURE 5.11 SEM IMAGE OF CREASED GRAPHENE PLATELET. THE PLATELET IS ALSO SEMI-TRANSPARENT 64

FIGURE 5.12 TEM IMAGE OF CREASED GRAPHENE PLATELET 65

FIGURE 5.13 TEM IMAGE OF AGGLOMERATED GRAPHENE PLATELETS 65

FIGURE 5.14 MICROSCOPIC IMAGES OF A) 40 AND B) 50 WT% GLASS FLAKE FILLED MOULDED DISCS PREPARED WITH DCM (CROSS SECTION) 66

FIGURE 5.15 SEM IMAGE OF 30 WT% GLASS FLAKE FILLED MOULDED DISC (CROSS SECTION) 67

FIGURE 5.16 SEM IMAGE OF 40 WT% GLASS FLAKE FILLED SAMPLE (CROSS SECTION) . 67

FIGURE 5.17 SEM IMAGE OF 50 WT% GLASS FLAKE FILLED DISC (CROSS SECTION) 68

FIGURE 5.18 SEM IMAGE OF 2 WT% GRAPHENE MULTILAYER SHEET WITH A THICKNESS OF 2 MM (CROSS SECTION)..... 69

FIGURE 5.19 SEM IMAGE OF THE GLASS FLAKE 30 WT% MULTILAYERED SHEET SHOWING THE DISPERSION OF THE FLAKES (SURFACE)..... 70

FIGURE 5.20 SEM IMAGE OF THE TOP LAYER OF THE GLASS FLAKE 30 WT% MULTILAYER SHEET (SURFACE) 71

FIGURE 5.21 SEM IMAGE OF THE CROSS-SECTIONAL AREA OF THE 30 WT% GLASS FLAKE MULTILAYER SHEET SHOWING THE ORIENTATION AND DISPERSION OF THE GLASS FLAKES IN VARIOUS LAYERS (CROSS SECTION) 71

FIGURE 5.22 HELIUM FLUX MEASUREMENTS OF GRAPHENE SAMPLES PREPARED WITH DIFFERENT TECHNIQUES 73

FIGURE 5.23 HELIUM FLUX MEASUREMENTS OF GRAPHENE FILLED DOCTOR BLADE SHEETS PREPARED WITH THE BLENDER 75

FIGURE 5.24 HELIUM FLUX MEASUREMENTS OF GLASS FLAKE FILLED DOCTOR BLADE SHEETS UP TO 6 WT%..... 77

FIGURE 5.25 HELIUM FLUX MEASUREMENTS OF GLASS FLAKE FILLED DOCTOR BLADE SHEETS UP TO 20 WT%..... 78

FIGURE 5.26 HELIUM FLUX MEASUREMENTS FOR GRAPHENE FILLED MOULDED DISCS . 80

FIGURE 5.27 HELIUM FLUX MEASUREMENTS FOR GLASS FLAKE FILLED MOULDED DISCS 82

FIGURE 5.28 HELIUM FLUX MEASUREMENTS OF MULTILAYER SHEETS 84

FIGURE 5.29 LINEAR FIT OF REFERENCE ARALDITE DOCTOR BLADE SHEET PERMEATION DATA..... 86

FIGURE 5.30 LINEAR FIT OF REFERENCE ARALDITE MOULDED DISC PERMEATION DATA86

FIGURE 5.31 MODEL FIT OF HELIUM FLUX DATA FOR REFERENCE ARALDITE SAMPLES . 87

FIGURE 5.32 MODEL FIT OF GRAPHENE DOCTOR BLADE SAMPLES..... 88

FIGURE 5.33 MODEL FIT OF GLASS FLAKE FILLED DOCTOR BLADE SHEETS..... 89

FIGURE 5.34 HELIUM PERMEABILITY COMPARISON OF GRAPHENE FILLED SAMPLES 95

FIGURE 5.35 HELIUM PERMEABILITY COMPARISON OF GLASS FLAKE FILLED SAMPLES . 96

FIGURE 5.36 DAC THRESHOLD FOR SCENARIO 1 99

FIGURE 5.37 DAC THRESHOLD FOR SCENARIO 2 100

FIGURE 5.38 DAC RESULTS FOR DOCTOR BLADE SHEETS (SCENARIO 1) 102

FIGURE 5.39 DAC RESULTS FOR MOULDED DISCS (SCENARIO 1) 103

FIGURE 5.40 DAC RESULTS FOR MULTILAYER SHEETS (SCENARIO 1) 104

FIGURE 5.41 DAC RESULTS FOR DOCTOR BLADE SHEETS (SCENARIO 2) 106

FIGURE 5.42 DAC RESULTS FOR MOULDED DISCS (SCENARIO 2) 107

FIGURE 5.43 DAC RESULTS FOR MULTILAYER SHEETS (SCENARIO 2) 108

FIGURE 5.44 SEM IMAGE OF MACHINED GRAPHITE SURFACE BEFORE COATING WITH EPOXY 110

FIGURE 5.45 MICROSCOPIC IMAGES OF CROSS HATCH LATTICE TAKEN WITH A A) STEREOMICROSCOPE AND B) SEM 111

FIGURE 5.46 SEM IMAGE OF CROSS HATCH LATTICE OF COATED POLYETHYLENE 112

FIGURE 5.47 SEM IMAGE OF GRAPHITE COATED WITH EPOXY RESIN 112

LIST OF TABLES

TABLE 2.1 NUMBER OF MAGNOX REACTORS SITUATED GEOGRAPHICALLY IN THE UK WITH THE AMOUNT OF GRAPHITE USED BY EACH REACTOR. ADAPTED FROM IAEA DOCUMENT (IAEA, 2006, PP 10-11) 8

TABLE 3.1 GRAPHENE DOCTOR BLADE SHEET FORMULATIONS 26

TABLE 3.2 GRAPHENE MOULDED DISC FORMULATIONS 27

TABLE 3.3 GLASS FLAKE DOCTOR BLADE SHEET FORMULATIONS 29

TABLE 3.4 GLASS FLAKE MOULDED DISC FORMULATIONS 30

TABLE 4.1 THE CONSIDERATIONS FOR SCENARIO 1 AND SCENARIO 2 50

TABLE 5.1 PERMEATION RESULTS OF DOCTOR BLADE SHEETS FILLED WITH GRAPHENE 72

TABLE 5.2 PERMEATION RESULTS OF DOCTOR BLADE SHEETS FILLED WITH GLASS FLAKES 76

TABLE 5.3 PERMEATION RESULTS FOR GRAPHENE FILLED MOULDED DISCS 79

TABLE 5.4 PERMEATION RESULTS FOR GLASS FLAKE FILLED MOULDED DISCS 81

TABLE 5.5 PERMEATION RESULTS OF MULTILAYER SHEETS..... 83

TABLE 5.6 HELIUM FLUX BEHAVIOUR OF DOCTORBLADE SHEETS FILLED WITH GRAPHENE..... 90

TABLE 5.7 HELIUM FLUX BEHAVIOUR OF DOCTOR BLADE SHEETS FILLED WITH GLASS FLAKES 91

TABLE 5.8 HELIUM FLUX BEHAVIOUR OF MOULDED DISCS FILLED WITH GRAPHENE 92

TABLE 5.9 HELIUM FLUX BEHAVIOUR OF MOULDED DISCS FILLED WITH GLASS FLAKES 92

TABLE 5.10 HELIUM FLUX BEHAVIOUR OF MULTILAYER SHEETS..... 93

TABLE 5.11 SAMPLES THAT MAY BE CONSIDERED FOR SCENARIO 1..... 101

TABLE 5.12 SAMPLES THAT MAY BE CONSIDERED FOR SCENARIO 2..... 105

1 INTRODUCTION

1.1 FOCUS OF THE RESEARCH

This research was conducted as part of a European initiative started in 2008 to address the retrieval, treatment and disposal of irradiated graphite waste generated from decommissioned reactors, as well as future generated waste (von Lenza, 2009).The so-called Carbowaste project consists of a global consortium of 28 partners with Necsa, as the South African research representative. One of the objectives of the project is the intermediate storage of irradiated graphite waste. A possible solution might be the use of a cladding material fabricated from a polymer composite that could contain the release of radioactive gases into the environment.

One area of polymer composites gaining interest is the improvement of the gas barrier properties of polymers by incorporating impermeable fillers. The incorporation of nano- and micro-sized impermeable fillers into polymer matrices has been reported to reduce the gas permeability when compared to permeability measurements of the homogenous polymer (Takahashi et al., 2006; Ogasawara et al., 2006; Gupta et al., 2009; Lape et al., 2004). Reduction of gas permeability by 50 to 500 times has been observed with relatively low loadings of certain fillers like nanoclays (Choudalakis & Gotsis, 2009). The introduction of graphene nanoplatelets have shown to improve the gas barrier properties of oxygen more than that of montmorollinite due to the higher aspect ratio of the platelets (Kalaitzidou et al., 2007). Glass platelets have also shown to improve the gas barrier properties significantly (Gupta et al., 2009).

Therefore, the aim of my research was to formulate an epoxy composite coating filled with impermeable platelet fillers which could be applied to irradiated graphite waste to limit or

prevent the release of radioactive gases containing radionuclides like carbon-14 (^{14}C), tritium (^{3}H) and chlorine-36 (^{36}Cl). Of these radionuclides, tritium was focused on because of the high diffusivity. Because of health and safety reasons, helium was chosen to model the gas permeability of the composite coating. Helium is sometimes used as a substitute test gas for hydrogen permeation studies due to the similar molecular size that the gases exhibit (Herring, 2003; Ogasawara et al., 2006; Schultheiß, 2007, p.30). It is assumed that a coating that can contain helium ought to be able to contain heavier elements as well. The suitability of the composite coating was determined by the proficiency of the gas barrier and adhesive properties of the material.

1.2 PROBLEM STATEMENT

Graphite is mainly used in nuclear reactors as neutron moderators and reflectors. When the reactors become defunct after long service periods and need to be decommissioned it raises the problem of irradiated radioactive graphite waste being generated from these large moderator blocks. This graphite waste is classified as Low to Intermediate Level radioactive Waste (LLW and ILW) due to the interaction of neutrons with impurities in the graphite, like lithium, nitrogen, chlorine, and cobalt (von Lenza, 2009).

The neutron capture by these impurities results in the formation of unstable radionuclides which leach or diffuse from the graphite structure over time. The radionuclides that are formed from this neutron capture include the following:

- Tritium (^{3}H) from the neutron activation of lithium-6
- Carbon-14 from the activation of nitrogen gas during the nuclear cycle
- Chlorine-36 from the activation of chlorine impurities in the graphite structure

Of the three radionuclides, tritium accumulation in underground storage facilities has become a concern due to the high permeability of tritium. A few methods have been researched and proposed in regards to containing the release of radionuclides from graphite waste like polymer encapsulation (Clifford, 2010), impregnation with resins (Costes et al., 1990), containment in metals, and storage in underground repositories (University of Manchester, n.d.). However, these methods might only be practically applicable to small quantities of low level radioactive graphite waste, but since the graphite waste is generated in large volumes, there is a need to develop methods that can contain or limit the release of radionuclides suitable for large quantities of graphite waste.

1.3 OBJECTIVES

The steps followed to evaluate the composite coating were as follow:

- Suitable resins and fillers were identified that exhibit a low permeability and ease of application to large graphite blocks.

- The obtained fillers were introduced into the resin with various mixing techniques. The techniques included mechanical, manual, and ultrasonic mixing.

- Sheets and moulds were produced by using a doctor blade, moulding the resin in special moulds, and applying thin layers of the composite resin in sequential stacked multilayers. The quality of the coating structures was determined by Scanning Electron Microscopy (SEM) and Transmission Electron Microscopy (TEM).

- The helium permeability of the composite coatings was measured using a helium leak detector.

- A mathematical permeability model was derived to predict the release of tritium gas.

- Cross hatch tests were done to determine the adhesion of the coating to a graphite surface.

2 LITERATURE REVIEW

2.1 IRRADIATED GRAPHITE WASTE

2.1.1 Carbowaste project initiative

It is estimated that the amount of irradiated graphite waste that currently exists world-wide is in the region of 250 000 tons (von Lenza, 2009). Most of this irradiated graphite is situated in the United Kingdom with more than 80 000 tons and the former Soviet Union countries with more than 50 000 tons (IAEA, 2006). Graphite is mainly used in nuclear reactors as moderators to slow down the movement of neutrons in a reactor core. The Magnox gas-cooled reactors in the UK and the water-cooled RBMK reactors (**Figure 2.1**) in Russia are two examples of reactors that use graphite as a moderator material. Reactor-4 that exploded in 1986 at Chernobyl was an RBMK reactor. These reactors have been in operation since the 1950s and the nuclear industry has so far been trying to find suitable methods to manage the long-term disposal of irradiated graphite waste. The option that appears to be the most sustainable is the one of long-term storage in underground repositories (Black, 2006; ElBaradei, 2003). This option has the benefit of isolation from human activity, for example terrorists, and limiting the migration of radionuclides into the environment (Grevoz, 2005).

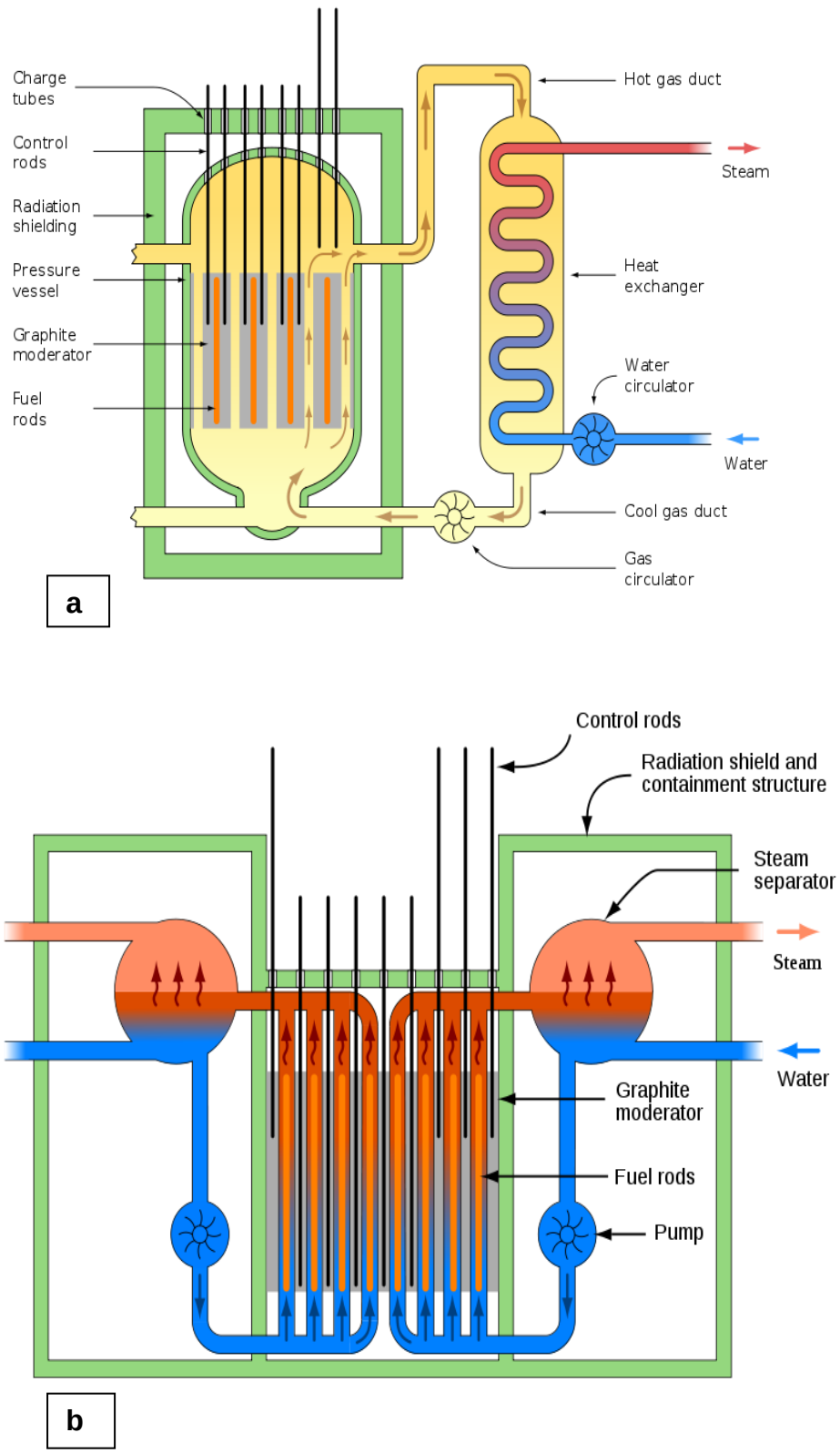

Figure 2.1 Diagram of the a) Magnox and b) RBMK reactors

†*Figures obtained from Wikipedia* (Wikipedia, 2007; Wikipedia, 2008)

Therefore, the Carbowaste project was initiated by the European Union in 2008 to address current problems associated with the retrieval, disposal, and conditioning of irradiated graphite waste. The Carbowaste project consists of a consortium of 28 partners from around the globe where Necsa, as a member of this consortium, contributes toward research. The main focus of the Carbowaste project is on potential and current graphite waste that might be generated from the decommissioning of nuclear reactors that have reached the end of their operation or are nearly approaching it.

2.1.2 Decommissioning of reactors and irradiated graphite waste

The decommissioning process can last as long as 50 years to allow most of the radioactivity to decrease before the reactors get dismantled. Studies have shown that most of the radioactivity comes from the irradiated graphite containing tritium and carbon-14 radionuclides in the first few years after the reactor has been shut down (Bushuev et al., 1992).

The amount of waste that is generated is dependent on the design, size and type of reactor. For instance, in the case of a Magnox gas-cooled reactor, the amount of graphite that is used as moderator and reflector material can range from 1 000 to 3 500 tons (**Table 2.1**). Just in the United Kingdom there are 26 Magnox reactors, some of them have already been decommissioned and others are approaching the end of their operational life. The waste generated is normally classified as low level waste (LLW) or intermediate level waste (ILW) due to the presence of radionuclides.

Table 2.1 Number of Magnox reactors situated geographically in the UK with the amount of graphite used by each reactor. Adapted from IAEA document (IAEA, 2006, pp 10-11)

Location (UK)	Number of reactors	Thermal power (MW)	Graphite in reactor (tons)
Bradwell	2	500	1810
Calder Hall	4	270	1164
Chapelcross	3	260	1164
Dungeness	2	780	2150
Hinkley Point	1	947	2210
Hinkley Point	1	947	3310
Oldbury	2	893	2061
Sizewell	2	800	2237
Wylfa	2	1760	3470
Berkeley	2	585	1938
Hunterston	2	545	1780
Trawsfynydd	2	860	1900

2.1.3 Radionuclide generation in graphite waste and gaseous release

The graphite used in nuclear reactors, either as neutron moderators or reflectors, are exposed to very high neutron fluxes and generate significant quantities of radionuclides which are formed from the activation of impurities such as lithium, nitrogen, chlorine, cobalt, iron, and caesium present in the graphite (IAEA, 2006, pp.29–32). Therefore the need to quantify the radionuclide content is necessary. Unfortunately, this task is difficult due to the unknown quantities of impurities contained in the graphite prior to commissioning of the reactor (Bushuev et al., 1992). Some of the β-emitting radionuclides that can be formed are:

- Tritium (^{3}H), which has a half-life of 12.33 years, from the neutron activation of ^{6}Li.
- Carbon-14 (^{14}C) from the neutron activation of nitrogen (N_2). The nitrogen may be present in the graphite or from the cooling gas used during the fission cycle. ^{14}C has a half-life of 5 730 years.
- Chlorine-36 (^{36}Cl) from the neutron activation of chlorine (^{35}Cl). Of the three, ^{36}Cl has the longest half-life of 300 000 years.

Other radionuclides are also formed, but for this study the focus was mainly on tritium and the long lived isotopes (^{14}C and ^{36}Cl).

During storage of the irradiated graphite waste, these radionuclides are released from the graphite structure in gaseous form (IAEA, 2006, pp.32–33; IAEA, 2008, p.18). Tritium and carbon-14 are the main gaseous radionuclides that are released. Tritium being an isotope of hydrogen should diffuse more readily than the other radionuclide gases. Carbon-14 is released as methane and carbon dioxide due to microbial breakdown of the graphite

structure, and chlorine-36 is released as chlorine gas. The diffusion mechanism of the radioactive gases is dependent on the porosity of the graphite structure (Yamaguchi et al., 1991; Spitsyn et al., 2007).

2.2 POLYMER RESINS AS GAS BARRIER MATERIAL FOR RADIONUCLIDE GASES

2.2.1 Immobilisation of graphite waste

Various metal alloys and carbon are used in the structural design of nuclear reactors to limit the release of radionuclide gases like tritium. Alumina (Al_2O_3) coatings (Aiello et al., 2004; Benamati et al., 1999; Guikai et al., 2011; Magielsen et al., 2002; K. Zhang & Hatano, 2011; H. G. Yang et al., 2011) and chemical vapour deposition silicon carbide coatings (Causey & Wampler, 1995) have been shown to reduce the permeability of tritium significantly. Unfortunately, these coatings are expensive to apply to large surface areas as in the case of irradiated graphite waste. Therefore, the use of cheaper alternatives, for example, cement or polymer resins with improved gas barrier properties has to be considered.

To date, polymers are not commonly applied in the immobilization of intermediate and low level radioactive waste because inorganic types of cement is the more traditional option used due to its desired properties like excellent mechanical, chemical, and thermal stability. The use of cement as a primary barrier is well established, but there exists the concern that the contained radionuclides might leach from the cement and corrode the secondary metal barrier over time (Duffó et al., 2010).

However, polymers do present an optional alternative where inorganic cement might not be applicable or beneficial to a specific scenario. The use of polyurathene coatings with disposal canisters for nuclear waste has shown that the mechanical properties of the coating is largely unaffected by small amounts of accumulated radiation dosages up to 2 MGy (Mortley et al., 2008).

2.2.2 Polymer resins and the effect of irradiation

Some thermoplastic polymers like high and low density polyethylene have been applied in the immobilization of low level and intermediate waste by encapsulation. Polyethylene has excellent moisture barrier properties which make it ideal to encapsulate ion-exchange resins which contain ^{137}Cs and ^{106}Ru radionuclides (UK Nirex Limited, 2005, pp.11–13). On the other hand, polyethylene has very poor gas barrier properties which make it inappropriate with radionuclides which are released as gases like tritium. The main radiolysis products of polyethylene are hydrogen and carbon dioxide.

Polyester resins have been used in countries like the USA to immobilize radioactive waste due to its good radiation resistance to LLW. These resins exhibit low leaching of soluble radionuclides like ^{137}Cs and lower the release rates of tritium from encapsulated polyester resin waste (UK Nirex Limited, 2005, pp.17–20). The problems associated with using polyester resins are the short shelf life and the flammability of the resin which makes it impractical with large amounts of waste.

Epoxy resins on the other hand are versatile resins which can be sourced in various viscosities, curing time, etc. which makes them very practical to encapsulate large waste structures. During the 90s, Costes et al. (1990) proposed a method whereby they impregnated irradiated graphite waste from dismantled gas cooled reactors with epoxy

resins mixed with pitch and bitumen. By using this technique it was claimed that the resin filled most pores above 1 μm sufficiently and therefore restricted the leaching of the radionuclide content. The authors concluded that the technique is truly a long term waste management solution and submitted a proposal for the technique to be examined by the French authorities.

Glass composites filled with graphite has been synthesised as an option to immobilize irradiated graphite waste (McGann & Ojovan, 2011). The results obtained indicate that glass might be an option for future use with low loadings of graphite. However, the sintering process is adversely affected in an oxidizing atmosphere. Sellafield Ltd (Clifford, 2010) recently researched the use of epoxy resins to encapsulate graphite waste from decommissioned windscale piles in the UK. The epoxy resin showed promising long-term waste performance trials and good irradiation resistance to γ-irradiation.

It must be noted that all polymers degrade or crosslink when exposed to radiation. The extent of the degradation depends on the polymer and the total dose of radiation emitted from the specific radionuclide. The radiolysis of polymers normally produces gases like hydrogen and carbon dioxide. Therefore, polymer resins that exhibit good radiation resistance must be considered when being applied to immobilize radioactive waste. Further, the incorporation of certain inorganic fillers like carbon fiber (Hoffman & Skidmore, 2009) and glass fiber (Z. X. Wu et al., 2010) can improve the radiation resistance of polymers (Nielsen et al., 2008).

The radiation resistance of glass fiber composite epoxy resin has been studied by Wu et al. (2010). They investigated the effect of radiation on glass fiber reinforced epoxy resin composites and noticed no severe changes in the physical properties of the composite

resin after being irradiated by ^{60}Co γ-rays. The total radiation dose received was 1 MGy. French researchers (Davenas et al., 2002; Lionel Vignoud et al., 2001) have investigated the effect of ionizing radiation and electron irradiation on polymers, mainly epoxy resin and elastomers that are used in the nuclear industry. With regards to epoxy resin, the researchers found that the main form of degradation occurs by further chain scissions occurring when the resin is irradiated at different doses.

2.2.3 Epoxy resin

Epoxy resin is a thermosetting copolymer which is synthesized from the reaction between an epoxide resin (part A) and a hardener (part B). The most common reaction (Petrie, 2006, p.30) to prepare the pre-polymer resin is by reacting epichlorohydrin with Bisphenol-A in the presence of sodium hydroxide (NaOH) to produce a diepoxide (**Figure 2.2**).

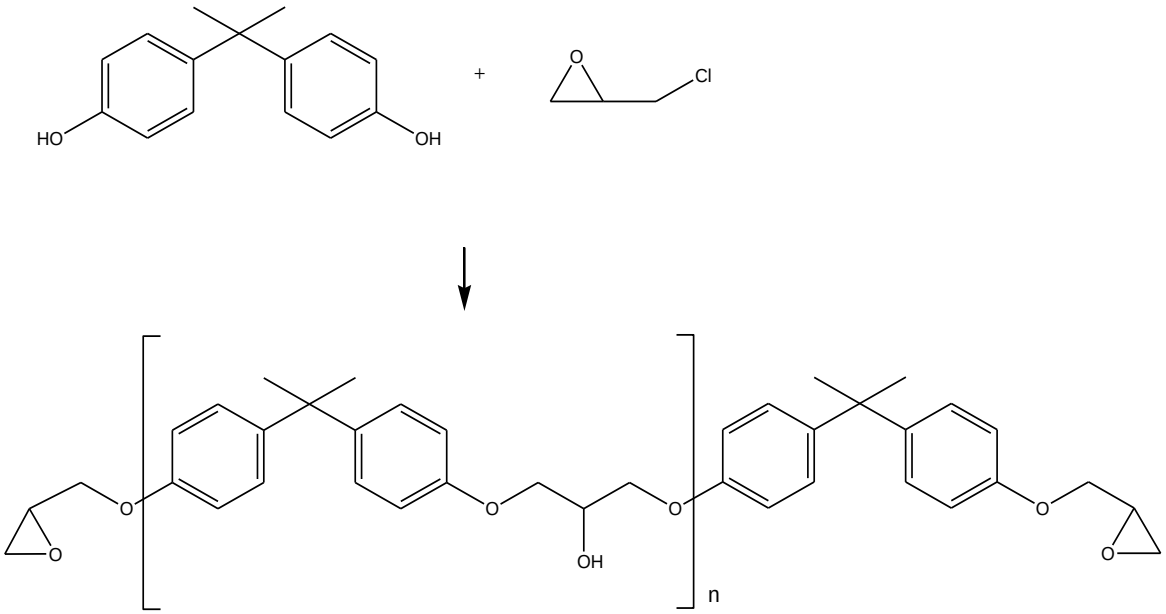

Figure 2.2 The addition of bisphenol A with epichlorohydrin to create epoxy pre-polymer

The molecular weight of the epoxy resin is controlled by the concentration of epichlorohydrin. In the presence of high concentrations of epichlorohydrin, low molecular resins are produced, which are the commercially useful resins (Petrie, 2006, p.30).

The curing reaction (**Figure 2.3**) occurs when a hardener is mixed with the epoxy resin. The hardener consists normally of a diamine that reacts with the epoxy groups to form a highly cross-linked structure (**Figure 2.4**). The curing reaction is exothermic and normally cures at room temperature depending on what type of curing agent is used. The curing reaction can be accelerated by curing at elevated temperatures.

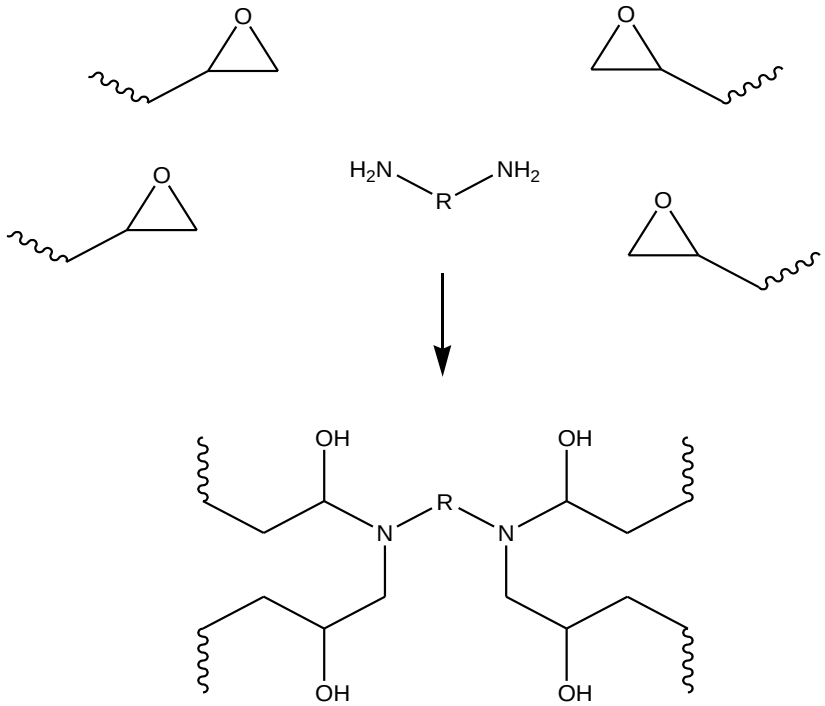

Figure 2.3 The reaction of a diamine with the epoxy pre-polymer resin

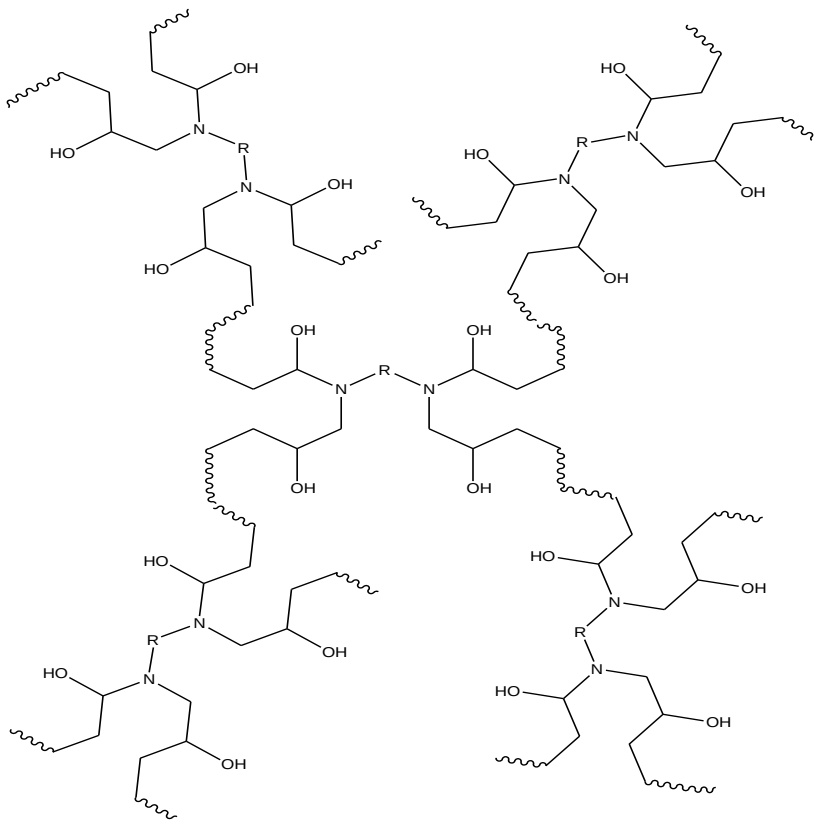

Figure 2.4 Cross-linked structure of epoxy resin

2.2.4 Additives to improve gas barrier properties

Epoxy resins can be mixed with specific additives to produce composite resins which exhibit improved physical properties. The desired effect is mainly determined by the type of additive. Fibres can improve mechanical properties like tensile strength and impact strength, whilst an additive like titanium dioxide aids in improving weatherability.

Extensive research is being performed on the property enhancing effect of incorporating nano-sized fillers into polymer resins to develop composite materials. Studies (Dumont et al., 2007; Frounchi et al., 2006; Ogasawara et al., 2006; Gupta et al., 2009; H. Kim et al., 2010; H. Wu & Drzal, 2012) over the past few years have shown that the incorporation of

nano-sized platelets and flakes like montmorillonite, glass flakes, and carbon flakes into polymer resins can improve the gas barrier properties quite effectively. The incorporation of impermeable platelet fillers at low weight fractions into a polymer matrix has been shown to improve the gas barrier properties.

This effect can be explained due to the increase in length of the diffusive path of gas molecules as the platelets invade the free volume in the polymer matrix (Bhattacharya et al., 2011) (**Figure 2.5**). The effectiveness of the filler to lower the diffusion of the gas molecule depends on the shape, orientation, and the amount of the filler dispersed in the polymer resin. The size of the gas molecule must also be considered when selecting an appropriate barrier material.

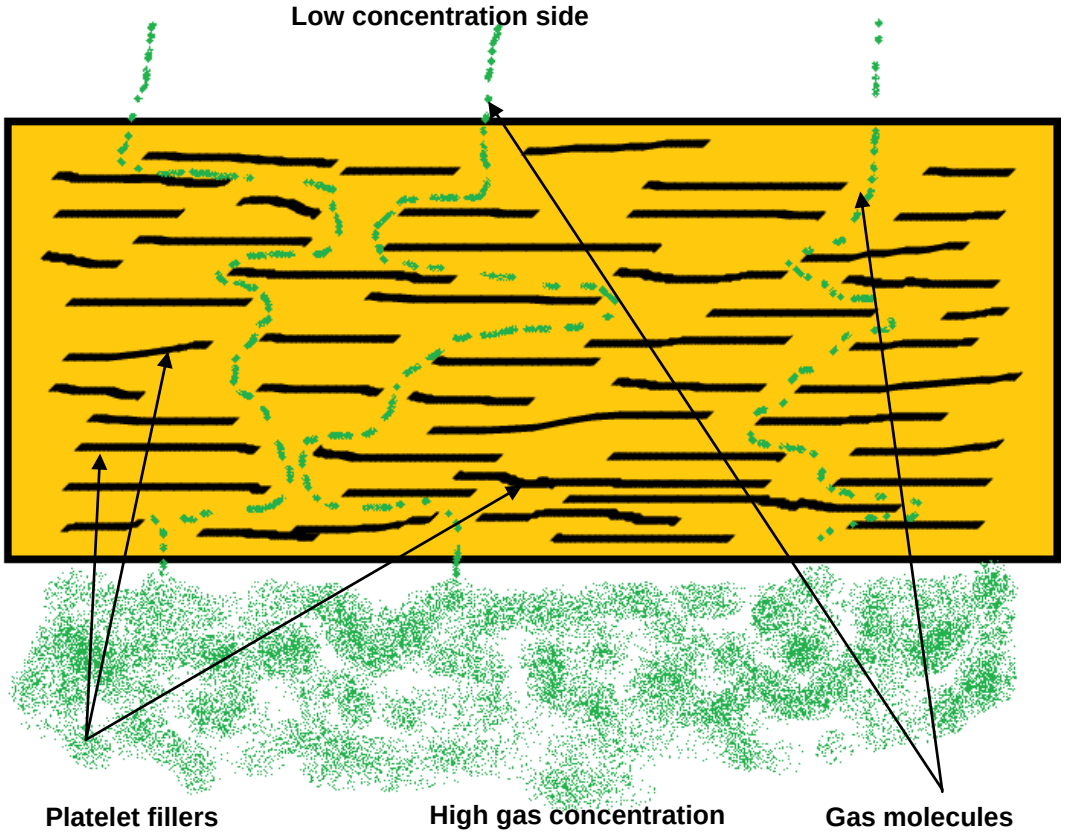

Figure 2.5 Diagram of a hypothetical composite membrane displaying the tortuous path created by exfoliated and orientated platelet fillers

Graphene is an allotrope of carbon, whose structure is one atom thick planar sheets of sp^2 bonded carbon atoms that are densely packed in a honeycomb crystal lattice (Stankovich et al., 2006). The crystalline or flake form of graphite consists of many graphene sheets stacked together. Graphene is the basic structural element of some carbon allotropes including graphite, charcoal, carbon nanotubes, and fullerenes. The incorporation of graphene platelets into polymers can improve the gas barrier properties significantly. For example, incorporating graphene platelets into polycarbonate reduces the helium gas permeation by 32% (H. Kim & Macosko, 2009) and the oxygen gas permeation of polyvinyl alcohol films has been improved by 17 times than that of pure poly(ethylene terephthalate) films (H. M. Kim et al., 2011). Graphene platelets have shown to be just as effective as montmorillonite clays to reduce the oxygen permeability of polypropylene (Kalaitzidou et al., 2007).

Glass flakes have been extensively used as barrier coatings in corrosive environments (González-Guzmán et al., 2010), yet there exists very limited research on the use of glass flake filled coatings as gas barrier coatings. Glass flakes incorporated into epoxy resins have displayed better corrosion resistance when compared to montmorillonite clays (Nematollahi et al., 2010). The incorporation of glass platelets and flakes can reduce the oxygen gas permeability of a polymer as much as two orders of magnitude (Gupta et al., 2009), while glass fibre epoxy composite resins are suitable replacements for metals to store helium at cryogenic temperatures due to the excellent barrier properties displayed (Disdier et al., 1998).

Therefore, with the improvement of the barrier properties that has been observed with the incorporation of graphene and glass flakes into polymer resins, the focus of this study was

to investigate the efficiency of graphene nanoplatelets and glass flakes to improve the gas barrier properties of the epoxy resin with regards to helium gas.

2.3 METHODS OF MEASURING GAS PERMEABILITY OF POLYMER MEMBRANES

The conventional method of measuring the permeability of polymer films is to use a specially designed apparatus with a permeation cell which measures the pressure differential across a membrane. The specified cell consists of two chambers with a membrane dividing the chambers. The one chamber is evacuated whilst the other chamber on the opposite end is pressurized with the test gas (helium, oxygen, or nitrogen). The pressure difference is then measured over a specified time as the gas diffuses through the polymer membrane (Hennessy et al., 1966, pp.32–35; ASTM, 2009a, pp.41–52). However, this technique does have some limitations like measuring the volume of the evacuated chamber and the problems of leaks during testing. Therefore, recent methods have been applying helium leak detectors to improve the accuracy of measurements and perform faster analysis of polymer and composite films (Muller et al., 2011, pp.62–67; Amanat et al., 2011).

Helium leak detectors are compact mass spectrometers equipped with a turbo-molecular pump and vacuum pump. The majority of helium leak detectors can measure leak rates as low as 1×10^{-12} mbar.l.s^{-1} with an effective range measured between 1×10^{-10} and 1×10^{0} mbar.l.s^{-1}.

Helium leak detectors were designed during World War II to detect leaks in uranium enrichment programs within the Manhattan Project (Varian Vacuum Products, 1995).

Helium leak detectors are being used as a relatively quick and easy method to apply in research areas to measure the permeability of polymer films or membranes (dos Santos, 2005) and to determine the quantities of tritium in radioactive waste drums (Demange et al., 2002). The helium leak detector technique was further used to examine the effect that matrix cracks have on the helium gas permeability of carbon fiber composite laminates for cryogenic applications (Yokozeki et al., 2009; Yokozeki et al., 2006; Yokozeki et al., 2004). This technique was used to investigate the helium permeability of films (Muller et al., 2011). The advantage of this technique is that it is not only faster than other pressure differential methods, which may take a few days or even weeks to analyse high gas barrier materials, but can also be used to predict the permeability of other gases like oxygen and carbon dioxide. Ogasawara et al. (2006) also used this technique to determine the helium permeability behaviour of montmorillonite/epoxy nanocomposites. They found that the incorporation of increasing amounts of the nano sized silicates reduced the helium gas permeability more than the base epoxy resin. The helium gas permeability and diffusion co-efficient was calculated according to a one-dimensional model based on Fick's second law of diffusion proposed by Yokozeki et al. (2004).

From the helium flux data, Fick's second law of diffusion can be applied to calculate the steady state flux and the diffusion co-efficient in the early stages of helium diffusion across the composite membranes with relatively low error (Yokozeki et al., 2004). This method has been successfully applied by other researchers to determine the helium gas permeability and diffusion co-efficient of polymers and composites (Yao et al., 2010; Choudalakis & Gotsis, 2009; Humpenöder, 1998).

For this study, the same method suggested by Ogasawara et al. (2006) and the model based on Fick's second law of diffusion suggested by Yokozeki et al. (2004) was used to

determine the diffusion coefficient and permeability coefficient. This method is explained in more detail in Chapter 4 of this dissertation.

3 METHODOLOGY

3.1 MATERIALS

Ciba-Geigy (now Huntsman) Araldite LY 5082 (resin) and Araldite HY 5083 (hardener) were purchased from Hi-Tech Polymers in Centurion. The Araldite LY 5082 resin consists of a type of bisphenol-F epoxy and the HY 5083 hardener consists of isophorone diamine. The supplier's recommended ratio of epoxy resin to hardener of 100:23 according to weight were used for all formulations.

The graphene nanoplatelets (Grade H) used were obtained from XG Sciences in the USA and the glass flakes (model C borosilicate) from the Tianrong Glass flake Co. LTD., were sourced from Glass Flake Coatings in Klerksdorp. SEM analyses of the fillers showed that the glass flakes (**Figure 3.1**) are larger than the graphene nanoplatelets (**Figure 3.2**). Chloroform ($CHCl_3$), dichloromethane (CH_2Cl_2), and tetrahydrofuran (THF) were purchased from Sigma-Aldrich, and N,N-dimethylformamide (DMF) from Associated Chemical Enterprises. These solvents were used to disperse the fillers into the resin for specific samples.

Afrox Helium 5.0 helium gas (99.99999 %) was used to measure the helium permeability of the epoxy resin disc samples.

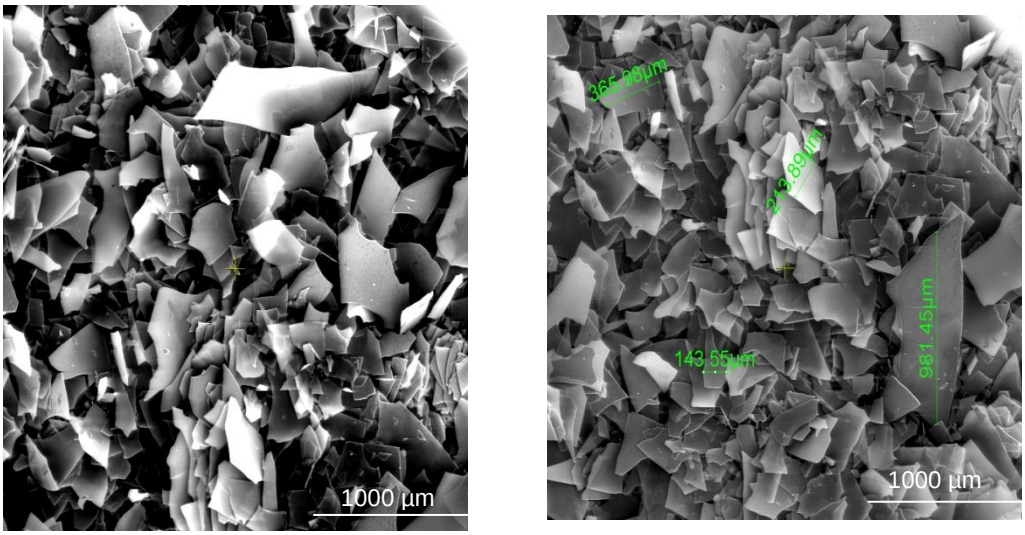

Figure 3.1 SEM images of (a) the glass flakes and (b) the dimensions

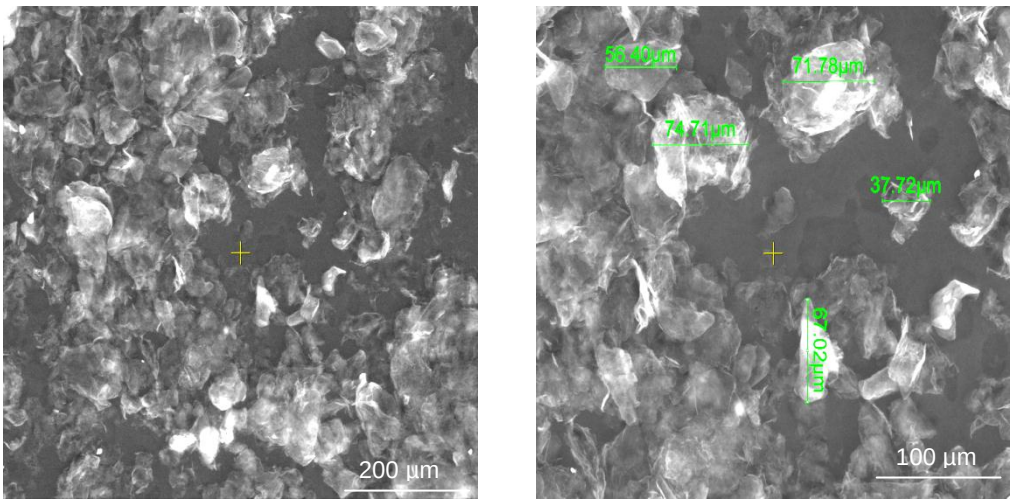

Figure 3.2 SEM images of the (a) graphene nanoplatelets and (b) the dimensions

3.2 TECHNIQUES FOR PREPARING THE COMPOSITE SHEETS

3.2.1 Doctor blade technique

Doctor blades are used in paint and ceramic technology to prepare thin films and to evaluate the degree of dispersion of additives like pigments. A doctor blade (**Figure 3.3**) works on the principle that a substrate (normally glass, metal, or plastic) is moved under a blade with an adjustable height, from a stationary position, to produce a thin film or sheet (Aegerter & Mennig, 2004, pp.89–92; Padinger et al., 2000). This shear action of the dragging orientates the filler parallel to the substrate surface. In this study, the doctor blade was used to control the thickness of the sheets to 2 mm and to aid in the orientation of the flakes and platelets. This was done to improve the barrier properties of the composite material. Sample discs (45 mm in diameter) were machined from the sheets with a Dremel tool to fit the permeation cell.

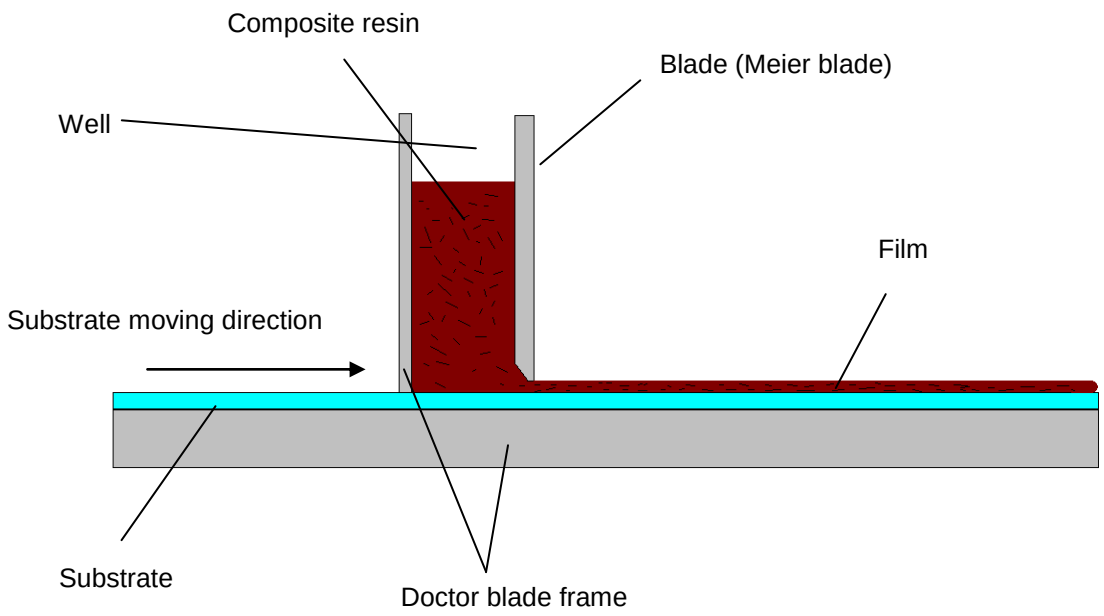

Figure 3.3 Diagram displaying the components of the doctor blade

3.2.2 Composite disc castings and use of solvents

Disc samples were cast in polyethylene moulds for samples thicker than 3 mm. Solvents were used to incorporate larger loadings and to disperse the fillers in the epoxy resin. Solvents are normally used to disperse fillers, like carbon nanotubes, into polymeric material and epoxy resins (Singh et al., 2011). The main problem encountered when using solvents is that the curing time of the epoxy can be affected if the solvent becomes trapped in the resin. Solvents that have very low boiling points were considered for dispersing the graphene into the epoxy resin. Therefore, the following solvents were chosen: chloroform, dichloromethane, tetrahydrofuran and N,N-dimethylformamide. According to literature, N,N-dimethylformamide gives very good dispersion and suspension of carbon nanotubes (Arepalli et al., 2008, p.20).

3.2.3 Multilayer sheets

Thin layers of the glass and graphene composite resin were coated on top of one another with a brush, to produce a sandwich structured sheet. One layer was applied onto a polyethylene sheet and once it was dry another layer was applied. Further layers were applied until the sheet was at the required thickness.

3.3 GRAPHENE/EPOXY NANOCOMPOSITE FORMULATION

3.3.1 Mixing methods

Graphene platelets, like carbon nanotubes, tend to agglomerate and the preferred methods to disperse these fillers in a resin are mechanical mixing and sonication techniques (Yasmin et al., 2006). The incorporation of the graphene platelets into the epoxy resin was the greatest challenge of the two fillers, due to the low bulk density (0.05 g/cm^3) of the

graphene. Therefore, the following available mixing techniques were used to separate and disperse the graphene platelets.

- *Mixing by hand*: The graphene powder was weighed and poured into the epoxy resin. The mixture was then stirred with a spatula for 5 min.
- *Generic kitchen blender*: A Russel Hobbs kitchen blender was used to mix the powder into the resin. The blender could only be used to mix for about 5 min because the motor of the blender started to overheat.
- *High shear mixing:* This technique was discarded because the composite resin started to overheat after a minute of mixing.
- *Ultrasonic mixing:* The beaker containing the epoxy resin and graphene was immersed in water in an ultrasonic bath and left to sonicate for 30 min at 50 ˚C. Hardener was added once the mixture had cooled to room temperature.

The mechanical mixing (kitchen blender) applies the principle of shearing the particles with high energy to separate them from one another and to disperse the particles into a resin system, whilst sonication uses ultrasonic waves to agitate and disperse particles uniformly in a resin system. Manual mixing by hand was included as a comparative technique because it was expected to exhibit poor dispersion of the graphene platelets.

3.3.2 Doctor blade graphene/epoxy composite sheets

The graphene platelets were mixed into 100 g of the Araldite epoxy resin with various loadings (**Table 3.1**) according to the weight percentage of the total composite resin system (**Equation 3.1**). Hardener (23 g) was added to the resin once the platelets were properly mixed and stirred by hand for 2 min. The resin was poured onto thin polyethylene sheet and the composite sheet was dragged out at 2 mm thickness with the doctor blade.

The sheet was allowed to fully cure for 7 days. Disc samples were then cut and measured for uniformity.

Table 3.1 Graphene doctor blade sheet formulations

Loading (wt%)	Mixing method	Weight (g)			Weight Fraction (%)		
		Araldite LY 5082	Araldite HY 5083	Graphene	Araldite LY 5082	Araldite HY 5083	Graphene
1	Manual	100	23	1.24	80.49	18.51	1
1	Ultrasonic	100	23	1.24	80.49	18.51	1
1	Shear	100	23	1.24	80.49	18.51	1
1	Blender	100	23	1.24	80.49	18.51	1
2	Blender	100	23	2.51	79.67	18.33	2
3	Blender	100	23	3.8	78.86	18.14	3

$$wt\ \% = \left[\frac{mf}{(mr + mh + mf)}\right] \times 100\% \qquad (3.1)$$

wt% = weight percentage (%)

mf = mass of filler (g)

mr = mass of resin (g)

mh = mass of hardener (g)

3.3.3 Graphene/epoxy composite moulded disc

The graphene powder was weighed according to the weight percentage and added to 50 ml of the solvent (**Table 3.2**). The solvent/graphene mixture was placed in an ultrasonic bath for 20 min and then added to 100 g of Araldite resin (LY 5082). The weight fraction is given in **Table 3.2**.

Table 3.2 Graphene moulded disc formulations

Loading (wt%)	Solvent	Weight (g)			Weight Fraction (%)		
		Araldite LY 5082	Araldite HY 5083	Graphene	Araldite LY 5082	Araldite HY 5083	Graphene
4	DMF	100	23	5.12	78.05	17.95	4.00
6	DMF	100	23	7.85	76.42	17.58	6.00
10	DMF	100	23	13.66	73.17	16.83	10.00
2	$CHCl_2$	100	23	2.51	79.67	18.33	2.00
4	$CHCl_2$	100	23	5.12	78.05	17.95	4.00
6	$CHCl_2$	100	23	7.85	76.42	17.58	6.00
4	THF	100	23	5.12	78.05	17.95	4.00
2	$CHCl_3$	100	23	2.51	79.67	18.33	2.00
4	$CHCl_3$	100	23	5.12	78.05	17.95	4.00

The epoxy/graphene/solvent mixture was placed in an ultrasonic bath for 2 h at 50 ˚C. The solvent was evaporated off with a Buchi rotary evaporation system. Once the solvent had been removed it was allowed to cool to room temperature. Hardener (Araldite HY 5083;

23 g) was added to the graphene/resin mixture and mixed by hand for 2 min. The resin was poured into polyethylene moulds with a diameter of 45 mm and a depth of 5 mm. The moulds were then left in an oven to cure for 15 h at 50 ˚C according to the supplier's guidelines (Ciba Geigy, 1991).

3.3.4 Stacked layers of graphene/epoxy nano-composite

The weighed graphene powder (0.251 g) was added to the Araldite epoxy resin (10 g). The beaker was sonicated for 5 h in an ultrasonic bath at 50 ˚C. When the mixture had cooled to room temperature, 2.3 g of hardener (Araldite HY 5083) was added and mixed manually by hand for 3 min. The resin was then coated onto a thin layer of polyethylene sheet with a brush. The thin layer was left to dry. Once the layer was dry another layer was coated on top of it. Further layers were coated until the required thickness was attained. Three samples for each graphene/resin mixture were prepared with thicknesses of 2, 3, and 4 mm respectively.

3.4 GLASS FLAKE/EPOXY COMPOSITE FORMULATION

3.4.1 Introduction

The glass flake/epoxy composite sheets were prepared by the following methods:

1. Doctor blade method to produce thin sheets
2. Casting discs in moulds
3. Stacked multiple layers of thin composite resin

3.4.2 Formulation of doctor blade glass flake/epoxy composite sheets

The glass flake filler was dispersed into the epoxy resin (100 g) at different weight percentages ranging from 1 to 30 wt% (**Table 3.3**). First it was mixed by hand for 2 min, followed by sonication in an ultrasonic bath at 50 ˚C for 1 h. The glass flakes were mixed into the resin. Hardener (23 g) was added to the glass flake/resin mixture after it cooled to room temperature and mixed by hand for 2 min. The resin was poured into the well of the doctor blade and the glass flake filled resin was dragged out on a polyethylene sheet at a thickness of 2 mm.

Table 3.3 Glass flake doctor blade sheet formulations

Loading (wt%)	Mixing	Weight (g)			Weight Fraction (%)		
		Araldite LY 5082	Araldite HY 5083	Glass flake	Araldite LY 5082	Araldite HY 5083	Glass flake
1	Ultrasonic	100	23	1.24	80.49	18.51	1.00
3	Ultrasonic	100	23	3.8	78.86	18.14	3.00
6	Ultrasonic	100	23	7.85	76.42	17.58	6.00
10	Ultrasonic	100	23	13.66	73.17	16.83	10.00
15	Ultrasonic	100	23	21.7	69.11	15.89	15.00
20	Ultrasonic	100	23	30.75	65.04	14.96	20.00

3.4.3 Formulation of glass flake moulded discs

The samples prepared without solvent, were weighed according to the weight percentage (**Table 3.4**) and mixed for 2 h at 50 ˚C in an ultrasonic bath. Hardener (23 g) was added to the resin and mixed for 2 min. The resin was poured into the polyethylene moulds and cured for 15 h at 50 ˚C according to the suppliers' guidelines (Ciba Geigy, 1991).

Table 3.4 Glass flake moulded disc formulations

Loading (wt%)	Solvent	Weight (g)			Weight Fraction (%)		
		Araldite LY 5082	Araldite HY 5083	Glass flake	Araldite LY 5082	Araldite HY 5083	Glass flake
25	None	100	23	41.00	60.98	14.02	25.00
30	None	100	23	52.72	56.91	13.09	30.00
35	None	100	23	66.22	52.85	12.16	35.00
40	$CHCl_2$	100	23	82.00	48.78	11.22	40.00
50	$CHCl_2$	100	23	123.00	40.65	9.35	50.00

For the samples that were prepared with solvents to mix in larger loadings above 35 wt% , the glass flakes were weighed according to weight percentage (wt%) and added to 50 ml of dichloromethane according to **Table 3.4**. The solvent/glass mixture was placed in an ultrasonic bath for 20 min and then added to 100 g of Araldite resin. The

epoxy/glass/solvent mixture was placed in an ultrasonic bath for 2 h at 50 ˚C. The solvent was evaporated using a Buchi rotary evaporator. Hardener (23 g) was added to the resin and mixed by hand for 2 min once the solvent was removed and cooled to room temperature. The resin was poured into polyethylene moulds with a diameter of 45 mm and a depth of 5 mm. The moulds were then left in an oven to cure for 15 h.

3.4.4 Formulation of stacked multiple layer glass flake/epoxy composite sheet

Glass flakes (5.271 g) were added to the Araldite epoxy resin (10 g) in a beaker. The beaker was sonicated for 5 h in an ultrasonic bath at 50 ˚C. When the mixture cooled to room temperature, 2.3 g of hardener was added and mixed manually by hand for 3 min. The resin was coated onto a thin layer of polyethylene sheet with a brush. The thin layer was left to dry. Once the layer was dry, another layer was applied. The layering steps were repeated until samples with thicknesses of 2, 3, and 4 mm respectively, were prepared.

3.5 HELIUM PERMEATION MEASUREMENT

A specially designed permeation cell was manufactured to house the disc sample with a diameter of 45 mm (**Figure 3.4**). The disc sample was supported between two centring rings with sealing o-rings (**Figure 3.5**). The top chamber was clamped down by a specially designed clamp.

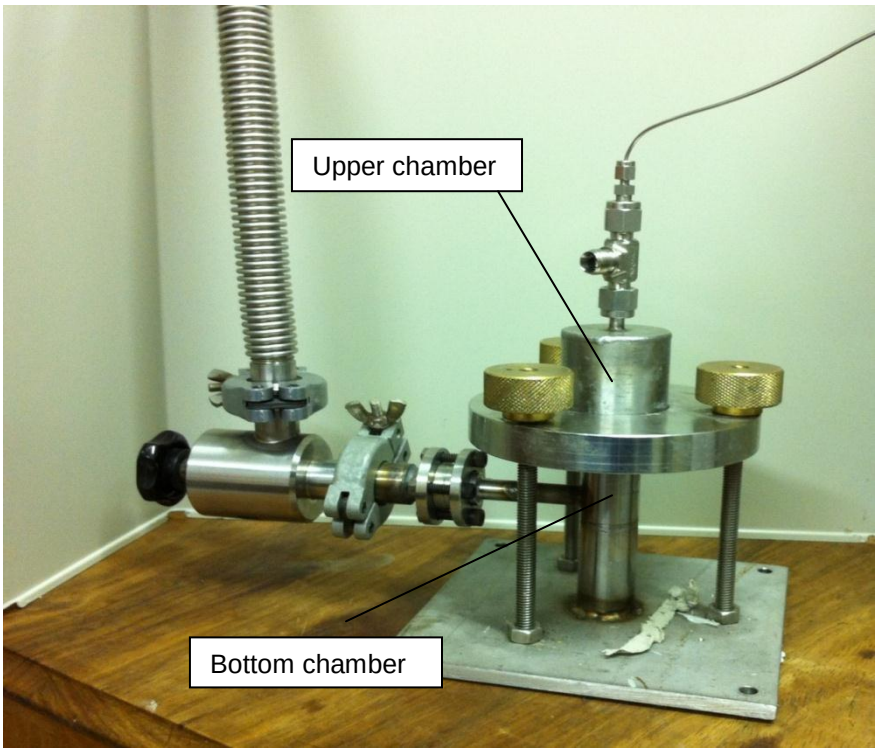

Figure 3.4 Photograph of permeation cell

Figure 3.5 Permeation cell with disc sample positioned between the o-rings

The permeation cell was connected to a Leybold L200^{+} helium leak detector with KF 25 stainless steel hose **(Figure 3.6**). The helium leak detector **(Figure 3.7**) is equipped with a mass spectrometer that could detect helium leak rates as low as 1 x 10^{-12} mbar.l.s^{-1} in vacuum mode.

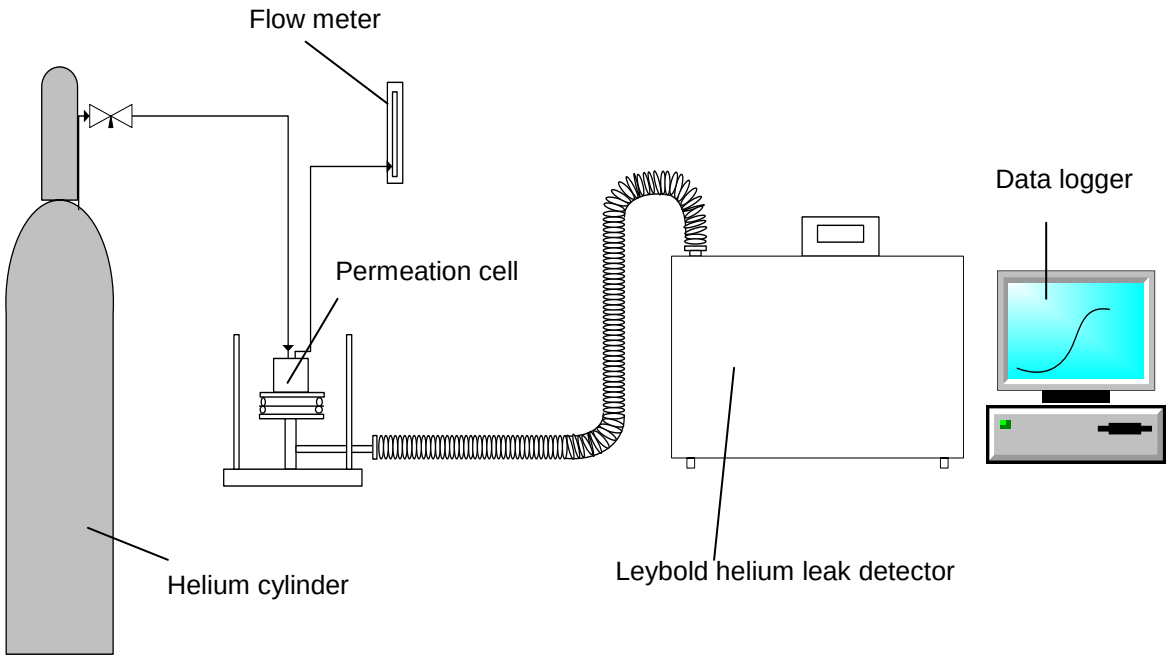

Figure 3.6 Helium permeation experimental setup

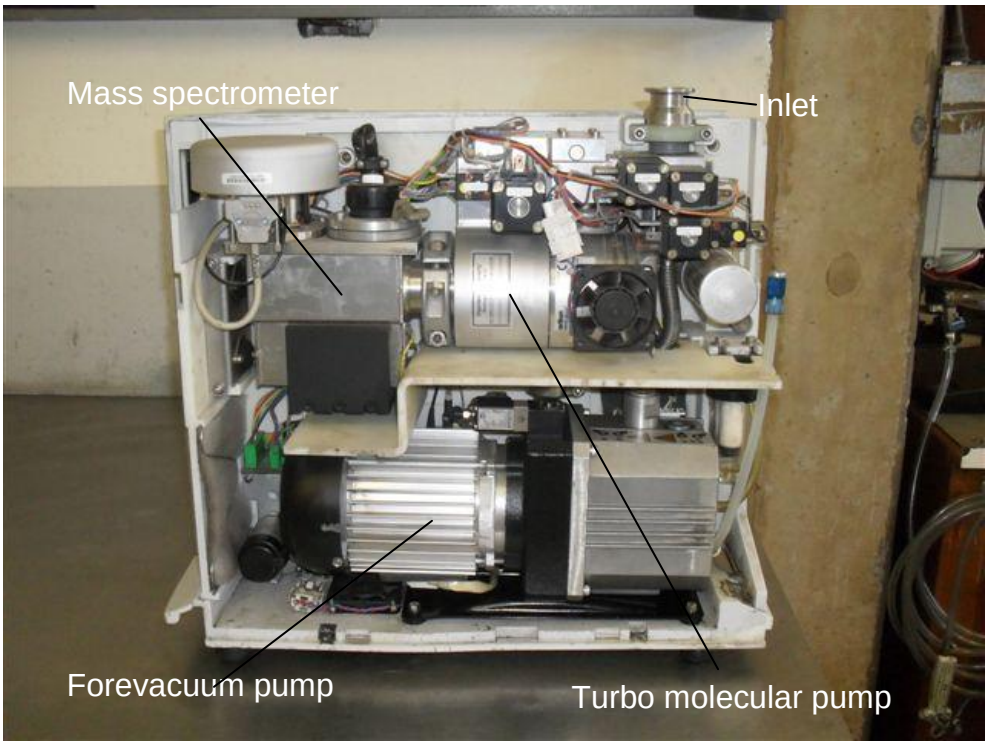

Figure 3.7 Photograph displaying the internal components of the helium leak detector

The startup procedure of the helium leak detector was to cycle the turbo-molecular pump and opening the gas ballast to vent for 5 min to remove any moisture which could influence the detector signal.

The gas ballast was then closed to start the evacuation of the bottom chamber to a pressure of 1.2 x 10^{-2} mbar. When the bottom chamber reached the required pressure, the vacuum would be maintained to determine if there were any leaks. The measurements were logged with the computer interface and software from National Instruments. This was initiated a few seconds before the helium was released into the upper chamber on the opposite side of the sample membrane.

The helium cylinder was opened and the helium released into the upper chamber at atmospheric pressure. The helium flowing into the upper chamber was controlled with a

pressure regulator and a valve at a rate of 50 ml/min. The helium leak rate was measured for 28 000 s or until steady state conditions were reached, as in the case of the reference samples. The measured leak rate was recorded on a logarithmic scale due to the small amounts of helium measured. When the required time measurement was obtained, the logging program was stopped and the helium cylinder shut off. The leak detector was stopped, vented to remove excess helium gas, and the disc sample removed.

3.6 CHARACTERISATION OF THE COMPOSITE COATINGS

3.6.1 Microscopic examination of composite coating morphology

Microscopic analysis was performed on the graphene and glass flake filled composite resins to determine how the fillers were dispersed and orientated in the resin matrix, since the dispersion and orientation of the fillers influence the gas barrier properties. Techniques like SEM and TEM are normally used to characterise the morphology of graphene composites (Potts et al., 2011) and glass flake filled samples (Gupta et al., 2010). The formation of a tortuous path from the incorporation of the glass flakes and graphene platelets can be verified with the use of these microscopic techniques.

Cubes were machined from selected composite samples and the cross sectional side (5 mm x 10 mm) of a cube was mounted in a moulding resin in order to polish the area for analysis. The polishing method used was according to the specifications found on the Struer website specifically tailored for brittle ceramics and glass (Struers, n.d.). The mounted samples were polished with a Tegra Force automated polishing unit and diamond paste with a grain size of 1 μm and with the final polishing step a silk disc was used.

The composite structures were examined using a Carl Zeiss Discovery V2 stereo microscope and FEI Quantum scanning electron microscope (SEM) (**Figure 3.8**). A low vacuum operational mode was used during the SEM imaging so that a large field detector could be employed. This detector has the advantage of eliminating charging from non-conductive specimens (such as the glass filled resin samples mounted in the casting resin for this study). Charging is caused by the build-up of electrons on the surface of an observed sample which deflects the electron beam in different directions and affects the image quality (Rice, n.d.).

With the FEI Quanta 200 3D SEM it was difficult to capture images of the graphene platelets suspended in the epoxy resin due to resolution limitations of the instrument. Only the surface of some of the samples filled with graphene produced clear and distinct images, but the orientation and degree of dispersion could not be observed with the specific SEM. Instead, an ultra-high resolution field emission scanning electron microscope (FESEM) (Carl Zeiss SMT AG, SUPRA^{TM} 40VP, Germany) was used to evaluate the surface of a 4 wt% graphene filled sample to determine the orientation of the platelets and the degree of dispersion. The observed surface was sputter coated with gold to improve the image quality. The graphene powder was examined using Transmission Electron Microscopy (TEM) due to the nanoscale of the graphene platelets.

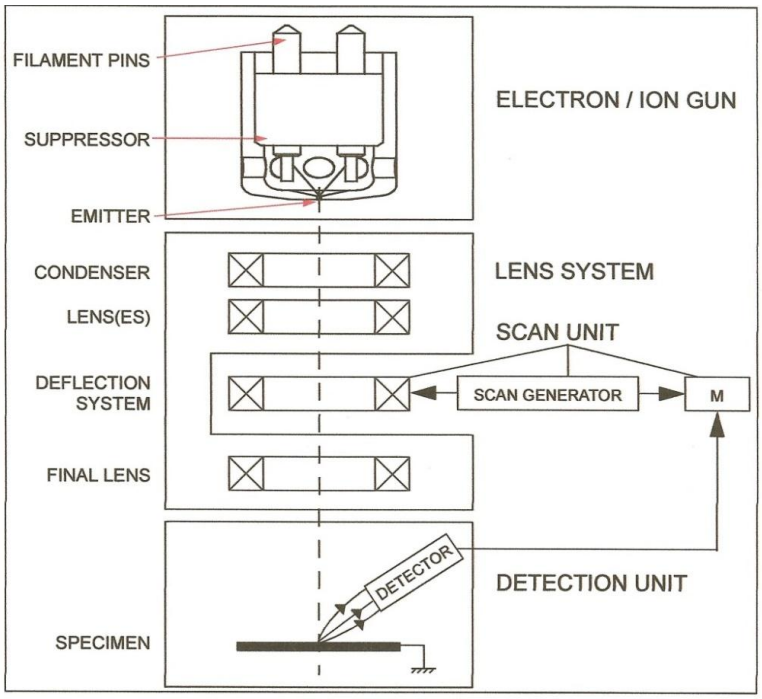

Figure 3.8 Diagram of the FEI Quanta 200 3D SEM

3.6.2 Adhesion to graphite surface

Reflector grade graphite and polyethylene blocks were used as reference surfaces to apply thin layers of epoxy resin to determine the adhesive properties of the epoxy resin. Epoxy resin (10 g) was prepared and a thin layer was applied to the specific surface with a brush. Cross hatch testing (ASTM D3359) was performed after the resin dried for 7 days. The cross hatches were cut close to one another to indicate if the resin is adhering to the graphite surface (**Figure 3.9**). Sticky tape was placed on the cut area and lifted. Good adhesion to the surface will show little or no flakes on the sticky tape. The cut areas were analysed with scanning electron microscopy. The visual assessment was determined from incisions made in the resin which was coated on the designated surface.

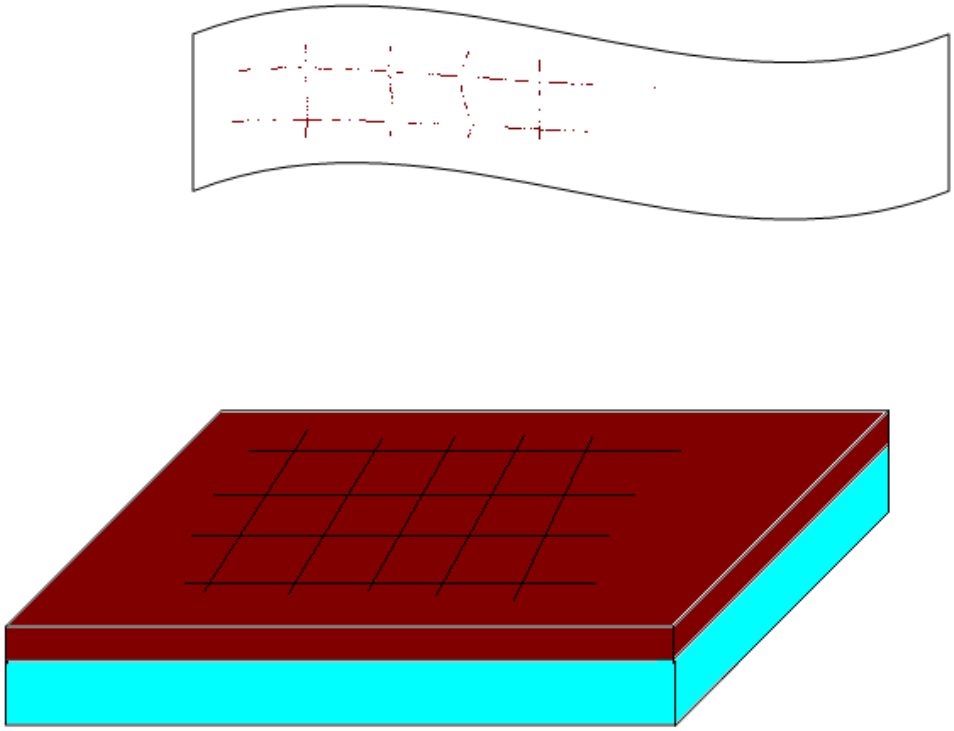

Figure 3.9 Cross-hatch adhesion test

4 PERMEABILITY OF COMPOSITE COATING

4.1 INTRODUCTION

Polymer membranes in general tend to have poor gas barrier properties (Qian et al., 2001), especially with regard to small gaseous molecules such as hydrogen, helium, oxygen, and nitrogen. It is established that the structure of a polymer membrane determines how the gas molecules migrate through the membrane (Cozmuta et al., 2007). The rate at which gas molecules travel through a polymer membrane depends on four stages, namely

1. Surface adsorption.
2. Absorption of the permeant into the membrane.
3. Diffusion through the membrane.
4. Desorption and release from the membrane.

This migration behaviour usually determines whether a polymer membrane is suitable for a specific barrier application or not and the study of membrane properties is essential for the understanding of gas barrier behaviour.

The migration of gas molecules through a polymer membrane is affected by factors like the size and shape of the gas molecule, and the nature of the polymer morphology (George & Thomas, 2001). Therefore, various theories and mathematical models have been used to explain permeability (Bucknall, 2004; Guo & Barbari, 2009; Lomax, 1980; Minelli et al., 2011). For this study, a derived mathematical model (Yokozeki et al., 2004) was used firstly to predict the possible transport mechanism of tritium gas through a composite barrier at steady state conditions and secondly, to determine the suitability of an epoxy

composite coating as a short-term solution to limit the release of tritium gas and other radioactive nuclides.

The first research on the diffusion of gases through a membrane was published in 1833 by a Scottish chemist, Thomas Graham (Philibert, 2006). He formulated a law which states that the rate of effusion of a gas is inversely proportional to the square root of the mass of its particles. Later, Adolf Fick would improve on this work in 1855 by introducing his own laws of diffusion (Philibert, 2006). He derived his equations from experiments on the fluxes and concentration of salts in water between two reservoirs connected with different lengths of pipe. He noticed that the behaviour of the concentration fluxes shared a common trait to Fourier's law of heat transfer and Ohm's law of electricity. Fick's laws of diffusion, as they came to be known, are still applied today to explain or model the general transport mechanisms of materials through a membrane. It must be noted, that not all diffusion processes behave according to Fick's law. These anomalies are termed to be non-Fickian in behaviour.

Since Fick's laws of diffusion have been used successfully to model the transport of gases through a membrane, it was used in this study to model the helium flux through the prepared graphene and glass flake composite membranes. The fitted model was also used to predict how much tritium gas might be released into the working environment and if unacceptable levels of exposure to radiation could occur in confined spaces due to tritium gas leaks.

4.2 FICKIAN MODEL DEVELOPMENT AND THEORETICAL CONSIDERATIONS

Fick's first law of diffusion describes the molecular flux (*J*) from a high concentration to a low concentration (*∂c*) through a membrane of a certain thickness (*x*). Introducing the diffusion coefficient (*D)*, as proportionality constant, gives the following equation:

$$J = -D\frac{\partial c}{\partial x} \tag{4.1}$$

In **Figure 4.1** a hypothetical membrane of an unknown thickness has been sketched to describe the migration of the gas particles, in one dimension, across a specific cross sectional area (A).

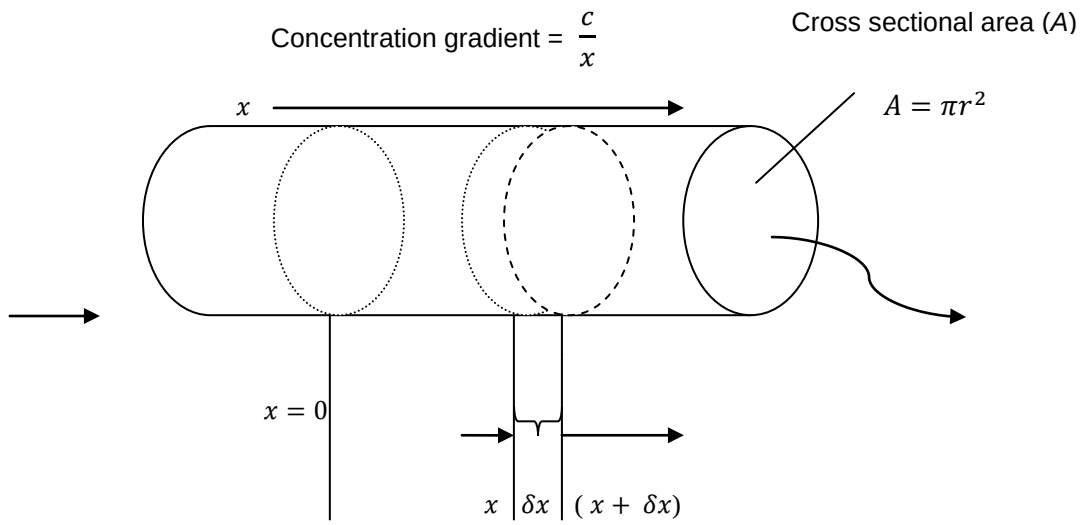

Figure 4.1 Diagram demonstrating how the concentration changes as molecules travel through a membrane of an unknown thickness

From **Figure 4.1** we can see that the concentration change along the x-axis as the permeant migrates across the membrane and this rate is defined as the concentration gradient ($^{c}/_{x}$).

The rate of diffusion is proportional to $-A\,{}^{\partial c}/_{\partial x}$ with the diffusion co-efficient (D) introduced as the proportionality constant, therefore

$$\text{Rate of diffusion} \quad = \; -\,DA\frac{\partial c}{\partial x}$$

By choosing a section of the membrane (**Figure 4.1**) defined from x to (x+δx), it may be considered that the molecules enters at x and exit at (x+δx). From this it can be noticed that the rate of entry will be the same as the rate of diffusion at any point along x.

$$\therefore \quad \text{Rate of entry at } x \quad = \; -DA\frac{\partial c}{\partial x}$$

$$\text{Rate of leaving at } (x+\delta x) \quad = \; -DA\left(\frac{\partial c}{\partial x} + \frac{\partial^2 c}{\partial x^2}.\partial x\right)$$

$$\therefore \text{ Rate of accumulation} \quad = -DA\frac{\partial c}{\partial x} - \left[-DA\left(\frac{\partial c}{\partial x} + \frac{\partial^2 c}{\partial x^2}.\partial x\right)\right]$$

$$= DA\left(\frac{\partial^2 c}{\partial x^2}.\partial x\right)$$

The rate at which the concentration changes with time can be equated to the rate of accumulation divided by the volume element, that is

$$\frac{\partial c}{\partial t} = \frac{\text{rate of accumulation}}{\text{volume element}}$$

where the volume element is Aδx, therefore

$$\frac{\partial c}{\partial t} = \frac{DA\left(\frac{\partial^2 c}{\partial x^2}\right)\cdot\frac{\partial x}{1}}{A\partial x}$$

$$= D\frac{\partial^2 c}{\partial x^2} \tag{4.2}$$

When applied to membranes, there are certain boundary conditions that need to be considered (Rogers et al., 1954; G. K. Vemulapalli & K. G. Vemulapalli, 1993, p.952) (see **Figure 4.2**). Initially the concentration is equal to zero since no particles have been absorbed into the membrane. As the particles start to enter the membrane, the concentration starts to increase as more of the particles diffuse into the membrane over a specific time frame.

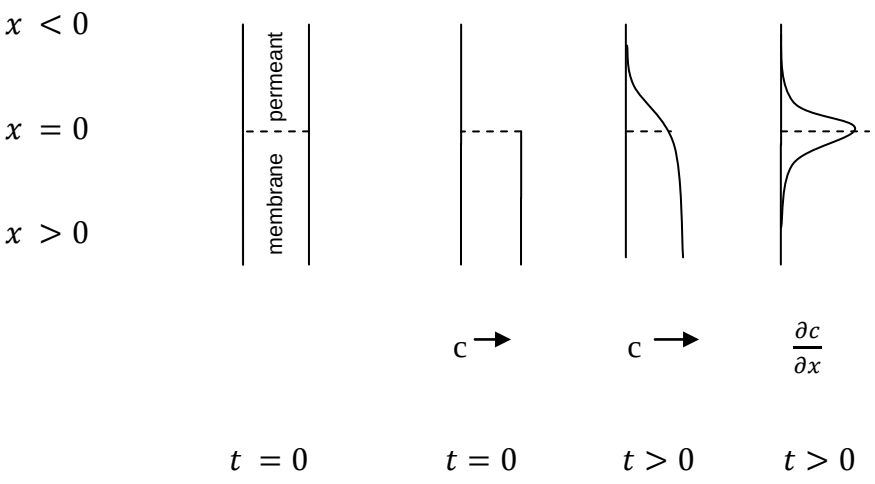

Figure 4.2 Listed boundary conditions

A mathematical solution of **Equation 4.2**, using the boundary conditions defined in **Figure 4.2** leads to **Equation 4.3**. **Equation 4.3** relates the gas flux through a membrane as a function of time and is given by

$$\left(\frac{\partial c}{\partial x}\right) t = \frac{c_0}{\sqrt{(4\pi D t)}} \exp \frac{-x}{4Dt} \tag{4.3}$$

Equation 4.3 describes the process known as diffusion. Diffusion may take place even through a membrane where the higher concentration of molecules tends to migrate to an area of low concentration. The exponential function in **Equation 4.3** is analogous to the random walk discovered by Robert Brown (Philibert, 2006). This arises from the fact that when molecules diffuse, the microscopic "picture" indicates a random walk scenario caused by molecular collisions, with a resultant movement towards areas of low concentration.

4.3 MODEL APPLICATION

The helium flux was calculated from the measured helium leak rate data as follow:

$$J = \frac{J^*}{ART} \tag{4.4}$$

Where J is the helium flux (mol.m^{-2}.s^{-1}), J^* the measured helium leak rate (measured in mbar.l.s^{-1} but converted to Pa.m^3.s^{-1}), A the surface area (m^2), R the gas constant (8.315 J.K^{-1}.mol^{-1}) and T the temperature in Kelvin.

Ogasawara et el. (2006) and Yokozeki et al. (2004) used the following variation of Fick's law to determine the diffusion coefficient (*D*) and the steady state flux (J_0).

$$J = J_0 \sqrt{\frac{4d^2}{\pi Dt}} \sum_{m=0}^{\infty} exp \left[- \frac{d^2}{4Dt} (2m+1)^2 \right] \tag{4.5}$$

In the earlier stages of gas diffusion, **Equation 4.5** can be approximated to

$$J \cong J_0 \sqrt{\frac{4d^{\ 2}}{\pi Dt}} \ exp \left(- \frac{d^2}{4Dt} \right) \tag{4.6}$$

This shortened form is then used to determine D and J_0.

Equation 4.6 can be re-arranged to the linear form

$$ln(J\sqrt{t}) \ \cong \ -(\frac{d^2}{4D})\frac{1}{t} \ + \ ln\, J_0 \sqrt{\frac{4d}{\pi\, D}} \tag{4.7}$$

The diffusion coefficient, *D*, can be determined from the slope (**Equation 4.8**) of the Arrhenius graph (**Figure 4.3**)

$$D \ = -\frac{d^2}{4} m \tag{4.8}$$

while the steady state flux, J_0, can be determined from the intercept (**Equation 4.9**) of the Arrhenius graph (**Figure 4.3**)

$$J_0 = {e^i}\Big/{\frac{4d^2}{\pi D}} \tag{4.9}$$

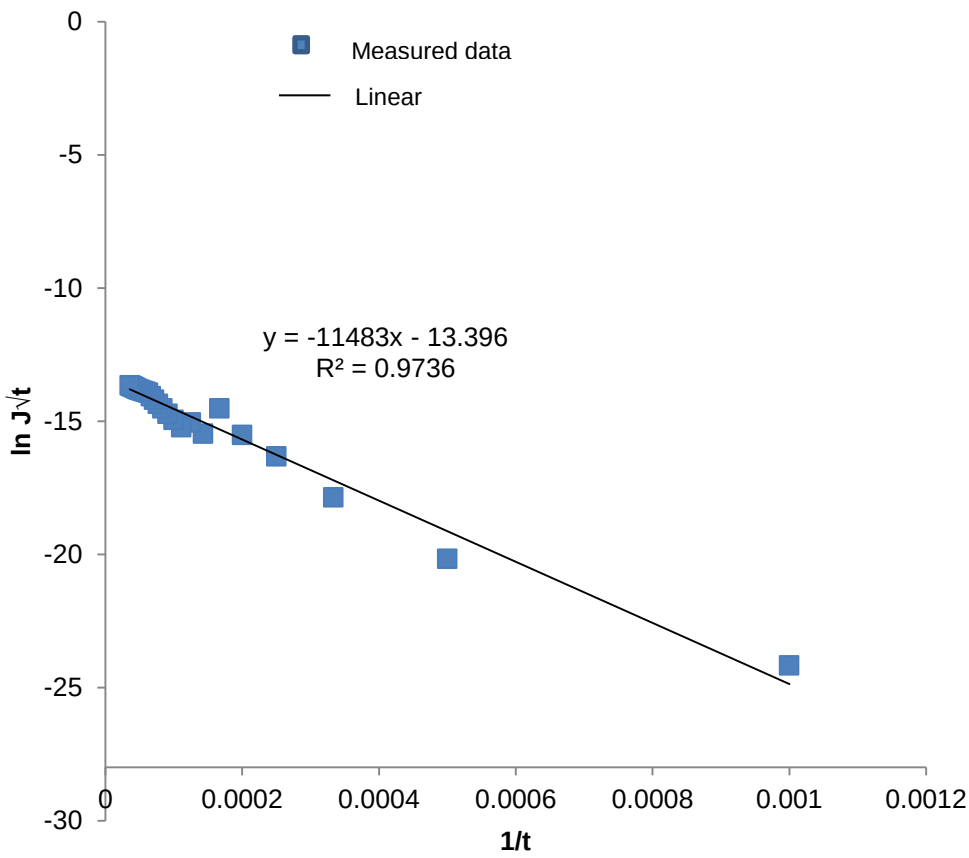

Figure 4.3 Linear plot of measured data and linear trendline

The linear trend line is fitted according to the data until the R^2 value is as close as possible to 1. Substitution of values for D and J_0 into **Equation 4.6** should produce a curve that

resembles the measured data (**Figure 4.4**) if the statistical deviation from the true value is within acceptable limits.

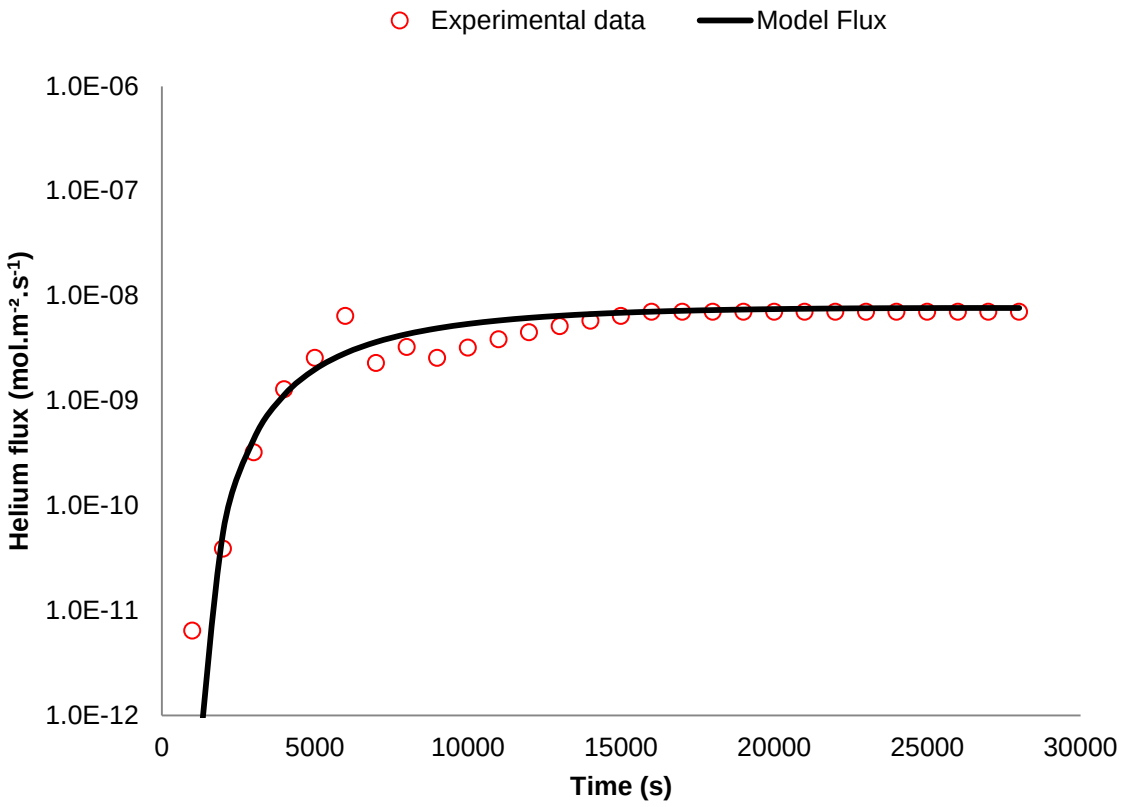

Figure 4.4 Example demonstrating good Fickian model fit of measured leak rate flux.

The permeability coefficient (P) was determined from the steady state flux (J_0) by the following equation:

$$P = \frac{J_0\, d}{\Delta p} \tag{4.10}$$

where P is the permeability coefficient (mol.m^{-1}.s^{-1}.Pa^{-1}); J_0 the steady state flux (mol.m^{-2}.s^{-1}); d the thickness of the membrane (m); and Δp the differential gas pressure (Pa).

4.4 TRITIUM MASS TRANSPORT

In order to use the measured helium flux to predict the activity and amount of radionuclides released, the following assumptions were made about the characteristics of tritium gas:

1. The tritium gas molecules exhibit the same transport properties as helium and hydrogen gas.
2. The tritium maintains its specific activity.
3. No reaction of the tritium gas occurs with other compounds to reduce the concentration of tritium.

The amount of tritium released through the coating was derived from the measured helium flux at steady state conditions as follows:

$$m_T = J_0 . m_a . A . t \tag{4.11}$$

where m_T is the mass (g) of tritium gas released, J_0 is the helium flux (mol.m^{-2}.s^{-1}) at steady state, m_a is the atomic mass (g.mol^{-1}) of tritium, A is the total surface area (m^2) of release, and t is the time (s).

The radioactivity can then be calculated as follows (Kotz et al., 2003, pp.975–976):

$$Q = \frac{m_t}{m_a} \cdot N_A \cdot \frac{\ln 2}{t_{1/2}} \tag{4.12}$$

where Q is the radioactivity in Becquerel (Bq); m_t is the mass (g) of tritium; m_a is the atomic mass ($g.mol^{-1}$); N_A is Avogadro's number (6.022141×10^{23} mol^{-1}); and $t_{1/2}$ is the half life of tritium in seconds.

4.5 TRITIUM RELEASE SCENARIOS AND CALCULATION

To simulate the performance of the coatings in a storage repository, it was necessary to make some assumptions. Therefore, a hypothetical storage repository was created based on assumptions about the surface area that needed to be coated, the thickness of the coating, the ambient pressure and temperature, ventilation of the working environment, the concentration of tritium in the graphite waste, and the long term release of the tritium into the working environment. The allowed concentrations were derived from the annual limit intake (ALI) and the derived air concentration (DAC) for the specific isotope conversion factor as prescribed by the Safety, Health, Environment, and Quality (SHEQ) (Beeslaar, 2012; ICRP, 1996, p.14; ICRP, 1997, p.38) regulating body.

The surface area was based on the volume of graphite waste that might be generated by a Magnox graphite moderated reactor. Two different scenarios were used to determine the effectiveness of the coatings (**Table 4.1**). With both these scenarios the graphite waste of one reactor would be stored in a facility and the tritium would be released into the working environment. The graphite volume is roughly 1500 m^3 and the surface area 600 m^2.

Table 4.1 The considerations for Scenario 1 and Scenario 2

	Scenario 1	**Scenario 2**
Surface area of graphite waste	600 m^2	600 m^2
Facility volume	125 000 m^3	500 000 m^3
Pressure	Ambient	Ambient
Temperature	< 25°C	< 25°C
Time frame	28 000 s	28 000 s
Ventilation	No	No

For both the scenarios, it was assumed that the repositories had little or no ventilation. This was to predict the accumulative effect of tritium gas in the repository environment if the ventilation system failed. For if the repository had sufficient ventilation then the accumulation of tritium gas would pose no real threat to radiological workers. The temperature of the repository was kept at room temperature conditions to reflect the temperatures (20 °C to 23 °C) that the composite samples were measured at in the laboratory. The concentration of tritium that diffuses from the graphite waste would be dependent on the volume of the repository and how quickly the tritium gas migrates through the composite coatings. The dimensions of the repositories (**Figure 4.5**) considered for this study was only to act as a guideline to estimate the concentrations of tritium gas accumulating in the repository environment. The helium leak rates of the

coatings could then be applied to determine if the tritium concentration was reduced below the recommended regulatory derived air concentration of 6 x 10^8 Bq.m^{-3}.

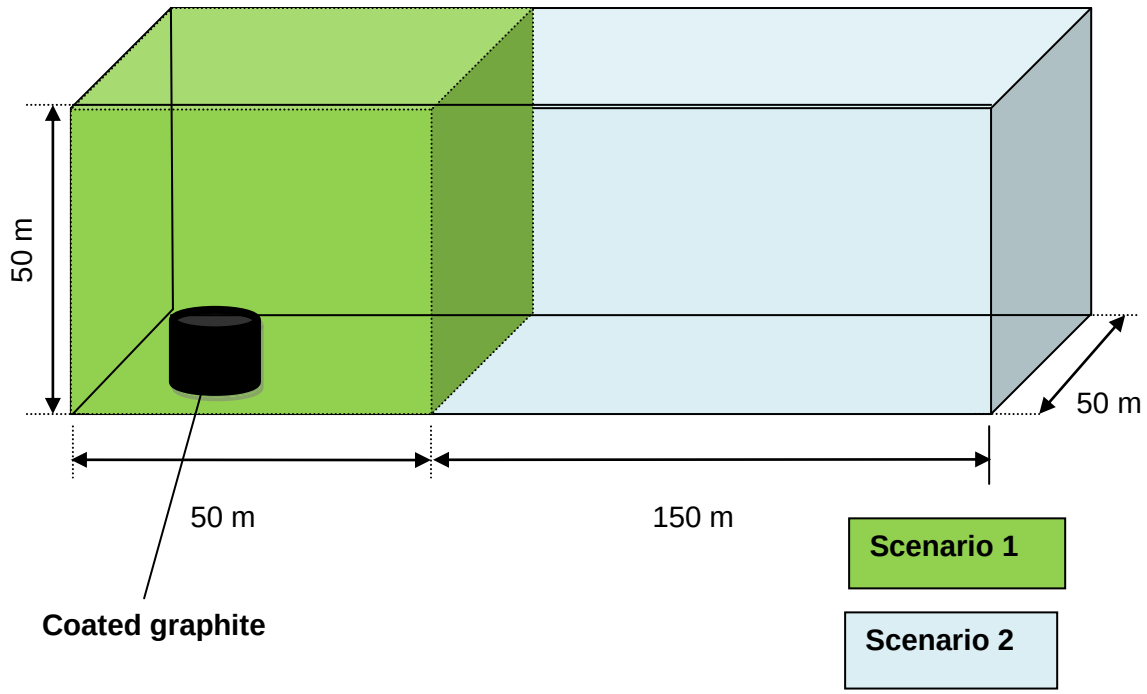

Figure 4.5 Schematic of Scenario 1 and Scenario 2 with given dimensions of the hypothetical repositories

In summary, the permeability model and tritium release predictions were applied to all the measured glass flake and graphene composite samples. The measured helium leak rates were modelled according to **Equation 4.6** to compare the effect that the glass flakes and graphene nano-platelets had on the helium permeability. From the model, the steady state flux can be determined which was used to determine the amount of tritium that could leak from irradiated graphite waste with a continuous inventory of tritium gas. These results are discussed in detail in Chapter 5.

5 RESULTS & DISCUSSION

5.1 EXPERIMENTAL AND CHARACTERISATION OVERVIEW

The volume of irradiated graphite waste generated by a Magnox nuclear reactor can be around 1500 m^3 (this equates to a minimum area of 600 m^2). To cover this large area, an epoxy resin which has a long workable pot life would have to be used. Huntsman Araldite LY 5082 epoxy resin and Araldite HY 5083 hardener was the only epoxy resin sourced for this study due to the specific properties required to coat graphite waste. This resin has a low viscosity (1700 to 2200 mPa.s) and a gel time of 170 to 200 min making it suitable for coating large areas like that of the graphite waste. The low viscosity of the resin and hardener also aided with the blending of the filler additives.

The incorporation of nano- and microscale platelet additives into polymer resins have shown to reduce the gas permeability due to the formation of a tortuous path which restricts the diffusion of gas molecules across the polymer matrix (See Section 2.2.4). Therefore, graphene nanoplatelets and glass flakes were blended into the Araldite epoxy resin to determine if the helium gas permeability of the epoxy resin could be reduced with the incorporation of these fillers. The platelets were introduced at concentrations starting from 1 wt% (weight percentage) of the total resin system and increasing the concentration until the resin has reached the weight fraction threshold.

The composite resin samples were prepared as doctor blade sheets, moulded discs, and multilayer sheets. The prepared composite structures were examined with a stereo microscope and Scanning Electron Microscope (SEM) whilst the graphene platelets were examined with a Transmission Electron Microscope (TEM).

Helium was used as the test gas to simulate the release of tritium from the graphite waste. A specially designed permeation cell in combination with a helium leak detector was used to measure the helium leak rate of the reference epoxy samples and fabricated composite samples.

The epoxy resin was applied onto reactor graphite and polyethylene blocks to determine the adhesion properties of the epoxy resin. The adhesion was evaluated using the cross hatch test method according to ASTM D3359.

5.2 EPOXY COMPOSITE PREPARATION & SAMPLE MORPHOLOGY

5.2.1 Doctor blade sheets

Individual graphene/epoxy samples were prepared with 1 wt% graphene by applying different mixing techniques to determine which technique could disperse the graphene platelets more effectively in the resin matrix and thereby reduce or prevent the permeation of helium molecules through the composite resin matrix.

The sample prepared with the IKA ultra torrax high shear mixer was omitted for permeability analysis because the 100 g resin overheated due to the high shear. Hardener was added to the graphene/epoxy mixture, but the heat generated appeared to have degraded the epoxy resin. The specific unit was designed to mix quantities larger than 2 dm^3 of resin, but the amount of epoxy resin available for the research was only 10 kg, it was therefore decided rather not to use this mixing technique further.

The advantage of sonicating the resin was that the viscosity of the epoxy resin was lowered further due to the agitation of the ultrasonic bath and raising the temperature of the mixture to 50 °C. Due to the decrease in viscosity, most of the graphene platelets settled in the bottom half of the beaker when 100 g of epoxy resin was sonicated. This indicated that the ultrasonic bath did not produce sufficient energy to disperse the graphene platelets in amounts of 100 g of epoxy resin. However, the ultrasonic bath was more suitable to disperse graphene in amounts less than 20 g of epoxy resin at 1 wt% loading which was observed with the multilayer samples.

It was expected that mixing the graphene by hand would produce poor dispersion of the platelets in the epoxy resin, but the technique appeared to disperse the graphene platelets well in the resin. During mixing no significant amount of clumping by the graphene platelets was observed.

Since the best mixing of the graphene platelets was obtained with the kitchen blender, the rest of the graphene/epoxy doctor blade sheets were prepared using this technique. The kitchen blender could mix the graphene loadings easily up to 2 to 3 wt% loading. Above 3 wt% the graphene/epoxy resin became so viscous that the graphene platelets did not disperse properly in the epoxy resin. This can be attributed to the diminishing free volume of the epoxy resin matrix which is known as the weight fraction threshold. The weight fraction threshold is the maximum concentration of filler that can be dispersed thoroughly in a polymer matrix.

For the glass flake filled resin, mechanical mixing was omitted in order to avoid deformation or possible damage of the glass flakes by the blender and high shear mixer. An ultrasonic bath was therefore used to disperse the glass flakes into the epoxy resin.

During the sonication, the temperature of the glass flake resin mixture rose to 50 ˚C and this resulted in a decrease in viscosity which helped to disperse the glass flakes. The glass flakes, with a higher bulk density (0.2 - 0.5 $g.cm^{-3}$) than that of the graphene platelets (0.05 – 0.25 $g.cm^{-3}$) allowed larger loadings of the glass flakes to be incorporated into the epoxy resin system. The dispersed glass flakes appeared to exhibit little or no agglomeration when compared to the graphene platelets dispersed in the resin. With the increase in loading of glass flakes the viscosity of the resin also increased.

The doctor blade sheets were prepared at a thickness of 2 mm and a length of about 400 to 500 mm. The increase in viscosity from the incorporation of the graphene platelets and glass flakes improved the stability and shape of the doctor blade sheets. However, with loadings above 3 wt% (graphene platelets) and 20 wt% (glass flake), the filler/epoxy resin mixtures became too viscous to drag 2 mm thick sheets with the doctor blade. The filler/epoxy resin mixtures would stick to the Meier blade edge and clump together in the well of the doctor blade. Therefore, sheets could not be produced with a glass flake loading above 20 wt% and for the graphene platelets 3 wt% was the maximum when using this method.

The sheets were left to cure for seven days at room temperature according to the supplier's specifications. The visual inspections of the cured sheets showed that with low loadings the graphene (1 wt%) and glass flake (1 to 6 wt%) fillers settled at the bottom of the sheets. Depending on the dispersion technique, it was observed that the graphene platelets agglomerated in regions within the doctor blade sheets. The graphene (2 to 3 wt%) and the glass flakes (10 to 20 wt%) at higher loadings showed less settling of the fillers than the lower loadings. The long gel time of the Araldite epoxy resin appears to be the reason why gravity caused the settling of the fillers in the epoxy matrix. One sheet was therefore

placed in the oven at 50 °C to cure quicker in an attempt to prevent the fillers from settling in the epoxy matrix. The sheet unfortunately warped from the heat at 50 °C because the sheet was only 2 mm thick. It was then tried to prepare thicker samples at 3 mm, but sheets thicker than 2 mm could not be controlled properly due to the low viscosity of the epoxy resin causing the sheet to sag and cure at around 2 mm thickness. Therefore, the sheets had to be left to cure at room temperature for seven days to maintain the thickness at around 2 mm.

The images (**Figure 5.1**) taken with the stereo-microscope showed that the doctor blade sheets prepared with the blender mixed the graphene platelets homogenously in the resin up to 3 wt% with few voids from entrapped air. As the weight fraction increased, the amount of voids increased. The 10 wt% glass flake filled sheet exhibited less voids as when compared to the 20 wt% glass flake filled sheet which had voids (**Figure 5.2**). Even with the voids, the glass flake sheets appeared to be properly mixed.

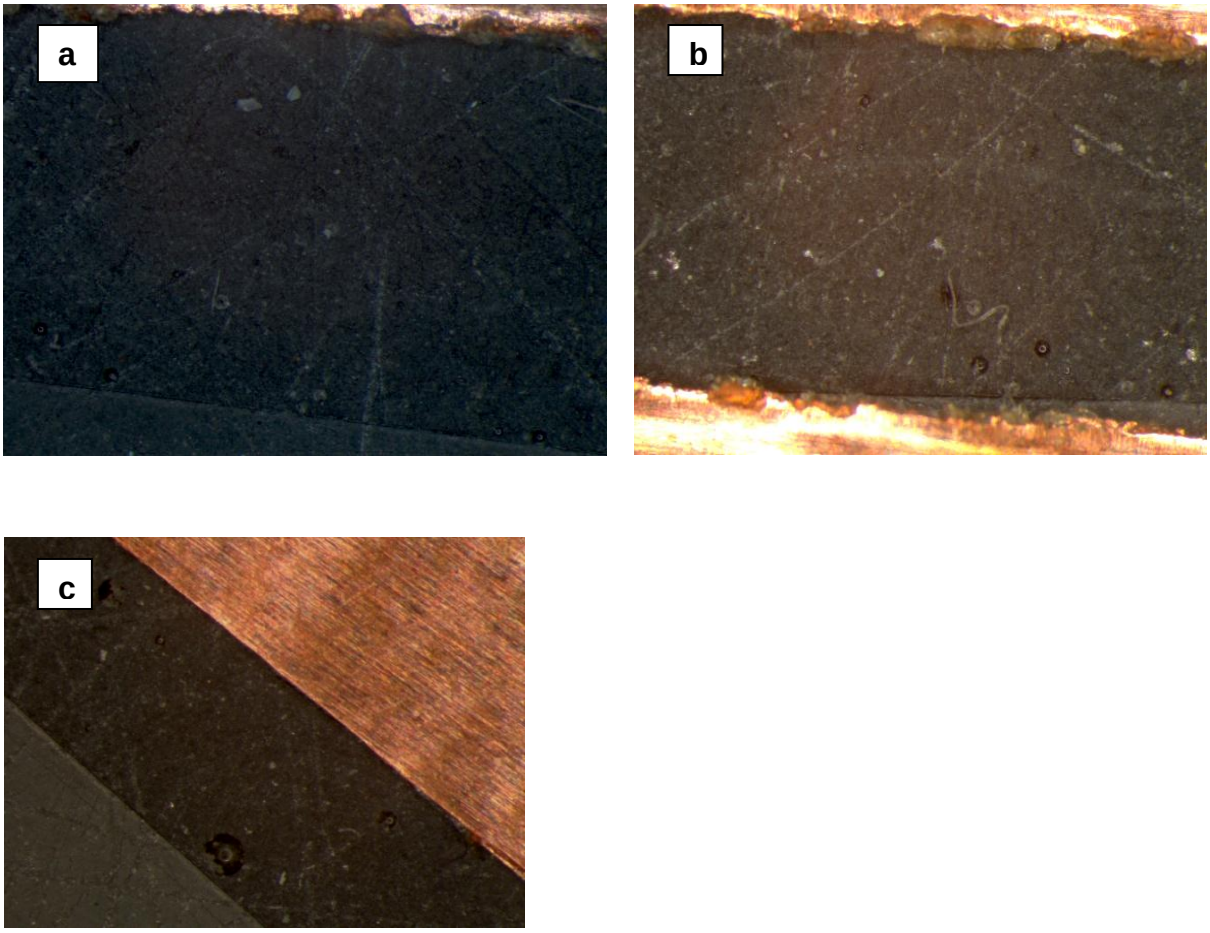

Figure 5.1 Microscopic images (40x) of the graphene filled doctor blade sheets (cross section) prepared with the blender at a) 1 wt%, b) 2 wt%, and c) 3 wt%

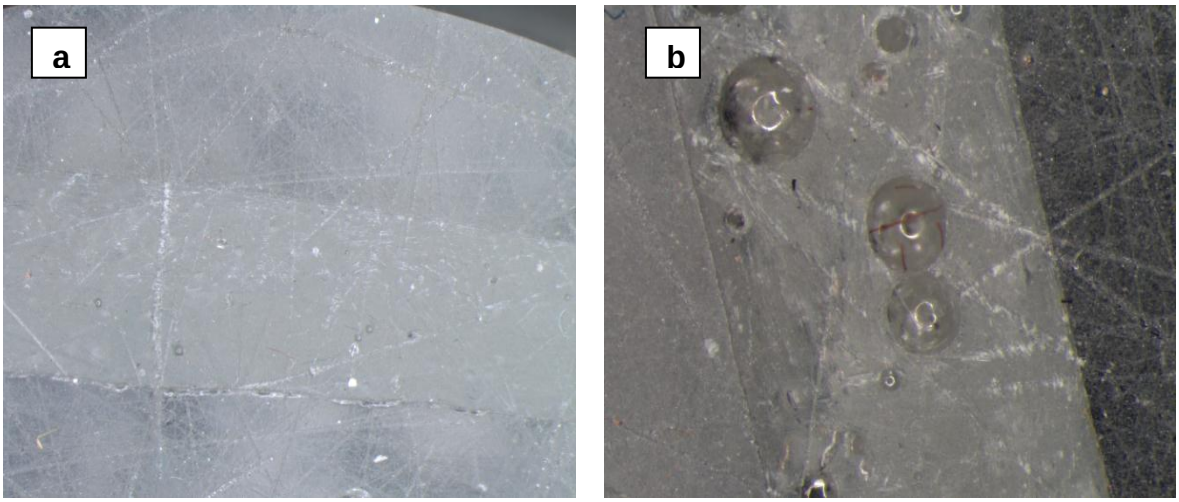

Figure 5.2 Microscopic images of a) 10 and b) 20 wt% glass flake filled doctor blade sheets (cross section)

SEM investigation of the graphene filled samples with the FEI Quanta 3D SEM revealed only the sample structure and it was difficult to determine the dispersion and orientation of the platelets in the epoxy resin (**Figure 5.3**).

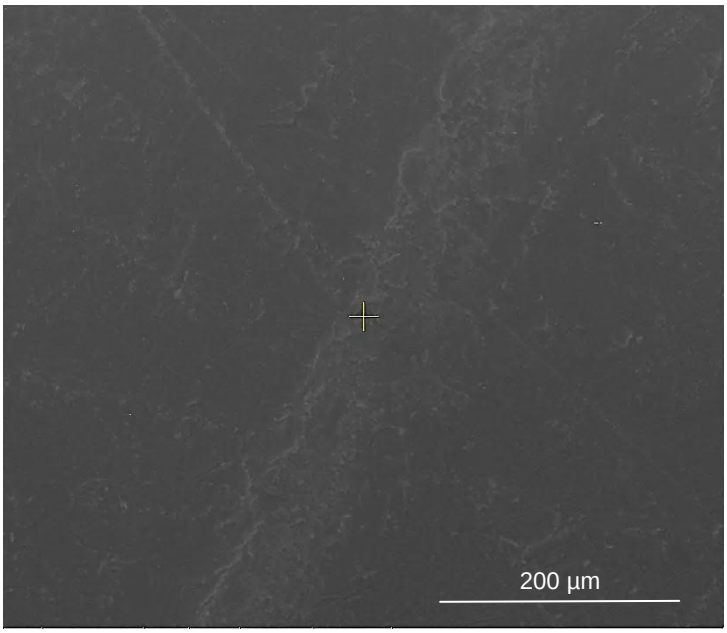

Figure 5.3 SEM micrograph of 1 wt% graphene filled doctor blade sheet prepared with blender (cross section)

The inspection of the glass flake filled samples with the FEI SEM clearly shows the degree of dispersion and high level of orientation in the resin structure. The doctor blade sheets filled with 10 (**Figure 5.4**) and 20 wt% (**Figure 5.5**) glass flakes showed that the width of the glass flakes at higher loadings tend to improve the orientation of the flakes as settling occurs in the epoxy resin due to gravity. The width of the glass flakes creates a stacking structure with other flakes in the close surrounding area in the resin as can be seen in **Figure 5.5**. The glass flakes appeared to orientate easier and disperse better than the graphene platelets with little or no agglomeration of the glass flakes.

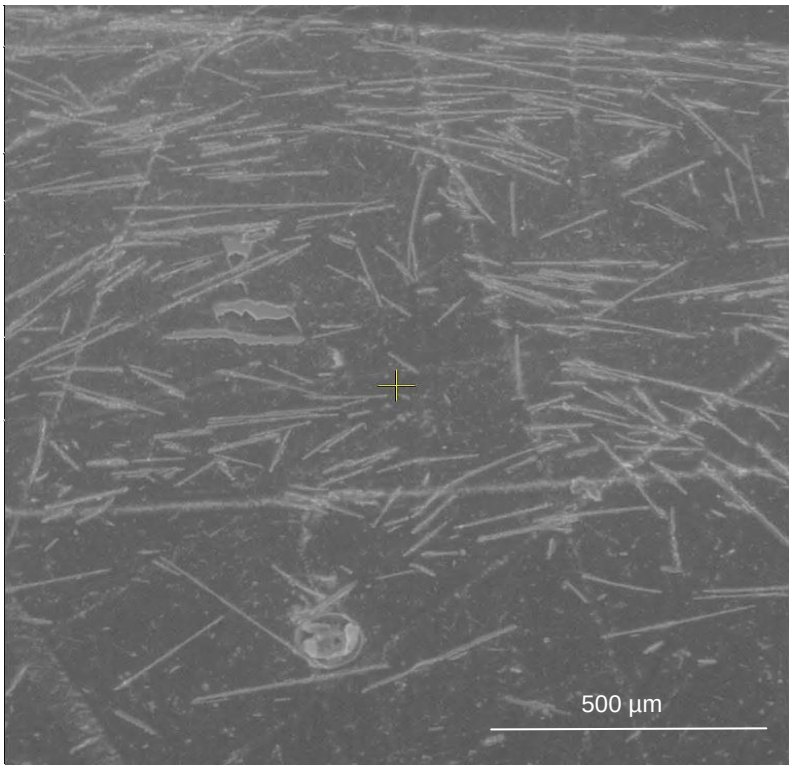

Figure 5.4 SEM image of 10 wt% glas flake filled doctor blade sheet (cross section)

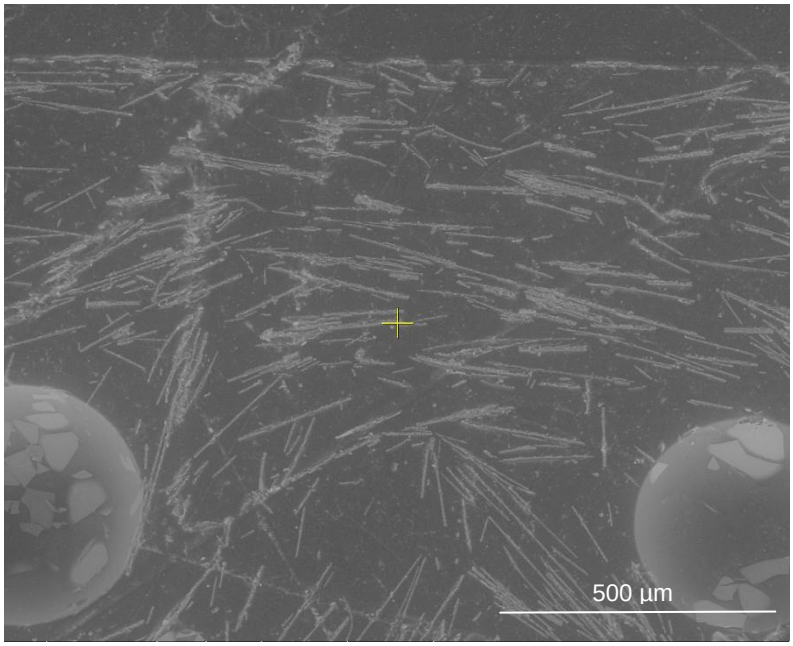

Figure 5.5 SEM image of 20 wt% glass flake filled doctor blade sheet (cross section)

5.2.2 Moulded discs

The preparation of doctor blade sheets had some limitations because of the low viscosity of the resin resulting in the settling of the fillers, long curing time of seven days, and the difficulty to control the thickness of doctor blade sheets above 3 mm. Therefore, thicker samples were moulded in plastic moulds made of polyethylene. The use of the plastic moulds made it easier to cast disc samples of a specified size and removed the need for machining. Also, higher loadings of the fillers could be moulded as in the case of the glass flakes above 20 wt%. The curing time was reduced from seven days, for the doctor blade samples, to 15 h in an oven at 50 ˚C for the moulded discs.

The difficulty of incorporating graphene loadings above 3 wt% necessitated the use of a dispersion aid like a solvent. Solvents are normally used in conjunction with solvent mixtures to lower the viscosity of epoxy resins to aid the mixing of fillers into resins (Jana & Jain, 2001) and therefore tetrahydrofuran (THF), chloroform, dichloromethane (DCM), and N,N-dimethylformamide (DMF) were used to disperse the graphene platelets at higher loadings in the epoxy resin (H. Kim et al., 2010; O'Neill et al., 2011; Park et al., 2009).

To determine which solvent disperses the graphene platelets the best in the epoxy resin, graphene moulded discs were prepared by dispersing the nanoplatelets at a loading of 4 wt% in the specified solvents in an ultrasonic bath, whereafter the solvent was removed by heating the mixture in a Buchi rotary evaporator. The graphene composite discs prepared with DMF, THF, and DCM improved the mixing and dispersion of the graphene platelets with higher loadings. However, the graphene samples prepared with chloroform (2, 4, and 6 wt%) remained tacky and were omitted for permeability analysis. The graphene moulded discs showed proper mixing with the use of solvents (**Figure 5.6**)

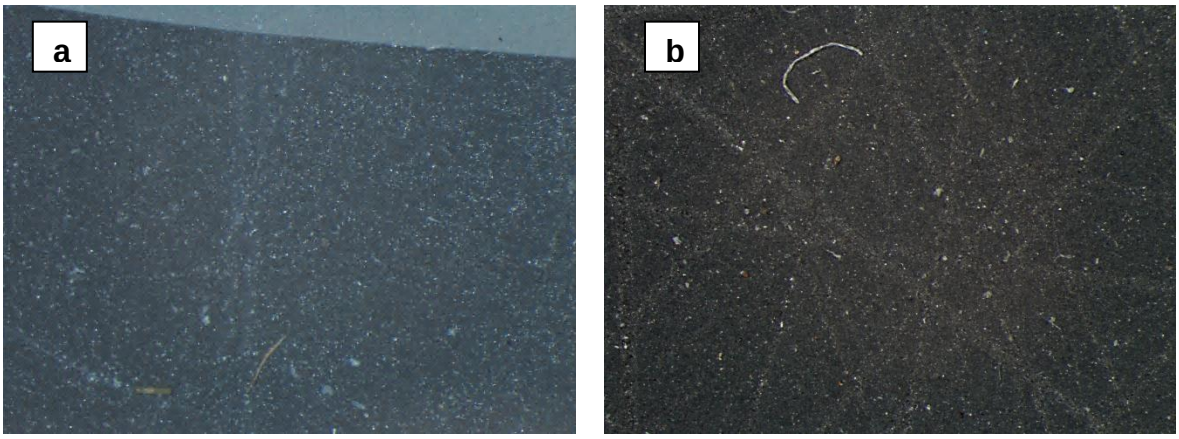

Figure 5.6 Microscopic images of the a) 4 and b) 6 wt% graphene filled samples prepared with DMF

With the higher loadings of graphene it was observed that the solvents had an adverse effect on the curing reaction of the graphene epoxy samples (Kotsilkova & Pissis, 2007, p.102; Petrie, 2006, p.117). This was clearly observed with graphene samples prepared at 6 and 10 wt% loadings with DCM as solvent (**Figure 5.7**). Voids were created from entrapped solvent trying to escape whilst curing in the oven. Some solvent must have become entrapped in the structure due to the platelets preventing the removal of all of the solvent. The DMF samples prepared at 6 and 10 wt% became flexible like an elastomer and porous. It has been observed by other researchers that the higher loadings of carbon nanotubes can affect the curing of epoxy resins (J. K. Kim & Ma, 2011, p.118).

Figure 5.7 Void formation from entrapped solvent (DCM) in 6 wt% graphene moulded disc

The 10 wt% graphene (**Figure 5.8**) moulded disc prepared with DMF exhibited highly agglomerated regions which created cracks in the structure of the resin by preventing further reaction with other epoxide groups. This confirms that higher loadings of graphene affected the curing of the epoxy resins and explains why the disc samples at higher loadings became more flexible and porous.

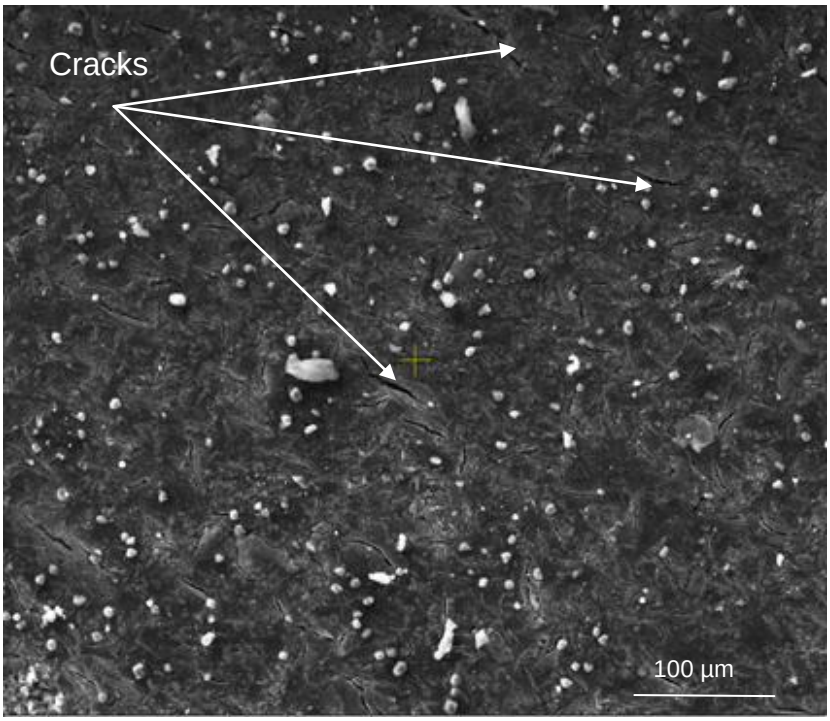

Figure 5.8 SEM image of the 10 wt% graphene filled disc prepared with DMF

From the SEM images (taken with the high resolution SEM) of the 4 wt% graphene moulded disc prepared with DMF (**Figures 5.9 – 5.11**), it could be seen that the composite structure contains areas where the graphene platelets were poorly dispersed. (**Figure 5.9**) shows large voids which were most likely produced by entrapped solvent. With closer investigation it could be observed that the graphene platelets were still highly agglomerated and this clumping produced poor alignment of the platelets in the resin structure which inhibits the formation of a tortuous path (**Figure 5.10**).

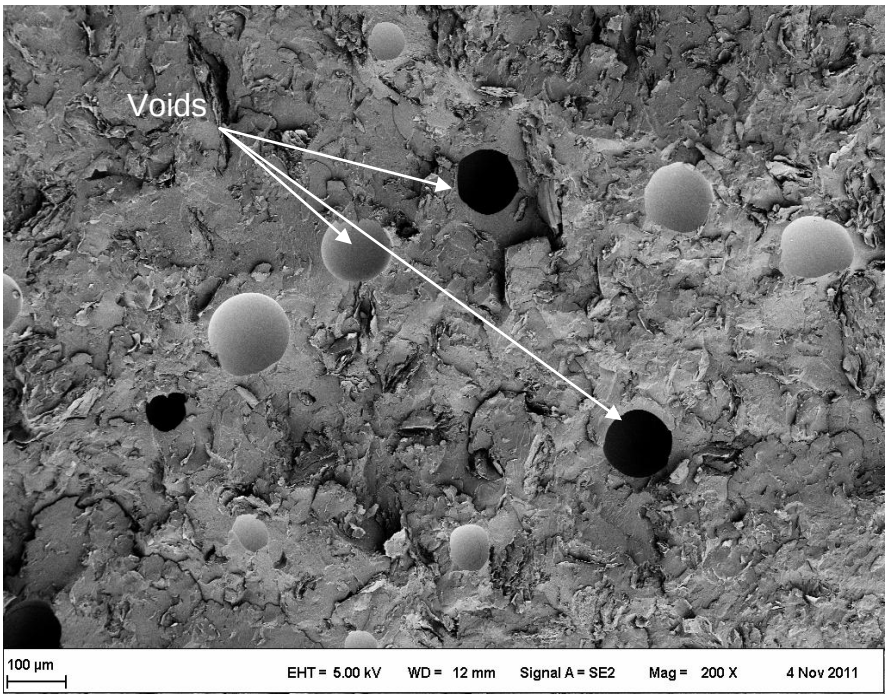

Figure 5.9 SEM image of 4 wt% graphene sample showing the formation of voids from entrapped solvent

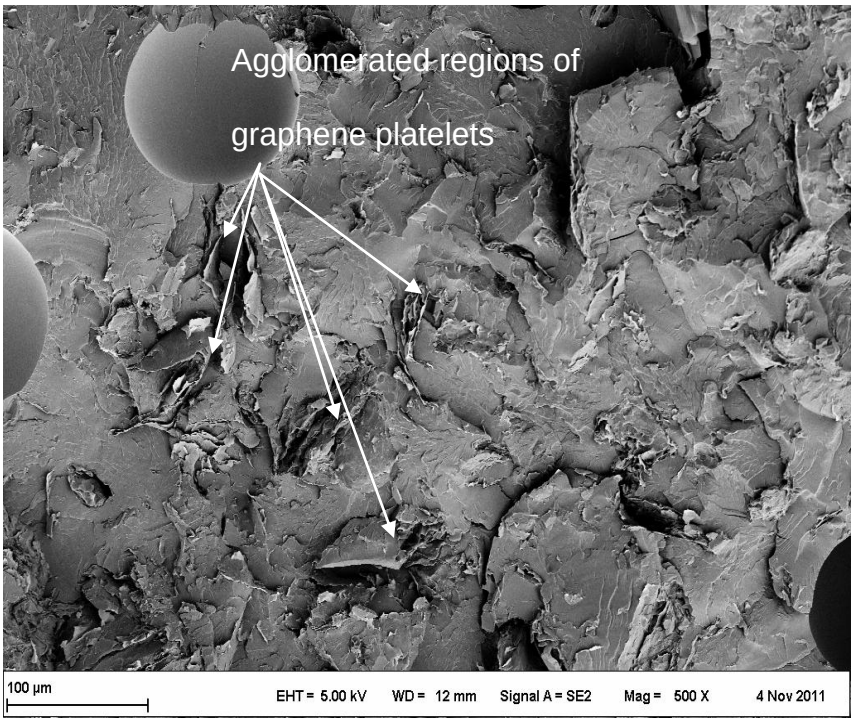

Figure 5.10 SEM image of disc sample displaying agglomerated regions of graphene platelets

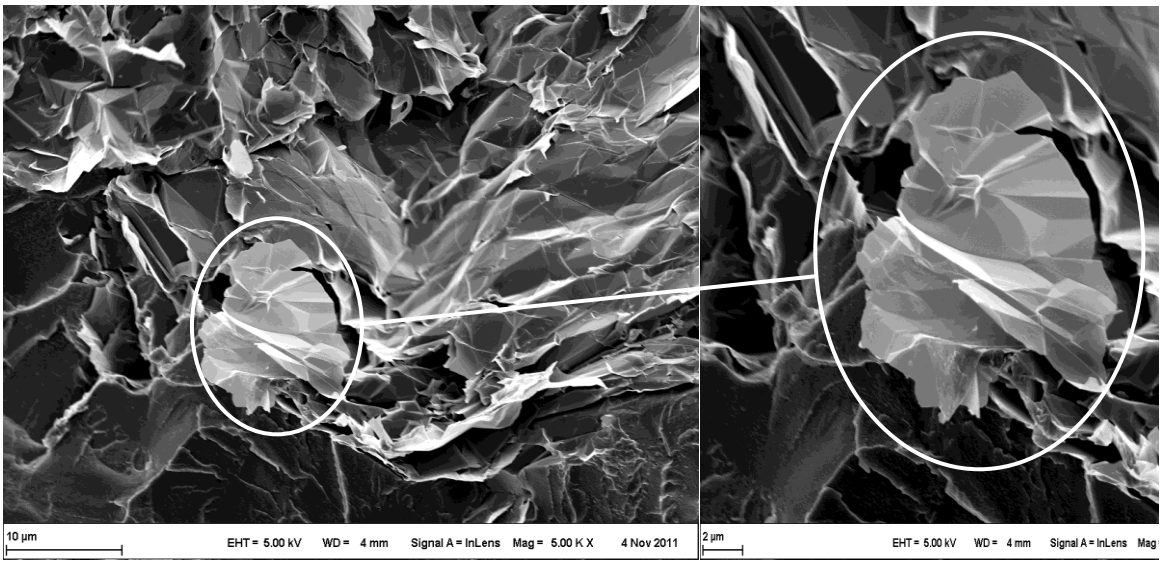

Figure 5.11 SEM image of creased graphene platelet. The platelet is also semi-transparent

Furthermore, the small size of the nanoplatelets made it difficult to orientate the platelets properly and it could be seen that the graphene platelets were very creased and semi-

transparent (**Figure 5.11)**. From the TEM images (**Figure 5.12** and **Figure 5.13**) of the graphene platelets it could be seen that the platelets tend to crease and agglomerate which indicates the difficulty to separate the platelets which was observed in **Figure 5.10**.

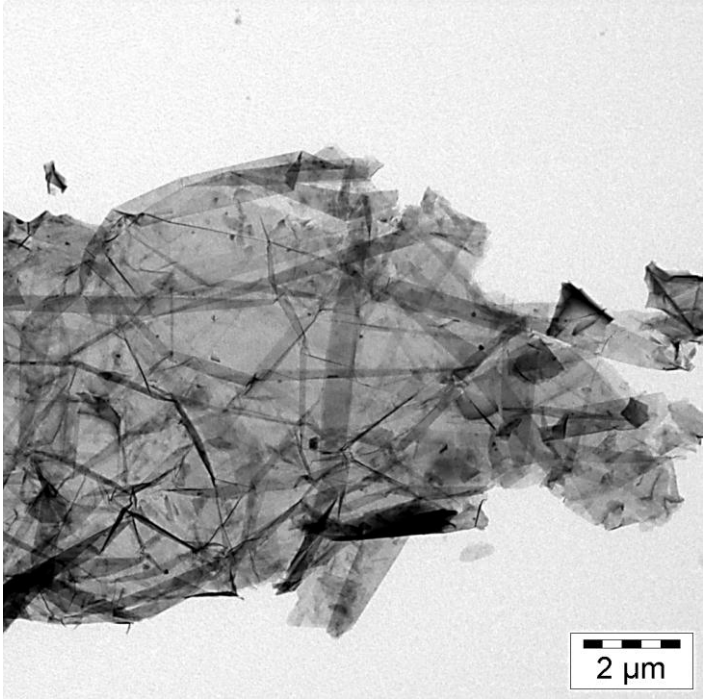

Figure 5.12 TEM image of creased graphene platelet

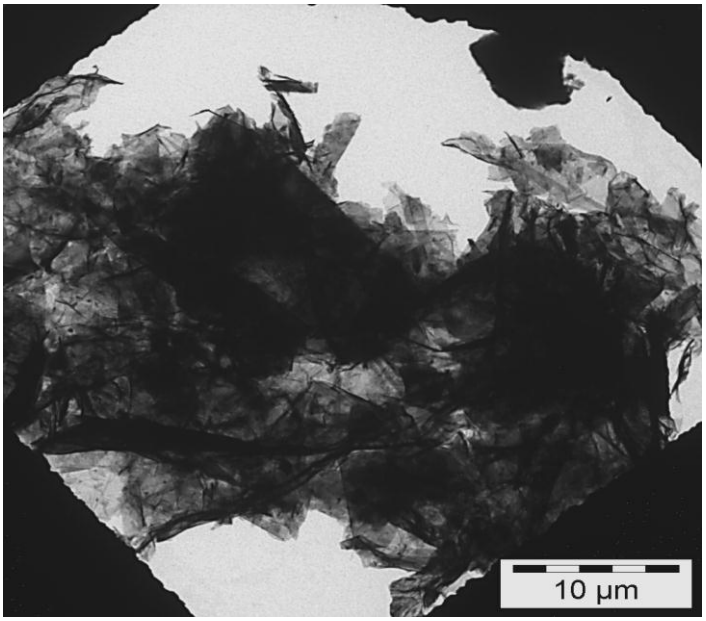

Figure 5.13 TEM image of agglomerated graphene platelets

The glass flake moulded samples mixed easily up to 35 wt% in the ultrasonic bath without solvent and were easier to prepare with the larger loadings of glass flakes than the doctor blade technique. DCM was only used to prepare samples with larger loadings of glass flakes (>35 wt%). The use of a solvent improved the capability to incorporate larger weight fractions, but the high glass content produced large voids and regions which contained clusters of glass flakes where the epoxy resin did not wet the flakes properly (**Figure 5.14**).

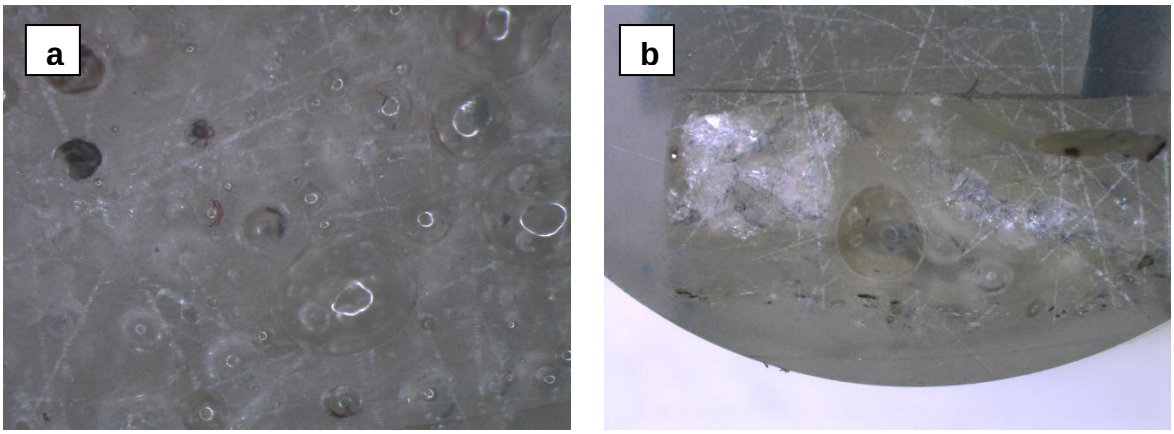

Figure 5.14 Microscopic images of a) 40 and b) 50 wt% glass flake filled moulded discs prepared with DCM (cross section)

The faster curing time limited the settling of the glass flakes in the epoxy resin matrix (**Figure 5.15**) which was a major improvement from the settling of the flakes which was observed with the doctor blade samples. The incorporation of larger loadings improved the orientation and dispersion of the glass flakes in the resin which also improved the tortuosity factor of the moulded discs. The use of DCM did improve the ability to incorporate glass flake loadings above 35 wt% which still maintained the good orientation and tighter packing of the glass flakes at 40 (**Figure 5.16**) and 50 wt% (**Figure 5.17**).

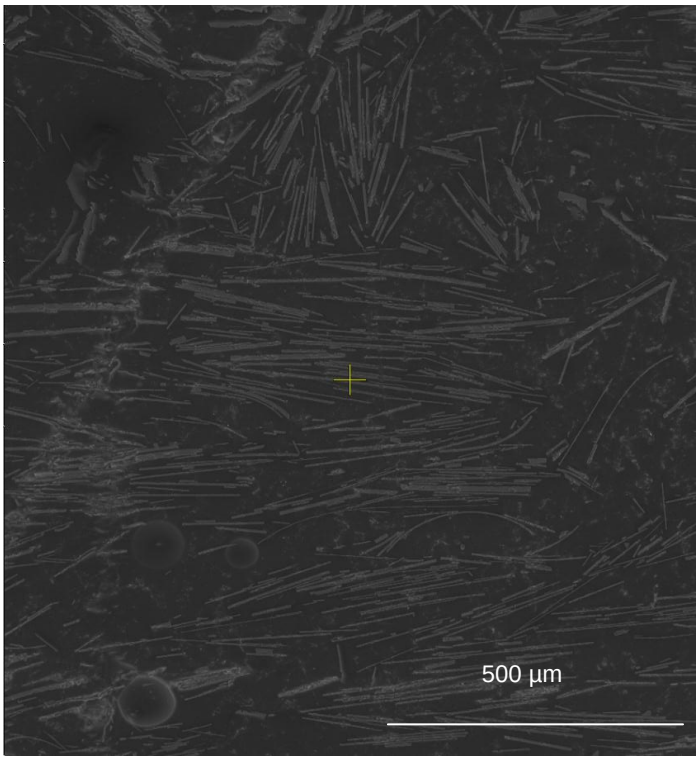

Figure 5.15 SEM image of 30 wt% glass flake filled moulded disc (cross section)

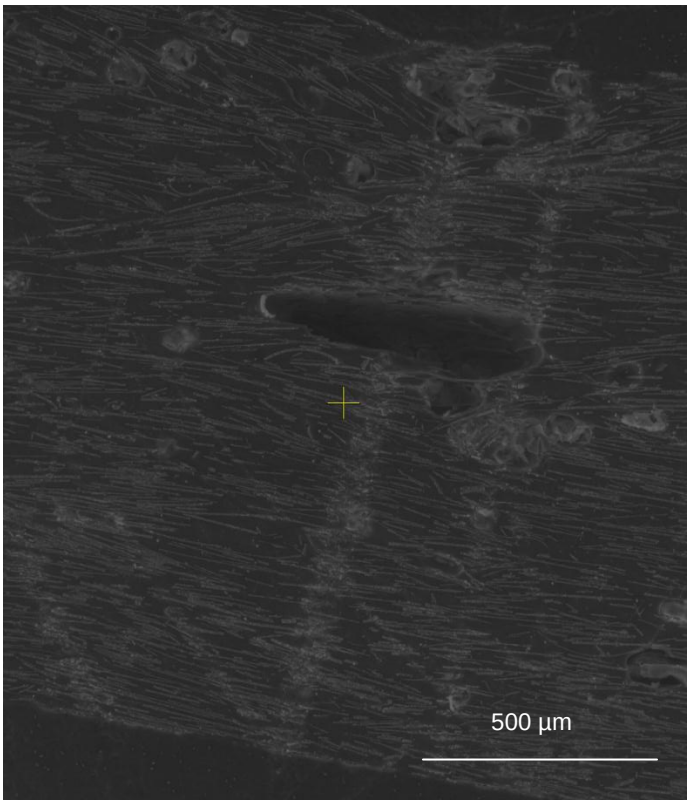

Figure 5.16 SEM image of 40 wt% glass flake filled sample (cross section)

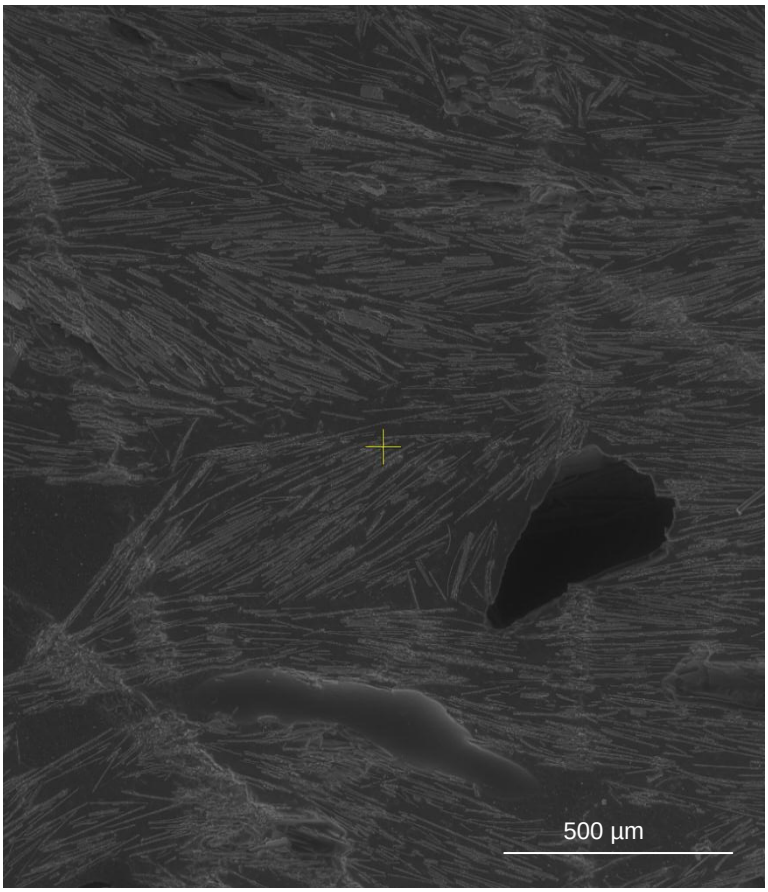

Figure 5.17 SEM image of 50 wt% glass flake filled disc (cross section)

However, the samples prepared with DCM produced large voids and the clustering of glass flakes in regions which failed to blend properly with the resin. Therefore, the samples prepared with DCM were omitted for helium permeation analysis.

5.2.3 Multilayer sheets

To limit and improve the settling of the fillers that was observed with the doctor blade samples, it was decided produce sheets, 3 to 4 mm thick, with thin multiple layers painted on top of one another with a paint brush until the required thickness was reached. The graphene or glass flake resin was firstly dispersed in epoxy resin and then applied with a brush to spread the composite resin as thin as possible, thereby dispersing the fillers and

orientating it parallel with the substrate surface. The coated layer was left to dry overnight, before the next layer was applied. The graphene platelets and glass flakes dispersed better with the smaller quantities of epoxy resin in the ultrasonic bath. Although smaller quantities of the epoxy resin were used, the filler content was still determined as part of the total resin system. The graphene filled resin was easily coated on the previously applied layer with good adhesion to the layer below. The samples showed no delamination when the disc permeation samples were machined from the composite epoxy sheets.

The multilayered samples looked similar to the moulded discs in appearance with very little voids. The SEM image (**Figure 5.18**) taken with the FEI Quanta 3D SEM could not indicate if the orientation of the graphene platelets was improved, but it was assumed that some agglomeration of the platelets would occur like with the 4 wt% DMF prepared disc sample.

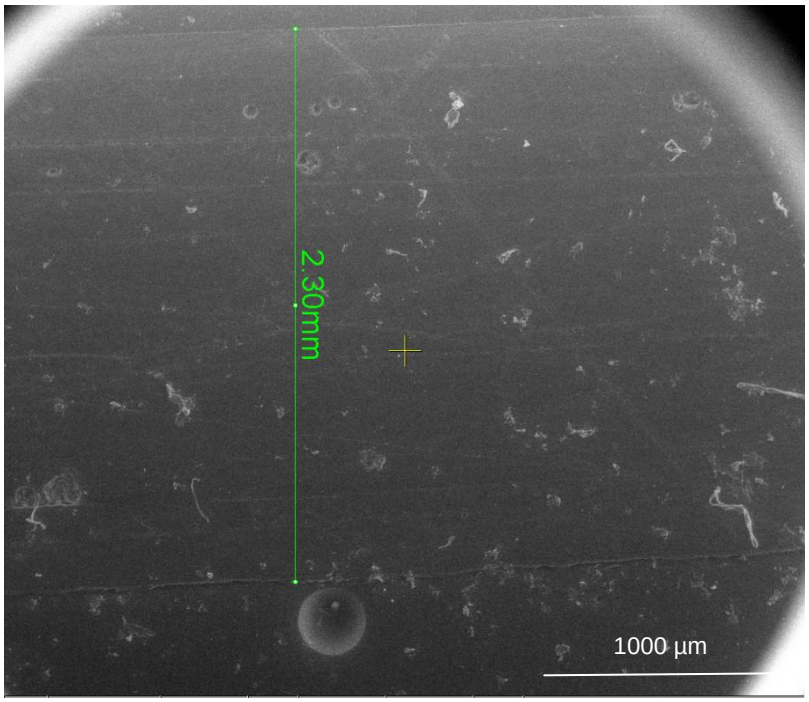

Figure 5.18 SEM image of 2 wt% graphene multilayer sheet with a thickness of 2 mm (cross section)

The inspection of the multilayered sample (3 mm thickness) structure filled with 30 wt% glass flake showed that the glass flakes were orientated parallel with the substrate surface and uniformly dispersed in the epoxy resin (**Figure 5.19** and **Figure 5.20**). The brushing of thinner layers improved the orientation and dispersion of the glass flakes in the epoxy resin to create a tortuous structure with the glass flakes (**Figure 5.21**). The thinner layers also limited the amount of settling of the flakes due to gravity.

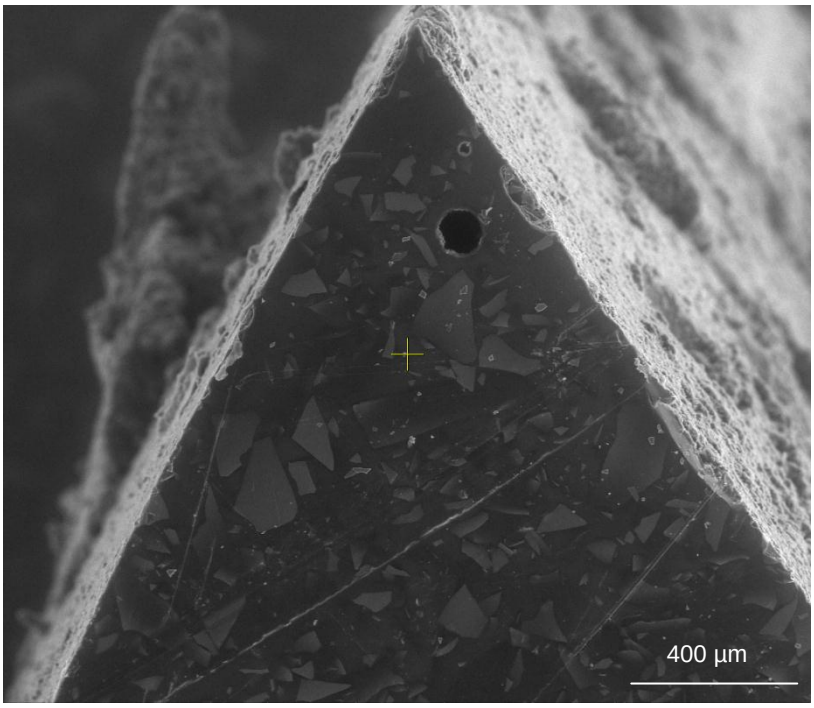

Figure 5.19 SEM image of the glass flake 30 wt% multilayered sheet showing the dispersion of the flakes (surface)

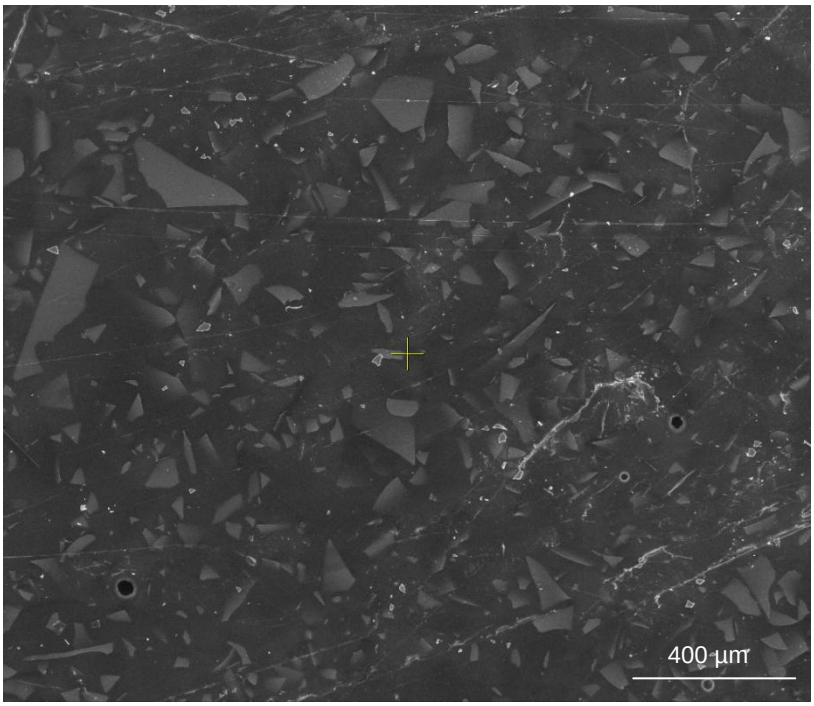

Figure 5.20 SEM image of the top layer of the glass flake 30 wt% multilayer sheet (surface)

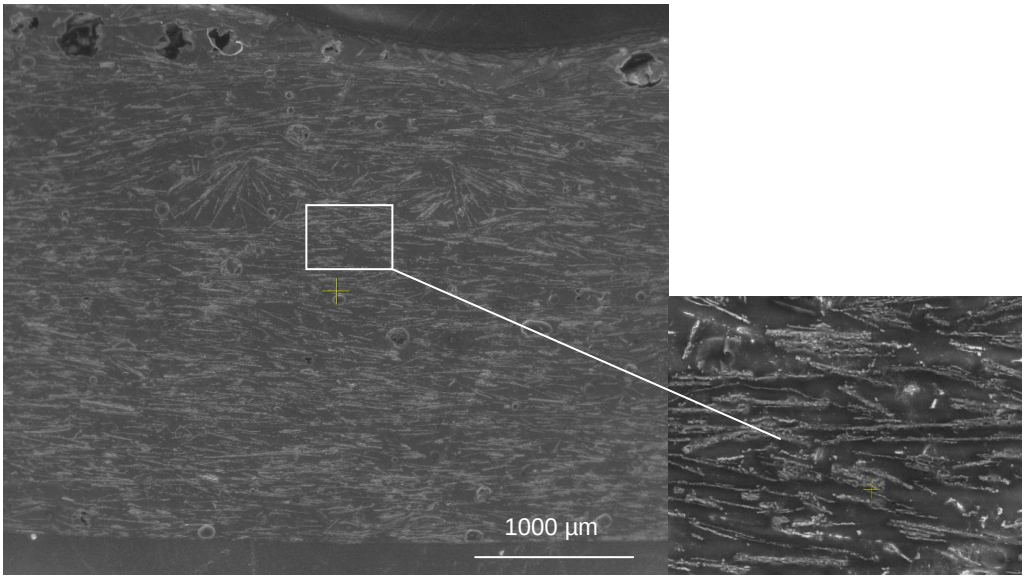

Figure 5.21 SEM image of the cross-sectional area of the 30 wt% glass flake multilayer sheet showing the orientation and dispersion of the glass flakes in various layers (cross section)

5.3 HELIUM LEAK RATE MEASUREMENTS

5.3.1 Doctor blade sheets

The incorporation of graphene platelets into the epoxy resin produced only a minor reduction in the helium leak rate (**Table 5.1** and **Figure 5.22**). The mixing methods used to disperse the graphene in the epoxy resin were unable to separate the platelets properly. As was observed with the SEM analysis, the graphene platelets tend to agglomerate in regions with poor orientation of the platelets. Therefore, no significant reduction of the helium leak rate was observed.

Table 5.1 Permeation results of doctor blade sheets filled with graphene

Loading (wt %)	**Mixing method**	**Steady state flux ($mol.m^{-2}.s^{-1}$)**	**Diffusion co-efficient ($m^2.s^{-1}$)**	**Permeability co-efficient ($mol.m^{-1}.s^{-1}.Pa^{-1}$)**
0	None	7.95×10^{-08}	1.36×10^{-10}	2.02×10^{-15}
1	Ultrasonic	7.25×10^{-08}	1.35×10^{-10}	1.77×10^{-15}
1	Hand	4.97×10^{-08}	0.95×10^{-10}	1.24×10^{-15}
1	Blender	4.96×10^{-08}	1.14×10^{-10}	1.33×10^{-15}
2	Blender	3.73×10^{-08}	0.78×10^{-10}	1.08×10^{-15}
3	Blender	4.89×10^{-08}	0.72×10^{-10}	1.23×10^{-15}

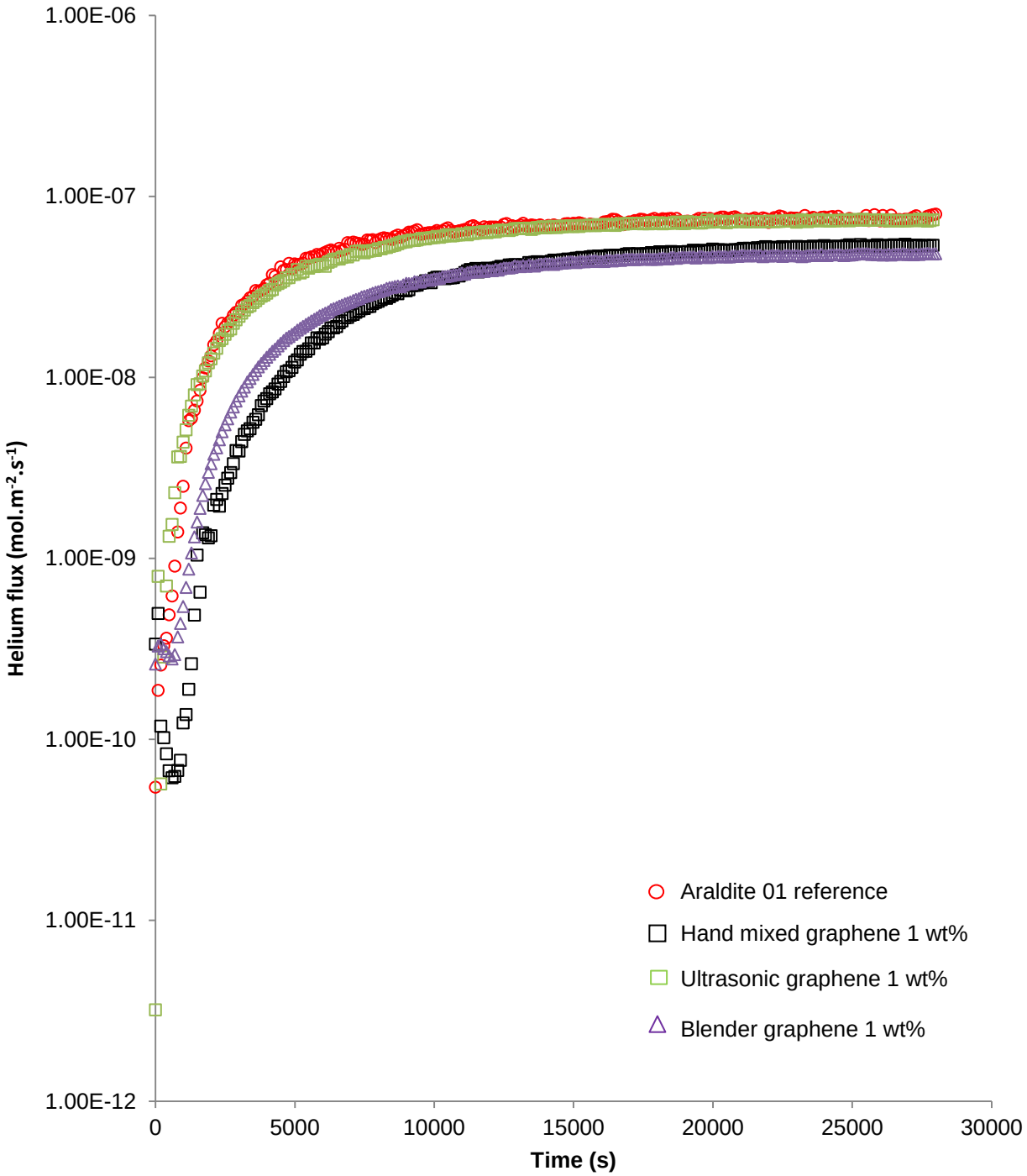

Figure 5.22 Helium flux measurements of graphene samples prepared with different techniques

The best result for the graphene/epoxy composite doctor blade sheets were obtained with the samples prepared with the kitchen blender at a loading of 2 wt% (**Figure 5.23**). This appeared to indicate that at about 2 wt% loading the resin/graphene mixture had reached the weight fraction threshold of the epoxy resin. When the weight fraction threshold is reached, the graphene platelets will tend to agglomerate because of van der Waals forces (Singh et al., 2011). This will cause the platelets to create regions in the composite matrix where the gas molecules can migrate with a lot more freedom through the graphene composite structure. It should be noted that with increasing weight fractions (H. Kim & Macosko, 2009) it becomes difficult to mix graphene into the resin because the viscosity increases dramatically.

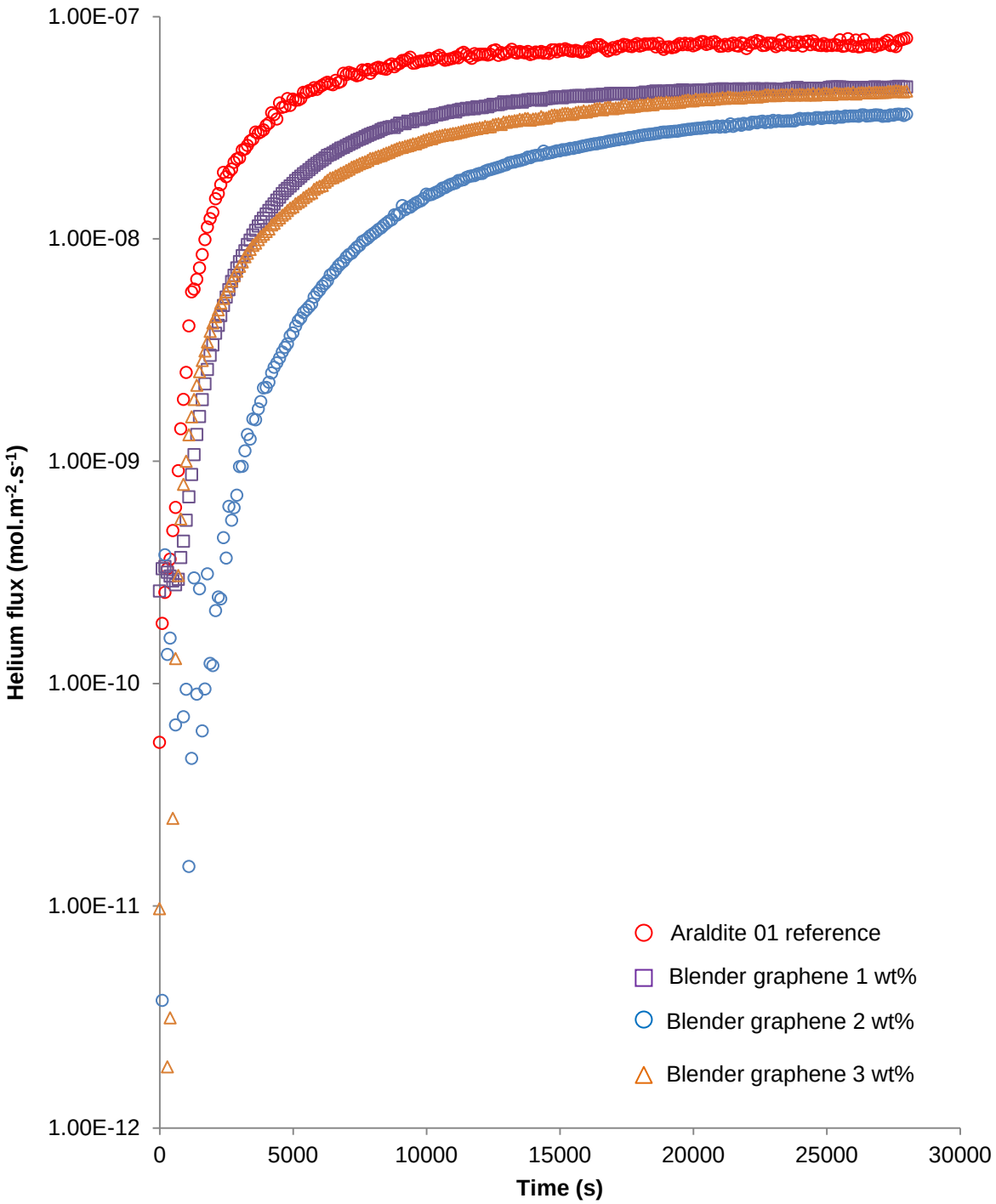

Figure 5.23 Helium flux measurements of graphene filled doctor blade sheets prepared with the blender

The helium leak rate results of the glass flake filled doctor blade sheets are shown in **Table 5.2**. It was found that the increase in loading of the glass flakes reduced the leak rate of the helium significantly up to 20 wt% (**Table 5.2**). **Figure 5.24** displays the helium flux results for the epoxy samples filled with 1, 3, and 6 wt% glass flake content, and **Figure 5.25** displays the results for the epoxy samples with content of 10, 15, and 20 wt% glass flake loadings. This reduction in helium leak rate therefore can be attributed to the larger size of the glass flakes and the better orientation and dispersion of the glass flakes improving the tortuosity factor.

Table 5.2 Permeation results of doctor blade sheets filled with glass flakes

Loading (wt %)	**Mixing technique**	**Steady state flux ($mol.m^{-2}.s^{-1}$)**	**Diffusion coefficient (m^2.s-1)**	**Permeability co-efficient ($mol.m^{-1}.s^{-1}.Pa^{-1}$)**
0	None	7.95×10^{-8}	1.36×10^{-10}	2.02×10^{-15}
1	Ultrasonic bath	5.17×10^{-8}	1.65×10^{-10}	1.61×10^{-15}
3	Ultrasonic bath	4.32×10^{-8}	1.20×10^{-10}	1.10×10^{-15}
6	Ultrasonic bath	2.97×10^{-8}	0.91×10^{-10}	0.75×10^{-15}
10	Ultrasonic bath	2.98×10^{-8}	0.68×10^{-10}	0.86×10^{-15}
15	Ultrasonic bath	2.90×10^{-8}	0.27×10^{-10}	0.58×10^{-15}
20	Ultrasonic bath	0.83×10^{-8}	0.31×10^{-10}	0.19×10^{-15}

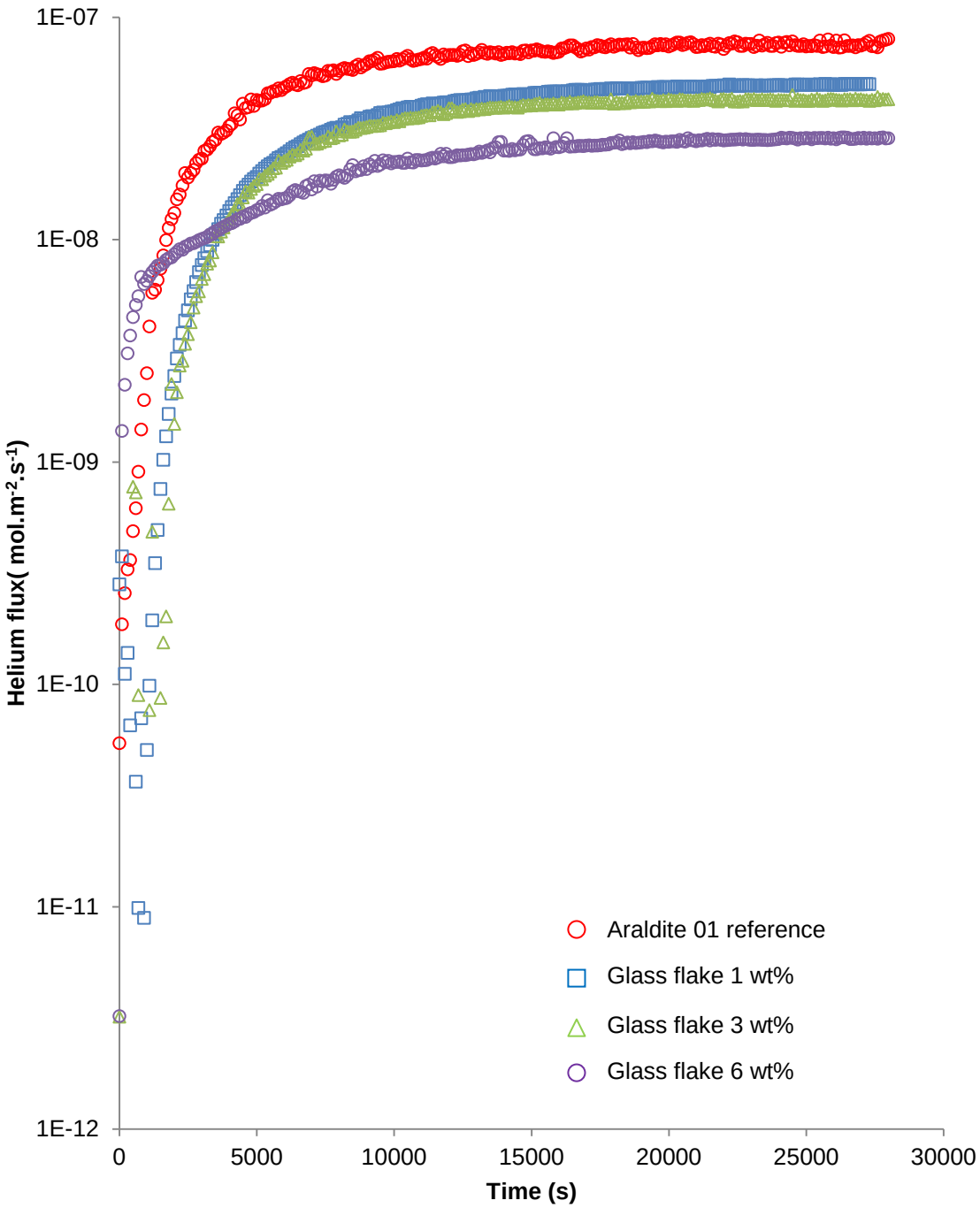

Figure 5.24 Helium flux measurements of glass flake filled doctor blade sheets up to 6 wt%

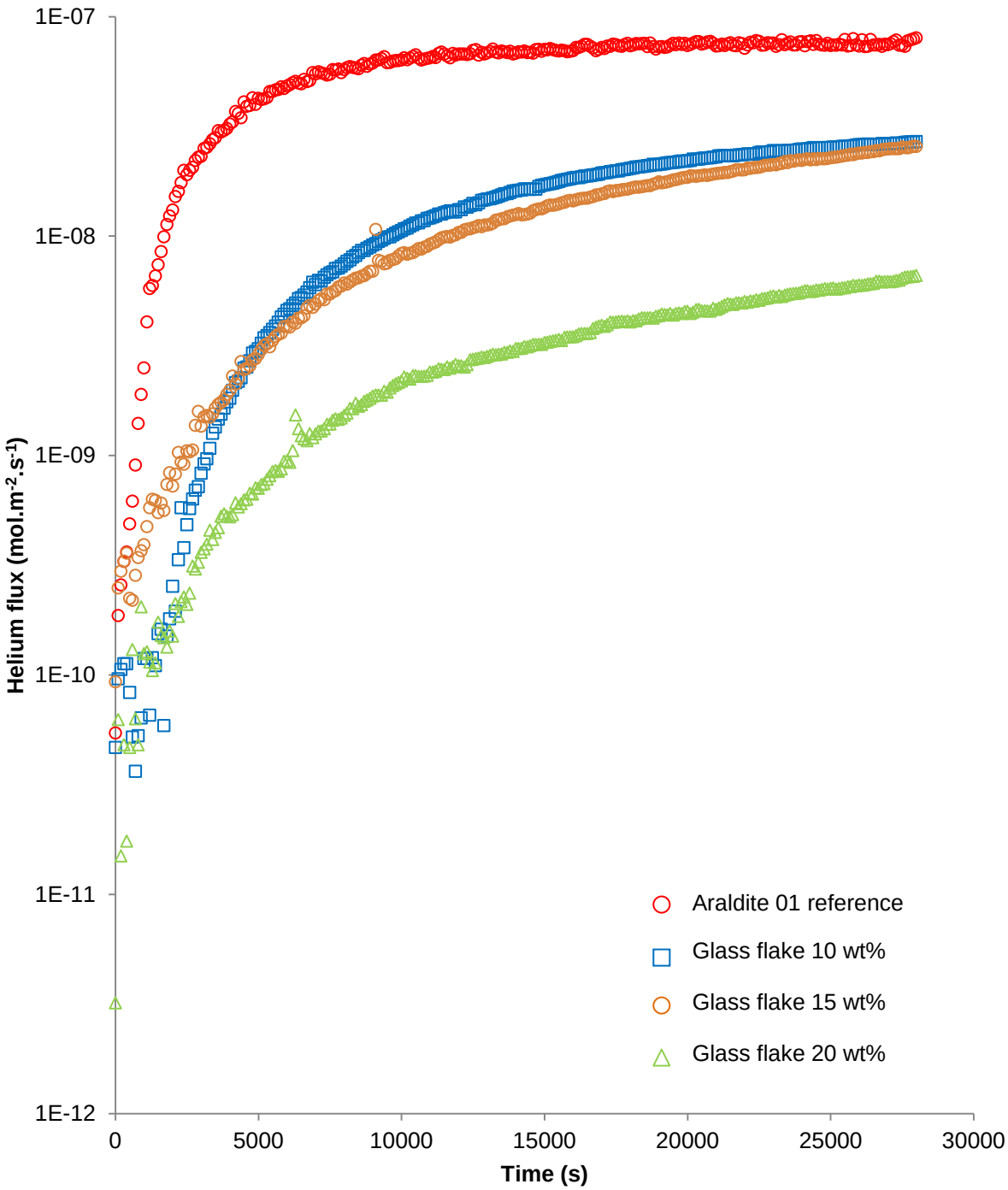

Figure 5.25 Helium flux measurements of glass flake filled doctor blade sheets up to 20 wt%

5.3.2 Moulded discs

The graphene composite samples prepared with the solvents (results in **Table 5.3**) improved the mixing and dispersion of the graphene platelets with higher loadings. However, all the samples displayed an increase, instead of a decrease in the helium leak rate (**Figure 5.26**). The entrapped solvents in the composite resin caused the samples to leak more than the reference epoxy resin.

The samples that used chloroform as dispersant could not be analysed due to the samples remaining tacky after seven days. The samples prepared with loadings at 6 and 10 wt% graphene were omitted from helium permeability analysis due to the high porosity of these samples.

Table 5.3 Permeation results for graphene filled moulded discs

Loading (wt %)	**Solvent used**	**Steady state flux ($mol.m^{-2}.s^{-1}$)**	**Diffusion co-efficient ($m^2.s^{-1}$)**	**Permeability co-efficient ($mol.m^{-1}.s^{-1}.Pa^{-1}$)**
0	None	1.76×10^{-08}	2.49×10^{-10}	0.70×10^{-15}
2	DCM	6.89×10^{-08}	3.61×10^{-10}	3.20×10^{-15}
4	DCM	5.20×10^{-08}	2.89×10^{-10}	2.32×10^{-15}
4	DMF	2.44×10^{-08}	2.22×10^{-10}	1.29×10^{-15}
4	THF	7.98×10^{-08}	4.79×10^{-10}	4.12×10^{-15}

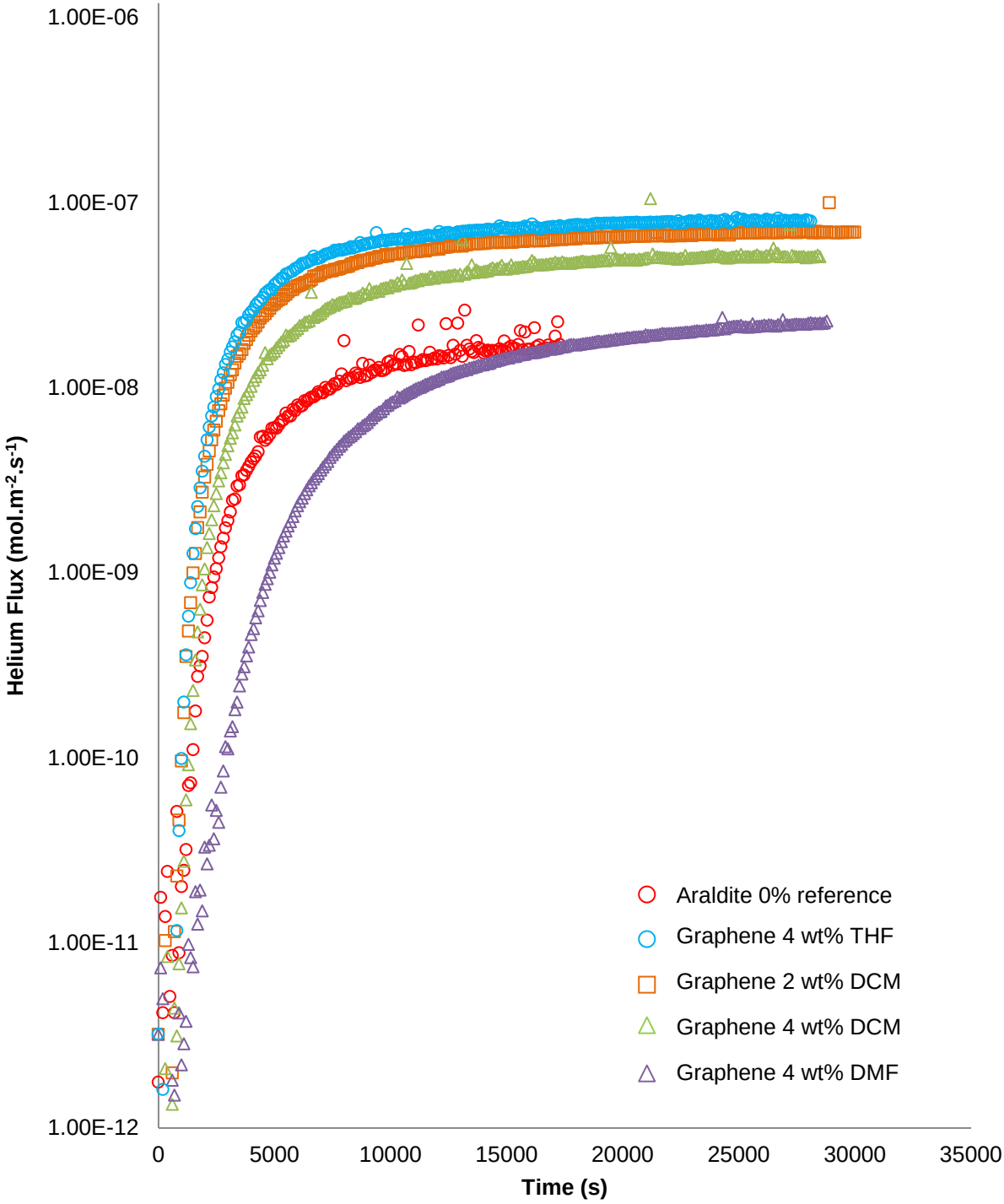

Figure 5.26 Helium flux measurements for graphene filled moulded discs

The helium leak rates of the glass flake samples mixed at 25 and 30 wt% (**Table 5.4** and **Figure 5.27**) improved significantly with the 30 wt% loading reducing the leak rate about three orders of magnitude. This was due to the tortuous path that was created from the glass flakes. It also appeared that 30 wt% was the weight fraction threshold of the glass flakes in the resin matrix, since the samples prepared at 35 wt% (**Figure 5.27**) leaked more than the reference sample. This was most likely due to the high glass flake content restricting the glass flake and epoxy resin to mix properly. This poor dispersion of the glass flakes and epoxy resin produced intercalated regions of glass flakes which increased the helium leak rate as was witnessed with the microscopic inspection of the sample.

Table 5.4 Permeation results for glass flake filled moulded discs

Loading (wt %)	**Solvent used**	**Steady state flux ($mol.m^{-2}.s^{-1}$)**	**Diffusion co-efficient ($m^2.s^{-1}$)**	**Permeability co-efficient ($mol.m^{-1}.s^{-1}.Pa^{-1}$)**
0	None	1.76×10^{-08}	2.49×10^{-10}	6.96×10^{-16}
25	None	4.61×10^{-09}	1.80×10^{-10}	2.14×10^{-16}
30	None	4.88×10^{-11}	9.09×10^{-10}	4.07×10^{-18}
35	None	2.11×10^{-07}	1.90×10^{-10}	1.49×10^{-14}

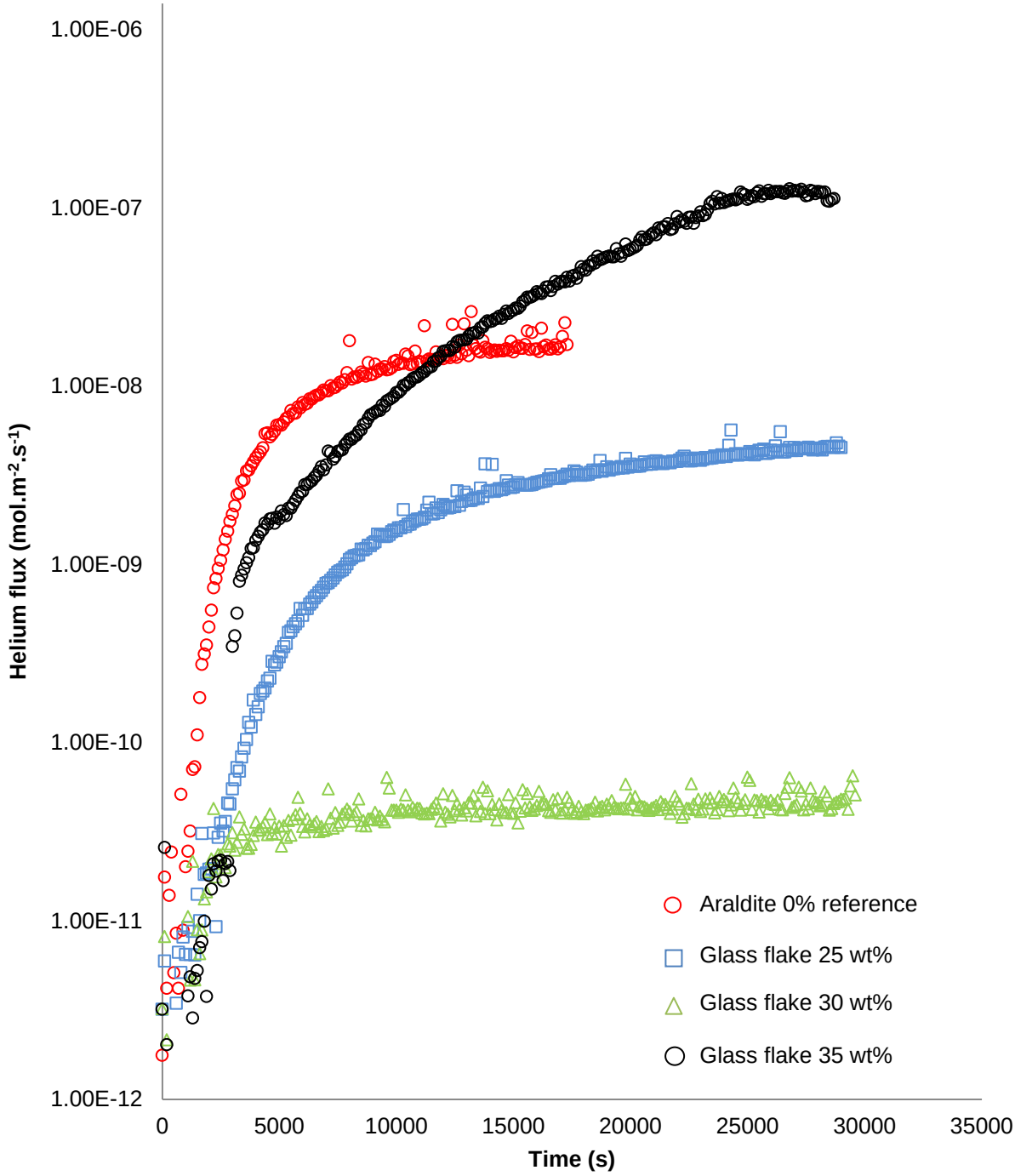

Figure 5.27 Helium flux measurements for glass flake filled moulded discs

5.3.3 Multilayer samples

From the results (**Table 5.5** and **Figure 5.28**) it can be seen that the improvement of the orientation and dispersion of the fillers in the composite structure by applying multiple layers reduced the helium leak rate significantly. The 4 mm graphene sample produced the best result for the graphene multilayered samples by reducing the leak rate by almost one order of magnitude when compared to the base reference epoxy resin. The 4 mm graphene sample displayed peculiar behaviour since it was the only sample which released the helium gas in two stages. The release in two stages indicate that the brushing helped disperse the graphene platelets better in the resin matrix and limited the agglomeration which was observed with the SEM analysis of the 4 wt% graphene moulded disc sample.

Table 5.5 Permeation results of multilayer sheets

Loading (wt %)	**Sample**	**Steady state flux ($mol.m^{-2}.s^{-1}$)**	**Diffusion co-efficient ($m^2.s^{-1}$)**	**Permeability co-efficient ($mol.m^{-1}.s^{-1}.Pa^{-1}$)**
0	Reference	1.76×10^{-08}	2.49×10^{-10}	6.96×10^{-16}
2	Graphene 3 mm	1.75×10^{-08}	1.30×10^{-10}	7.33×10^{-16}
2	Graphene 4 mm	3.91×10^{-09}	0.47×10^{-10}	1.88×10^{-16}
30	Glass flake 3 mm	3.38×10^{-11}	2.02×10^{-10}	1.52×10^{-18}
30	Glass flake 4 mm	2.50×10^{-11}	5.17×10^{-10}	1.41×10^{-18}

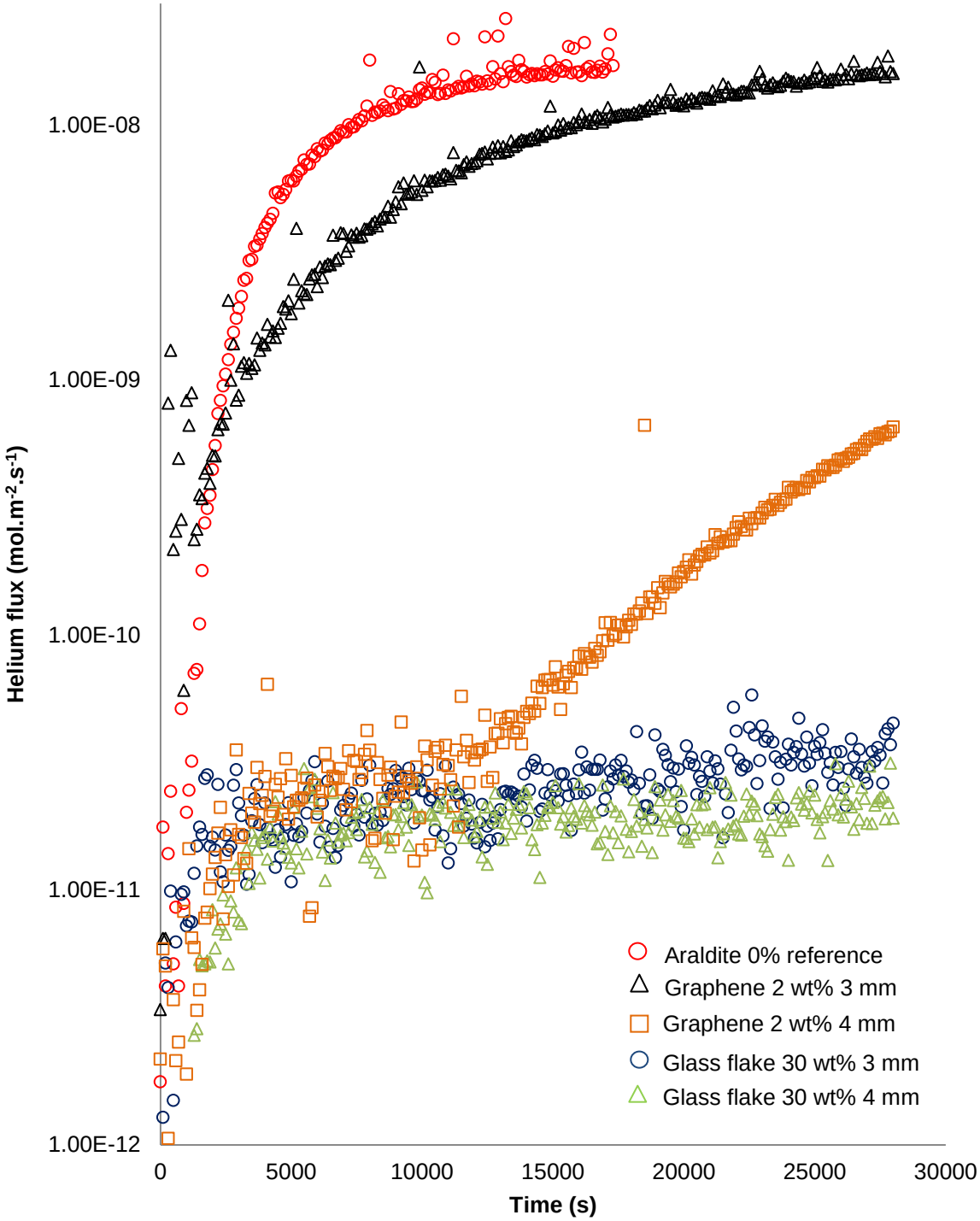

Figure 5.28 Helium flux measurements of multilayer sheets

The glass flake multilayer samples at both 3 mm and 4 mm thickness produced a significant improvement in reducing the helium leak rate almost three orders of magnitude (**Figure 5.28**). Gupta et al. (2010) also observed this improvement in oxygen gas barrier properties with glass sphere multi-layered samples of glass poly(propylene-graft-maleic anhydride)/phosphate glass composites. Both of these samples confirm the ideal loading of 30 wt% to improve the helium leak rate effectively, which was also observed with the helium permeation results of the 30 wt% glass flake moulded disc sample.

The excellent dispersion and orientation of the glass flakes in the thinner layers improved the tortuous path of the glass flake filled samples, which in turn improved the helium gas barrier properties of the composite resin.

5.3.4 Fit according to Fick's law

To determine the permeability- and diffusion co-efficients of the composite samples, the method described by Yokozeki et al. (2004) was used (this method has been discussed in detail in Chapter 4, Section 4.3). The values of the diffusion co-efficient and steady state flux (J_0) were calculated from the linear plot of $ln(J\sqrt{t})$ and the values substituted into the equation which governs Fick's law of diffusion. The epoxy reference samples prepared at 2 and 4 mm thickness which contained no fillers produced linear plots which showed little statistical deviation from the linear fit (**Figure 5.29** and **Figure 5.30**). The measured helium flux was then plotted along with the theoretical model data to match the measured results to the theoretical model. From **Figure 5.31**, it can be noticed that the theoretical model flux fitted the measured flux data and behaves in a Fickian manner for both the reference epoxy samples.

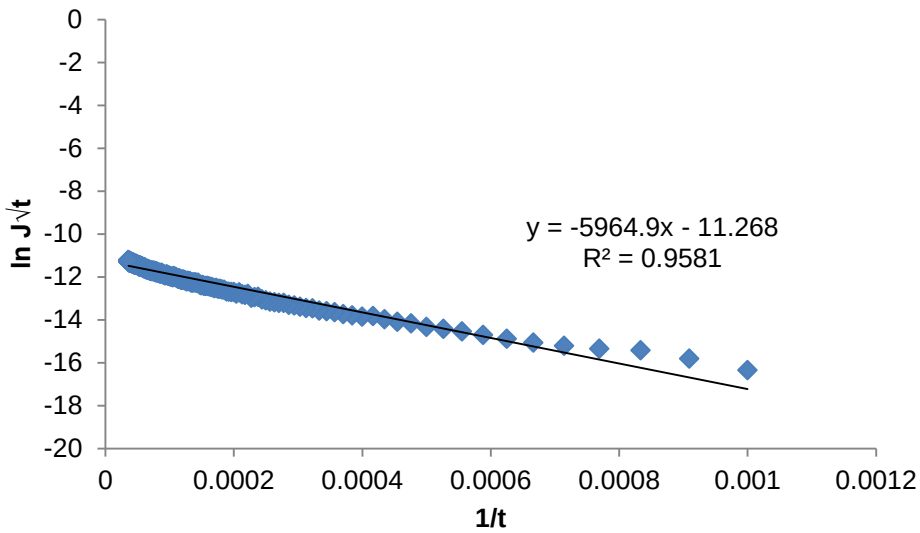

Figure 5.29 Linear fit of reference Araldite doctor blade sheet permeation data

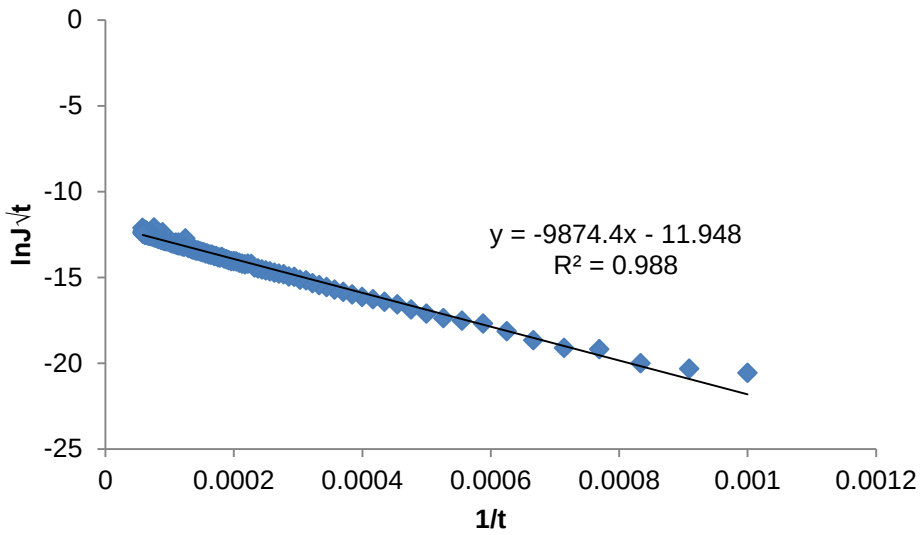

Figure 5.30 Linear fit of reference Araldite moulded disc permeation data

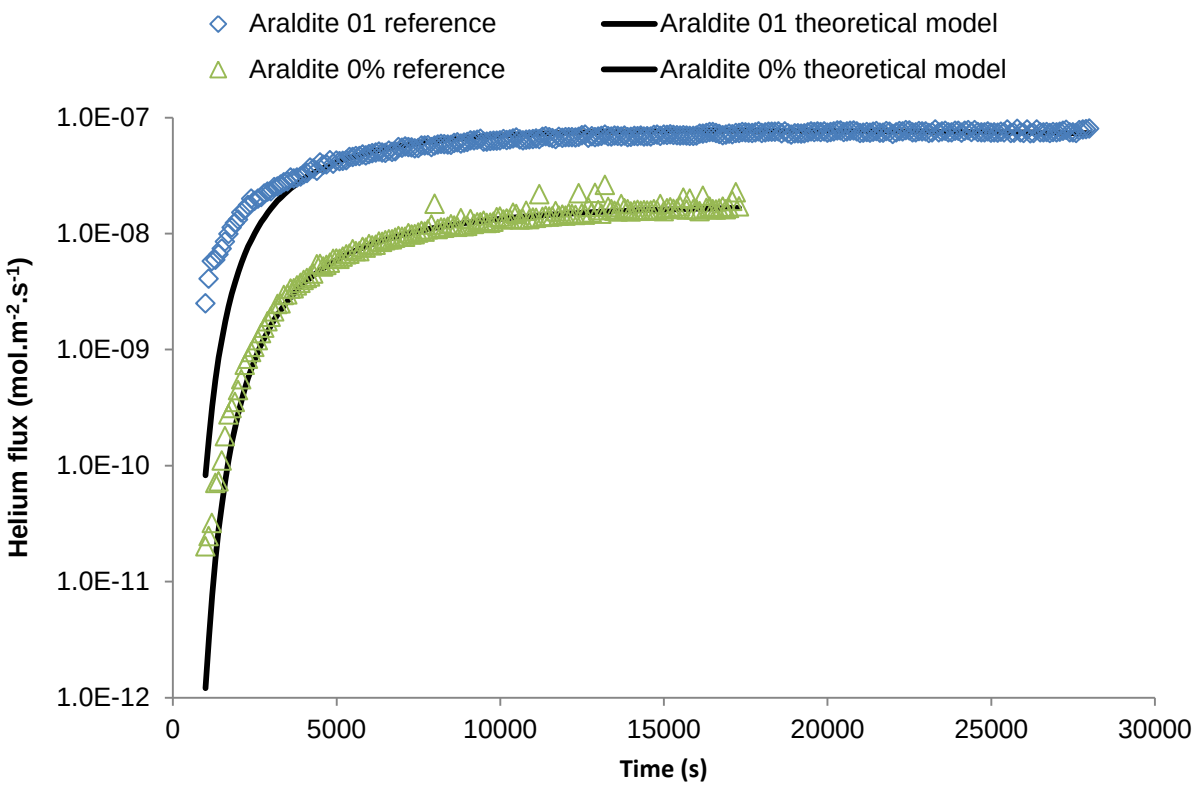

Figure 5.31 Model fit of helium flux data for reference Araldite samples

With the addition of the graphene platelets and the glass flakes the linear plots of $ln(J\sqrt{t})$ vs $1/t$ yielded no straight lines. As the weight fractions of the fillers increased the plotted graphs became more curved which can be seen in **Figure 5.32** and **Figure 5.33**. This same behaviour was observed by Humpenöder (1998) who used the same method to determine the permeability of fibre reinforced plastics. He suggested that the method be used for homogenous materials instead of composite materials because of the complex theory and lack of models to explain the behaviour properly. However, other researchers (Ogasawara et al., 2006; Schultheiß, 2007, pp.25–26; Yokozeki et al., 2004)(Schultheiß, 2007) have determined the diffusion co-efficient and permeability co-efficient successfully using this method and verified the Fickian behaviour by superimposing the model flux with the measured experimental gas flux. Therefore, the linear $ln(J\sqrt{t})$ vs. $1/t$ plot deviation and the model flux vs. experimental flux were used to determine the diffusion co-efficient. The diffusion co-efficient could only be determined accurately if the experimental flux behaved

in a Fickian manner. The experimental flux and theoretical model flux plots are compiled in Annexures A, B, C,and D.

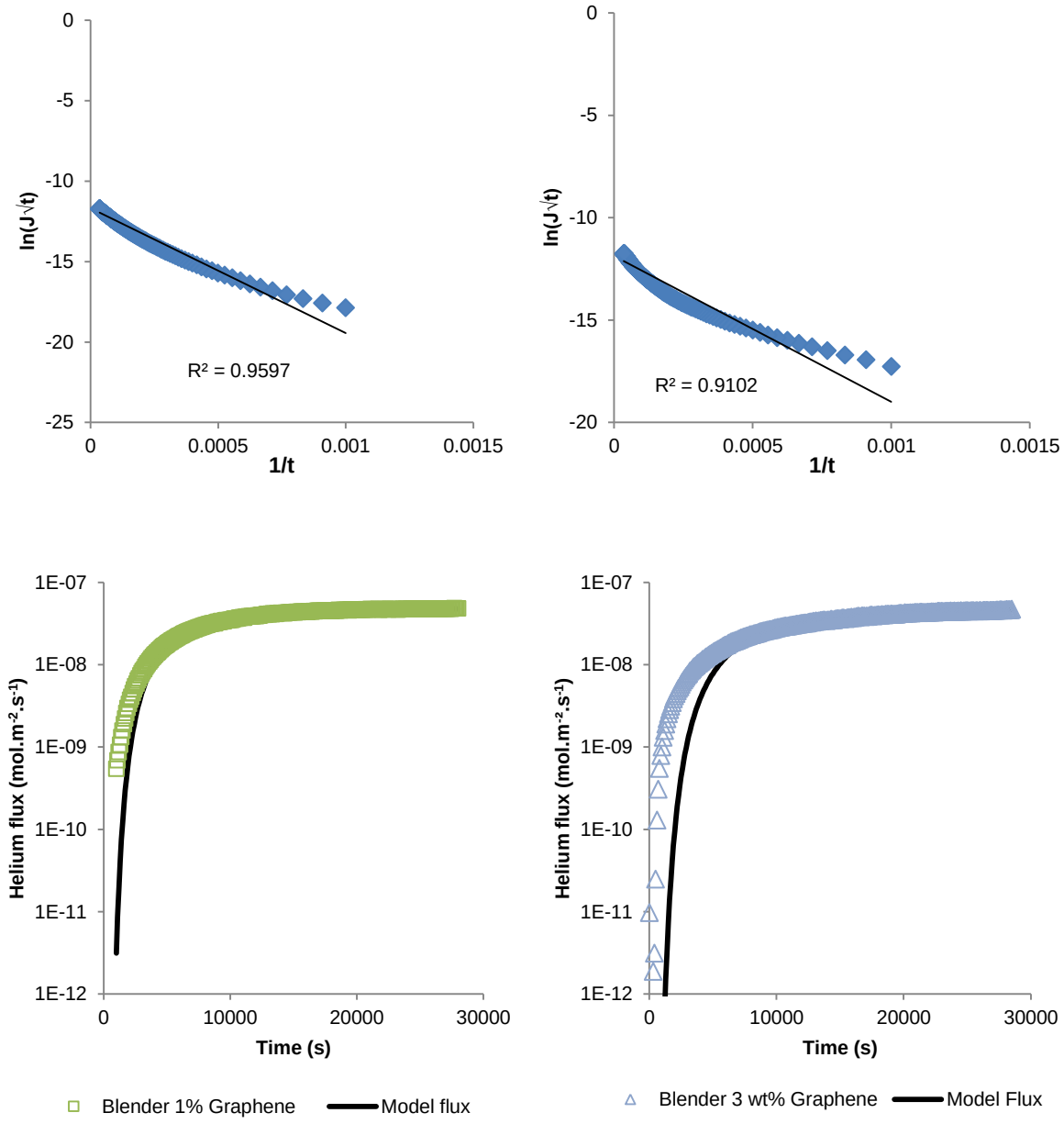

Figure 5.32 Model fit of graphene doctor blade samples

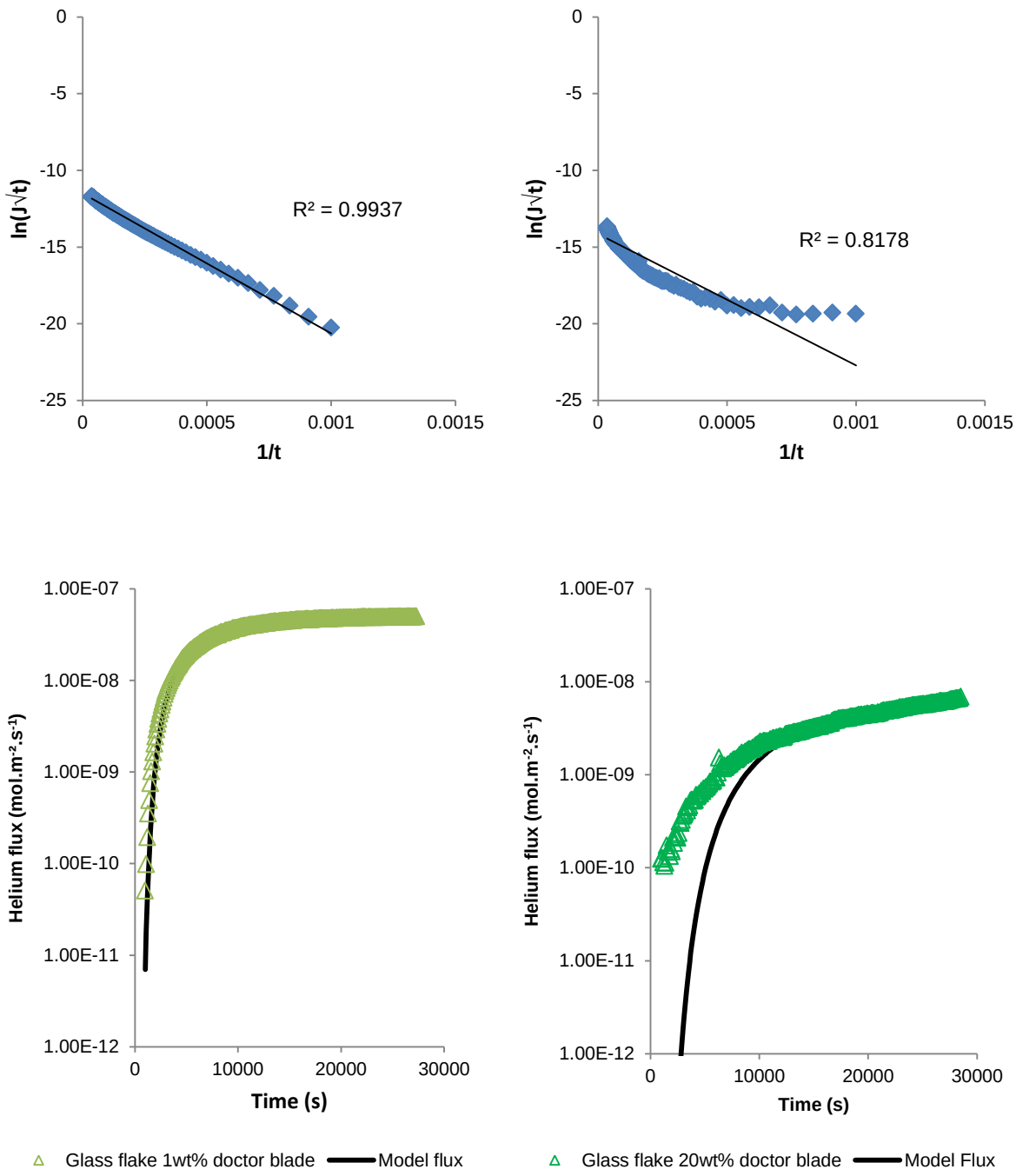

Figure 5.33 Model fit of glass flake filled doctor blade sheets

The helium flux results displayed good model flux fits for the doctor blade sheets according to the mathematical model for the graphene (**Table 5.6**) and for some of the glass flake (**Table 5.7**) composite samples. This can be ascribed to the incorporation of the fillers into the resin matrix altering the migration path of the helium molecules through the epoxy matrix. As the free volume of the polymer matrix decreases, from higher weight

fractions of the impermeable additives, the helium release from the molecules also changes and the behaviour becomes more of a pseudo-Fickian release from the membranes. The good fit to the flux model for the graphene composite samples indicated that the helium gas molecules still moved easily through the polymer matrix. This is due to the difficulty of dispersing the graphene platelets uniformly in the epoxy resin and therefore, not reducing the epoxy filled regions (free volume) of the composite membrane. As the weight fraction increased, the graphene samples started to deviate from the linear fit which indicated that the flux behaviour was differing from the Fickian model flux (**Figure 5.33**).

Table 5.6 Helium flux behaviour of doctorblade sheets filled with graphene

Loading (wt %)	**Mixing method**	**Helium flux behaviour**	**Linear fit (R^2)**
0	None	Exactly Fickian	0.96
1	Ultrasonic	Near Fickian	0.93
1	Hand	Exactly Fickian	0.96
1	Blender	Exactly Fickian	0.96
2	Blender	Near Fickian	0.91
3	Blender	Near Fickian	0.91

Table 5.7 Helium flux behaviour of doctor blade sheets filled with glass flakes

Loading (wt %)	Mixing method	Helium flux behaviour	Linear fit (R^2)
0	None	Exactly Fickian	0.96
1	Ultrasonic	Exactly Fickian	0.99
3	Ultrasonic	Exactly Fickian	0.99
6	Ultrasonic	Not Fickian	0.82
10	Ultrasonic	Near Fickian	0.90
15	Ultrasonic	Not Fickian	0.81
20	Ultrasonic	Not Fickian	0.82

The model fit to Fick's law of diffusion was good for all the graphene moulded disc samples (**Table 5.8)**. The graphene samples prepared with solvents produced fits which indicated that the samples were very porous by offering no resistance to the helium molecules. These samples all behaved in an exact Fickian manner. For the glass flake filled samples in (**Table** 5.9**)**, the 25 wt% sample still exhibited Fickian behaviour. The higher loading at 30 wt% produced tighter packing of the glass flakes which reduced the mobility of the helium molecules in the resin matrix. The fit to the model showed that the gas release from the sample behaved in a near-Fickian manner. This change in behaviour indicated that the change in morphology of the composite resin produced areas with well aligned and dispersed glass flakes. The 35 wt% glass flake filled composite disc did not display Fickian behaviour at all.

Table 5.8 Helium flux behaviour of moulded discs filled with graphene

Loading (wt %)	Solvent used	Helium flux behaviour	Linear fit (R^2)
0	None	Exactly Fickian	0.99
2	DCM	Exactly Fickian	0.99
4	DCM	Exactly Fickian	0.99
4	DMF	Exactly Fickian	0.92
4	THF	Exactly Fickian	0.99

Table 5.9 Helium flux behaviour of moulded discs filled with glass flakes

Loading (wt %)	Solvent used	Helium flux behaviour	Linear fit (R^2)
0	None	Exactly Fickian	0.99
25	None	Exactly Fickian	0.97
30	None	Near Fickian	0.90
35	None	Not Fickian	0.88

The model fit to the multi-layered samples (**Table 5.10**) showed that the samples no longer behaved according to Fickian behaviour except for the glass flake sample at a thickness of 4 mm. The better orientation of the fillers in thinner layers changed the behaviour dramatically to be rather considered as pseudo Fickian.

Table 5.10 Helium flux behaviour of multilayer sheets

Loading (wt %)	Sample	Helium flux behaviour	Linear fit (R^2)
0	Reference	Fickian	0.99
2	Graphene 3	Not Fickian	0.87
2	Graphene 4	Not Fickian	0.64
30	Glass flake 3	Not Fickian	0.68
30	Glass flake 4	Fickian	0.90

The method suggested by Yokozeki et al. (2004) was used successfully to model the helium leak results of the composite samples according to Fick's law of diffusion. The plain reference epoxy samples and the samples with low amounts of glass flakes and graphene platelets displayed model fits which matched the measured helium leak rates.

From the helium permeability results for the graphene (**Figure 5.34**) and glass flake samples (**Figure 5.35**) it can be summarized that the glass flakes displayed superior improvements in the gas barrier properties when compared to the graphene platelets. The improvement in the gas barrier properties is dependent on the aspect ratio (the aspect ratio is the width divided by the thickness of a flake/platelet) of the filler, orientation in the

polymer matrix, and the degree of dispersion of the platelet fillers (Kalaitzidou et al., 2007). Lape et al. (2004), Derocher et al. (2005) and Bharadwaj (2001) showed that aligned larger sized flakes have a better improvement on the gas barrier properties over smaller flakes. The glass flakes were larger (300-1000 μm), as was confirmed with the SEM analysis, than the graphene platelets (25 - 40 μm) and orientated easier in the epoxy matrix than the graphene platelets.

The shape and size of a gas molecule plays a major role in how it travels through a polymer matrix. The smaller diameter of the helium gas molecule allows it to travel with a lot more ease through a polymer matrix when compared to other gas molecules like nitrogen, oxygen, and hydrogen. Even though helium and hydrogen have similar atomic diameters, helium has been shown to diffuse faster through thermoplastic and thermosetting polymers than hydrogen (Humpenöder, 1998; Molyneux, 2001).

Therefore, the tritium gas should leak less than helium and the composite coatings containing larger glass flakes should act as an effective barrier to limit the release of tritium gas as has been shown with the helium permeability measurements.

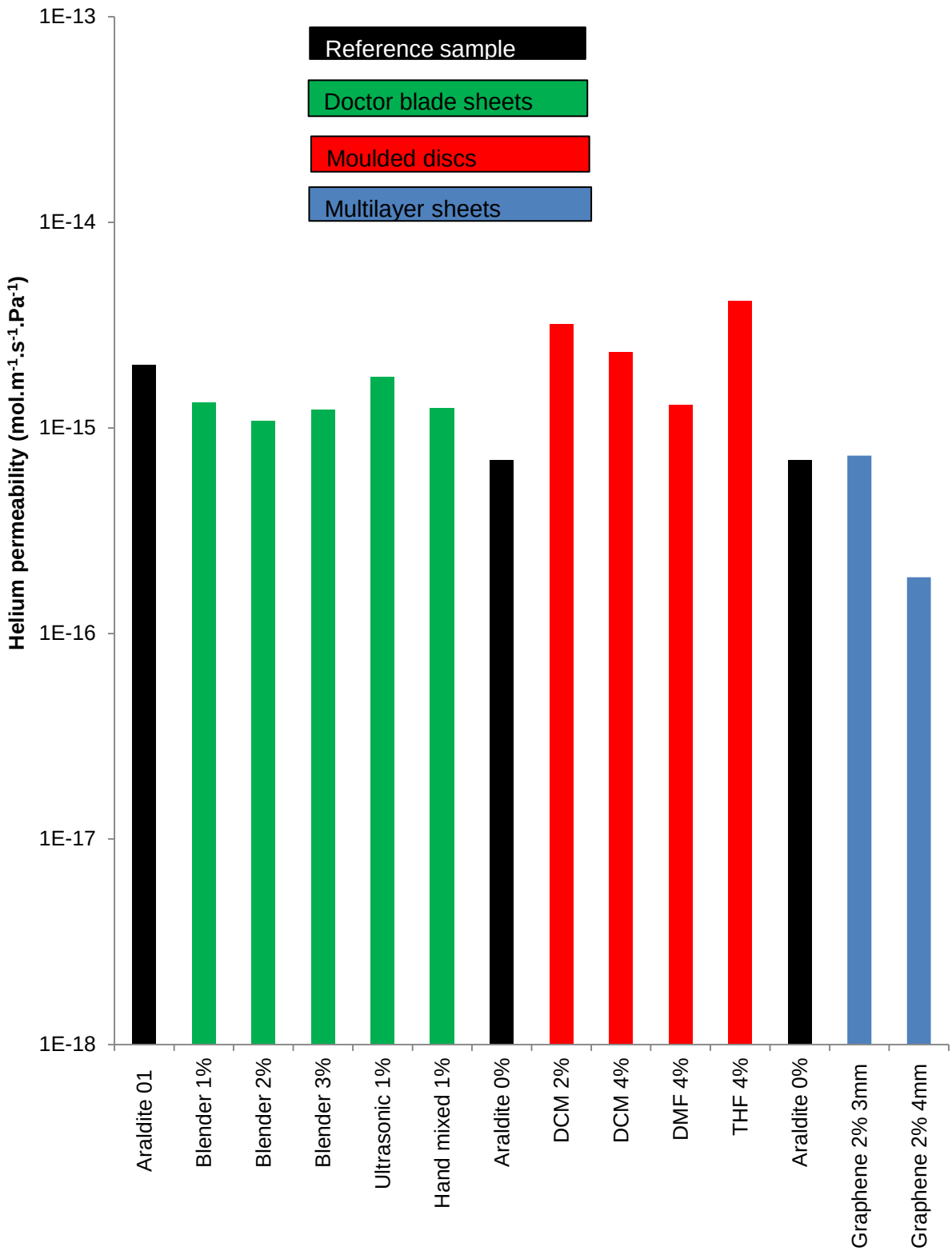

Figure 5.34 Helium permeability comparison of graphene filled samples

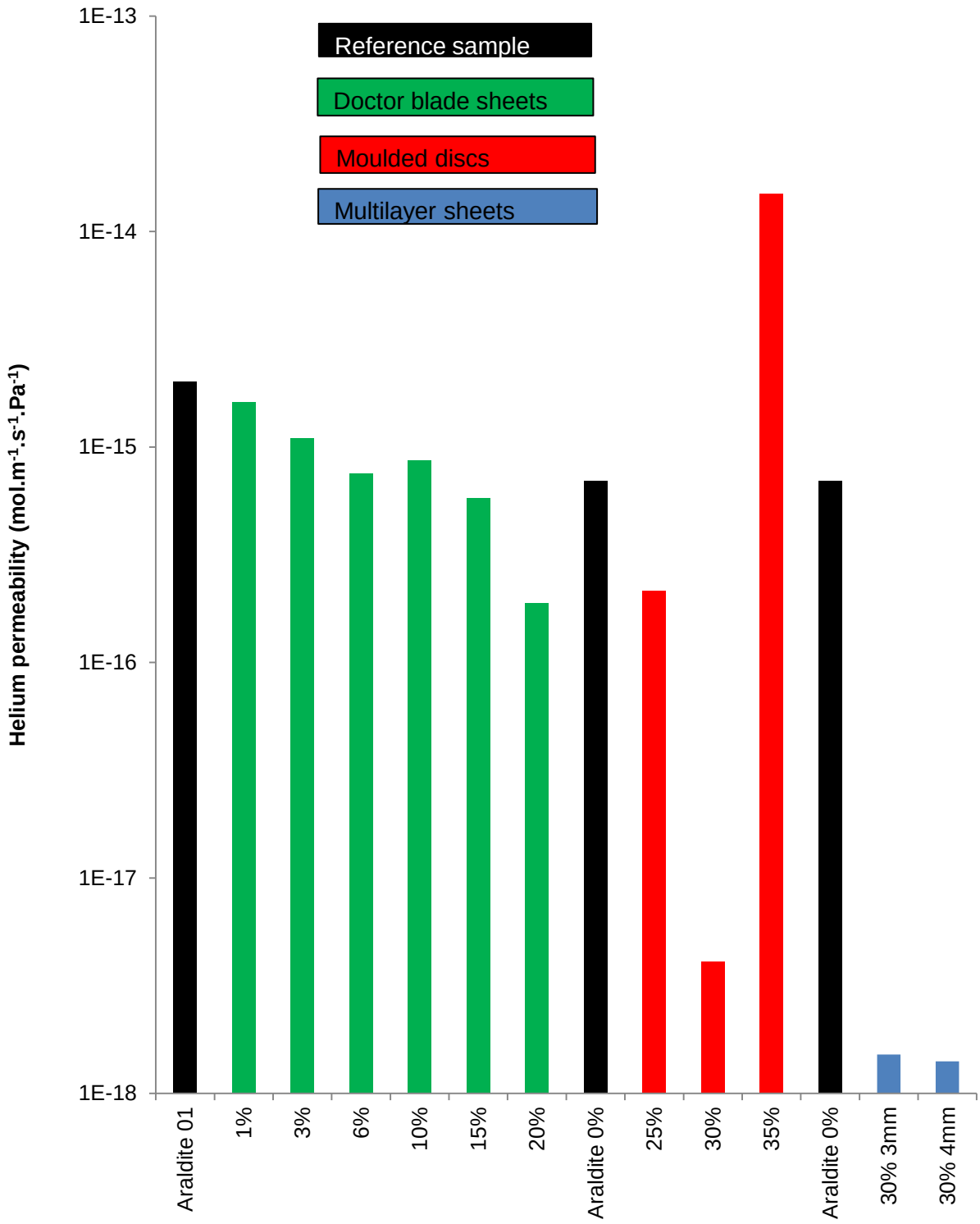

Figure 5.35 Helium permeability comparison of glass flake filled samples

5.4 TRITIUM RELEASE PREDICTIONS

5.4.1 Threshold determination

The prediction of the amount of tritium that might permeate through the composite coatings was essential to determine if the composite epoxy coatings could be used to coat low level radioactive graphite waste. The helium permeability analysis showed that the incorporation of glass flakes and graphene platelets into the resin structure could reduce the helium leak rate. However, the amount of tritium gas that might be released into a repository environment had to be determined from the measured helium leak rates of the various graphene and glass flake filled samples. For the composite resins to effectively immobilize the release of tritium gas from low level radioactive graphite waste, the leak rate would have to be reduced sufficiently below the allowable concentration of tritium regulatory limits (Beeslaar, 2012; ICRP, 1996; ICRP, 1997). Therefore, two hypothetical scenarios were created to evaluate if the incorporation of the glass flakes and graphene platelets could reduce the helium/tritium permeability below the required limits to be considered as an option for actual immobilization of irradiated graphite waste. Researchers have used similar methods to simulate the potential exposure of people to radioactive gases in working environments and confined spaces for a specific time period (Yamanishi et al., 2010; El-Hussein, 2005; Iwai et al., 2001).

In these scenarios, the “worst case scenario” was simulated with the irradiated graphite waste stored in a corner of the repository, no ventilation, and continual leaching of the tritium into the repository environment for 28 000 s which is equal to an 8 h shift for radiological workers. With these exaggerated conditions, which only serve as an indication of how the tritium might permeate from the irradiated graphite waste, the tritium predictions were calculated. The only variable that was changed with the scenarios was the

dimensions of the repositories which would determine if the coatings may be suitable for specific scenarios. The method used to determine the tritium radioactivity in the repository has been discussed thoroughly in Chapter 4, Sections 4.4 and 4.5.

The amount of tritium that might leak from the waste was calculated from the helium leak rate by firstly converting the steady state helium flux ($mol.m^{-2}.s^{-1}$) to tritium mass flux ($g.m^{-2}.s^{-1}$). The mass flux is then multiplied with the tritium atomic mass of 3 $g.mol^{-1}$, area of coated surface, and the total time for a radiological worker's daily shift according to **Table 4.1**. The amount of predicted tritium released from the waste was then used to determine the tritium radioactivity according to **Equation 4.12**. The derived air concentration ($Bq.m^{-3}$) was determined from the radioactivity and the volume of the repositories of Scenario 1 and 2 (**Figure 4.5**).

The derived air concentration (DAC) that a radiological worker is allowed to be exposed to for tritium gas is 6×10^{8} $Bq.m^{-3}$ (Beeslaar, 2012; ICRP, 1997). A series of helium leak rates between 1×10^{-13} to 1×10^{0} $mol.m^{-2}.s^{-1}$, were used to determine the DAC for Scenario 1 and 2. The calculated release of tritium for the two scenarios produced the release limits for the composite coatings. For the first scenario (**Figure 5.36**), the leak rate would have to be less than 4.1×10^{-9} $mol.m^{-2}.s^{-1}$ to fall within the regulatory safety threshold for tritium exposure while for Scenario 2 (**Figure 5.37**), the leak rate is raised to 1.65×10^{-8} $mol.m^{-2}.s^{-1}$ for the bigger repository. The measured helium leak rates of the doctor blade sheets, moulded disc, and the multi-layered sheets could then be compared with the hypothetical leak rates to determine if the composite coatings lowered the leak rate sufficiently below that of the regulatory limits.

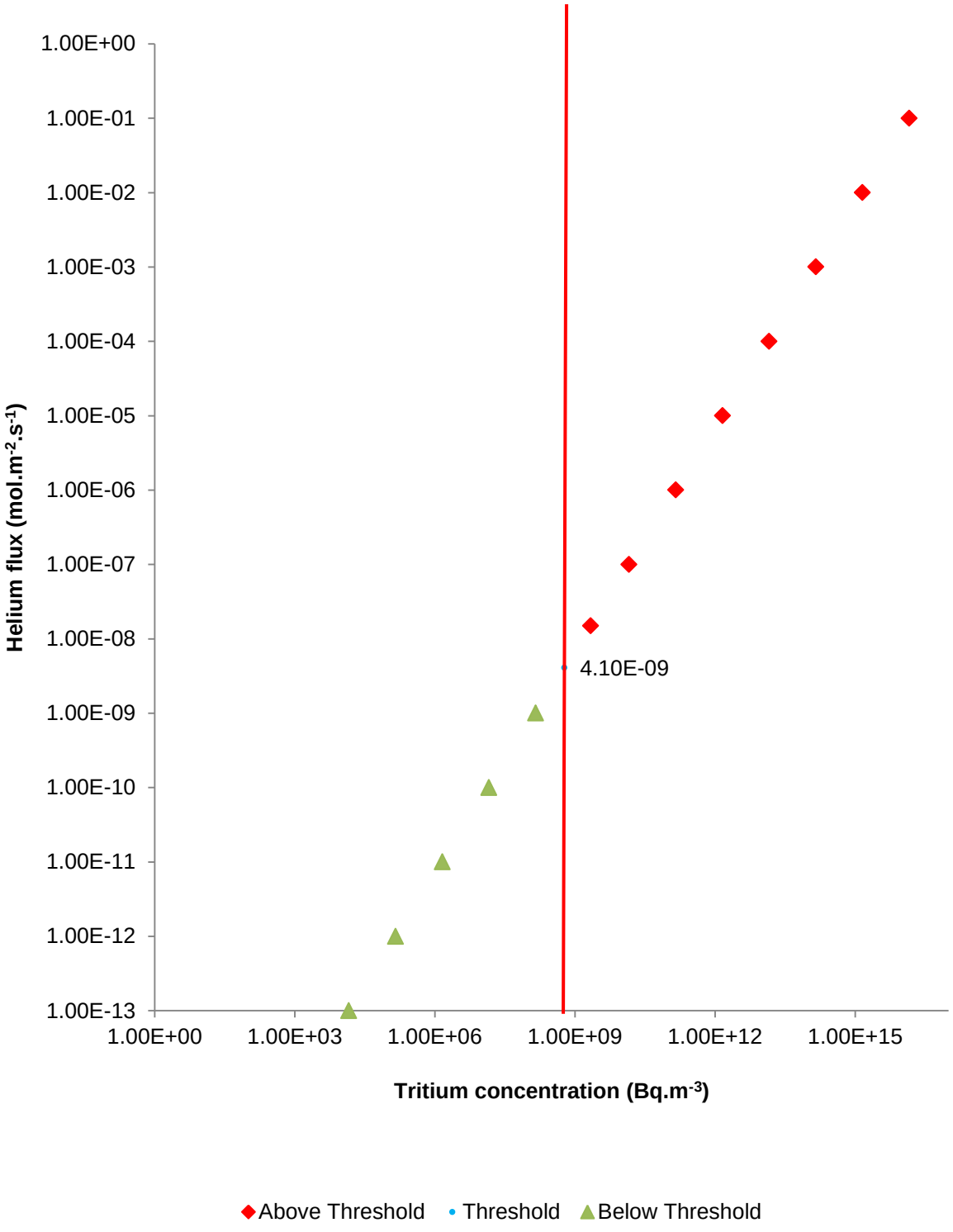

Figure 5.36 DAC Threshold for Scenario 1

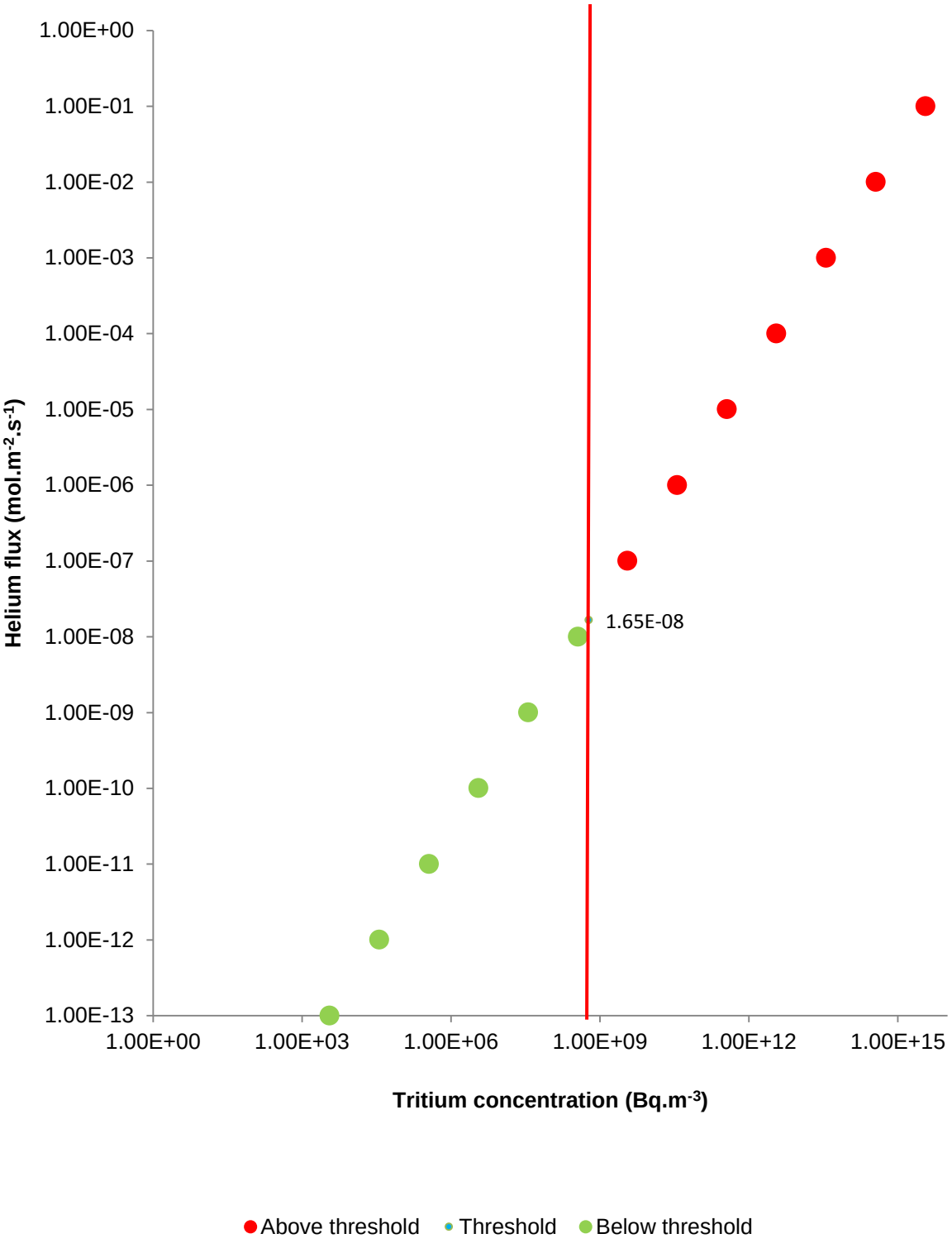

Figure 5.37 DAC threshold for Scenario 2

5.4.2 Scenario predictions of radioactivity concentrations

None of the doctor blade sheets reduced the helium leak rate enough to be considered for Scenario 1 (**Figure 5.38**). The moulded disc samples filled with graphene leaked too much due to the effect of solvents on the resin structure. However, the 25 wt% moulded disc filled with glass flake came close to the required leak rate, but the 30 wt% glass flake sample reduced the leak rate sufficiently below the required leak threshold (**Figure 5.39**). Both the 3 and 4 mm multilayer sheets filled with glass flakes reduced the leak rate below the required threshold and the 4 mm graphene multilayer sheet was the only graphene filled sample that could be considered for Scenario 1 (**Figure 5.40**). A summary of the composite samples which could be applied for Scenario 1 are listed in **Table 5.11**.

Table 5.11 Samples that may be considered for Scenario 1

Sample type	**Filler**	**Loading (wt%)**	**Steady state flux ($mol.m^{-2}.s^{-1}$)**	**Derived air concentration ($Bq.m^{-3}$)**
Moulded disc	Glass flake	30	4.88×10^{-11}	7.05×10^{06}
Multi-layer 4 mm	Graphene	2	3.91×10^{-09}	5.65×10^{08}
Multi-layer 3 mm	Glass flake	30	3.38×10^{-11}	4.88×10^{06}
Multi-layer 4 mm	Glass flake	30	2.50×10^{-11}	3.61×10^{06}

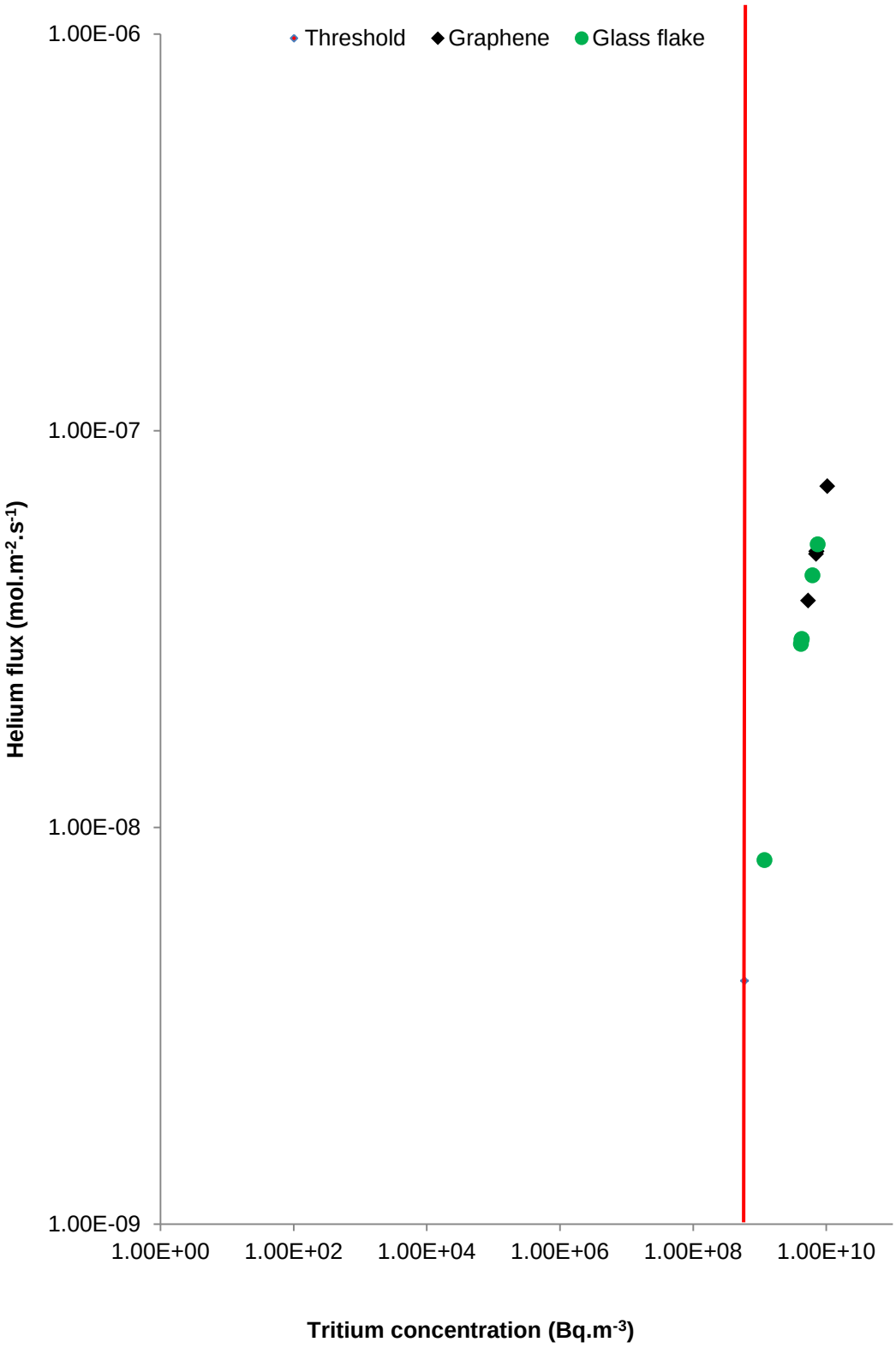

Figure 5.38 DAC results for doctor blade sheets (Scenario 1)

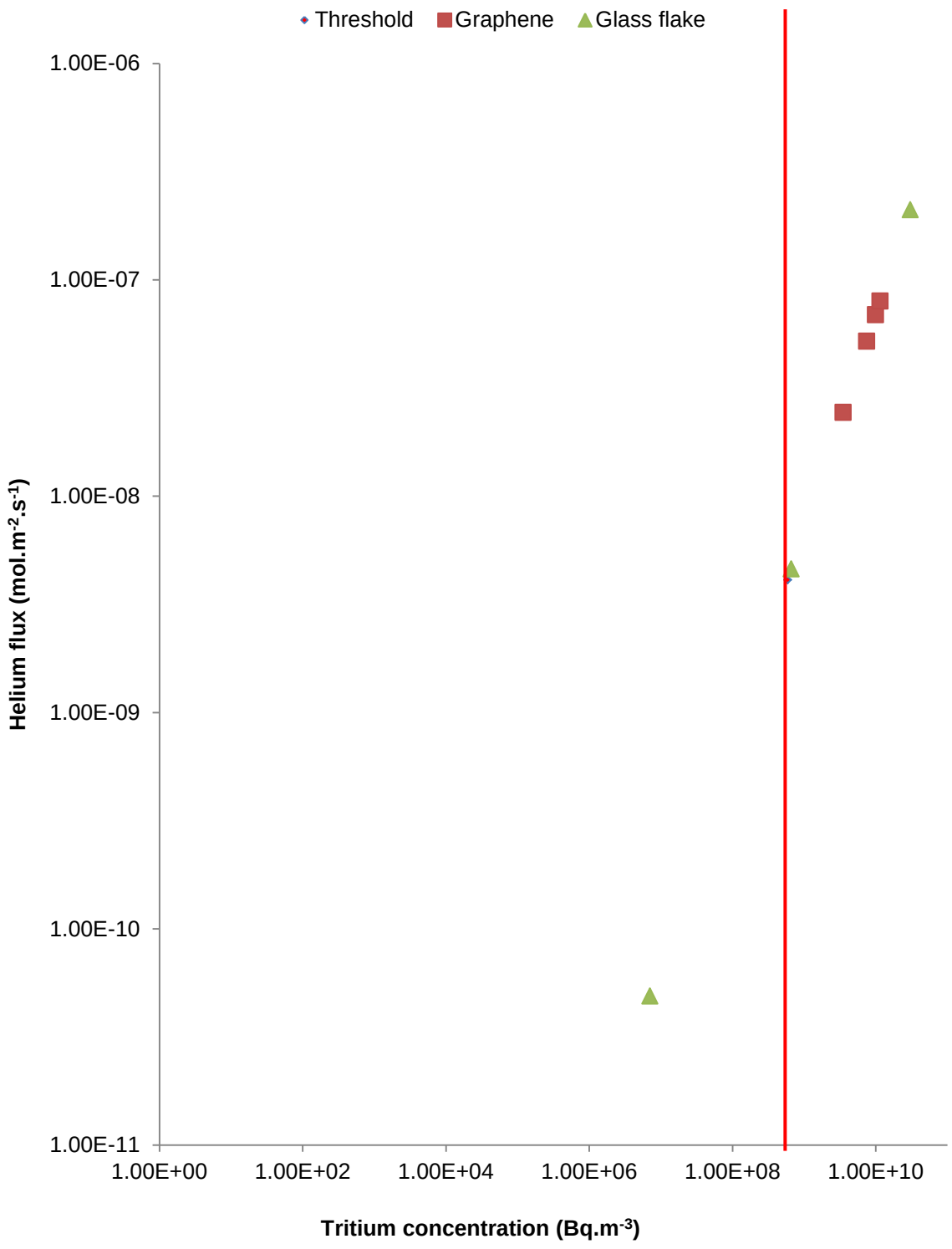

Figure 5.39 DAC results for moulded discs (Scenario 1)

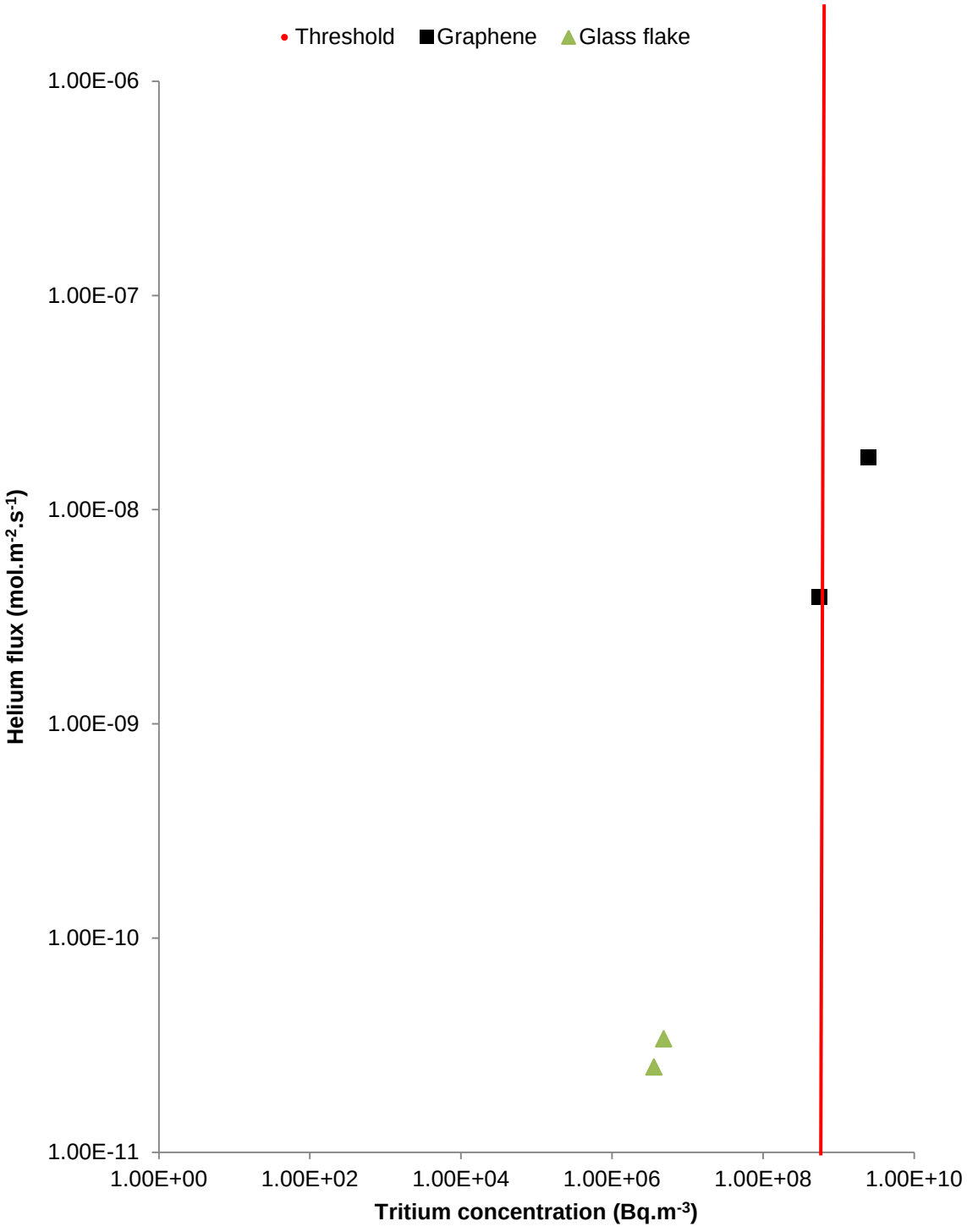

Figure 5.40 DAC results for multilayer sheets (Scenario 1)

With Scenario 2 (**Table 5.12**) the increased threshold saw the inclusion of two additional samples that nearly made it for application in Scenario 1, namely the doctor blade sample with 20 wt% glass flakes (**Figure 5.41**) and the 25 wt% glass flake filled moulded disc (**Figure 5.42**). The 30 wt% glass flake moulded disc (**Figure 5.42**), the 3 and 4 mm glass flake filled multilayer sheets (**Figure 5.43**), and the 4 mm graphene filled multilayer sheet (**Figure 5.43**) were the other samples that could be considered for application in this scenario.

Table 5.12 Samples that may be considered for Scenario 2

Sample type	**Filler**	**Loading (wt%)**	**Steady state flux ($mol.m^{-2}.s^{-1}$)**	**Derived air concentration ($Bq.m^{-3}$)**
Doctor blade	Glass flake	20	8.26×10^{-09}	2.98×10^{08}
Moulded disc	Glass flake	25	4.61×10^{-09}	1.66×10^{08}
Moulded disc	Glass flake	30	4.88×10^{-11}	1.76×10^{06}
Multi-layer 4 mm	Graphene	2	3.91×10^{-09}	1.41×10^{08}
Multi-layer 3 mm	Glass flake	30	3.38×10^{-11}	1.22×10^{06}
Multi-layer 4 mm	Glass flake	30	2.50×10^{-11}	9.02×10^{05}

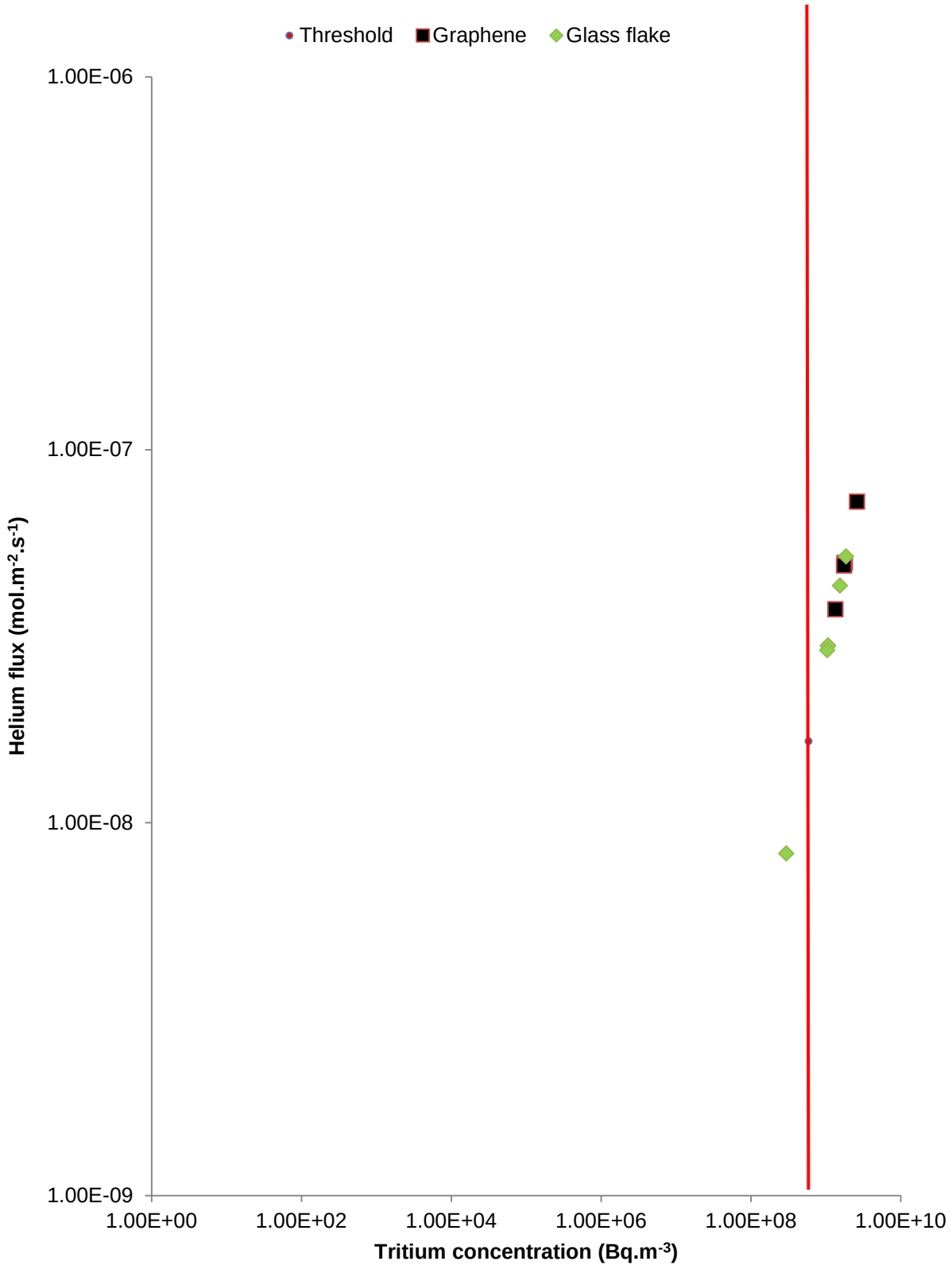

Figure 5.41 DAC results for doctor blade sheets (Scenario 2)

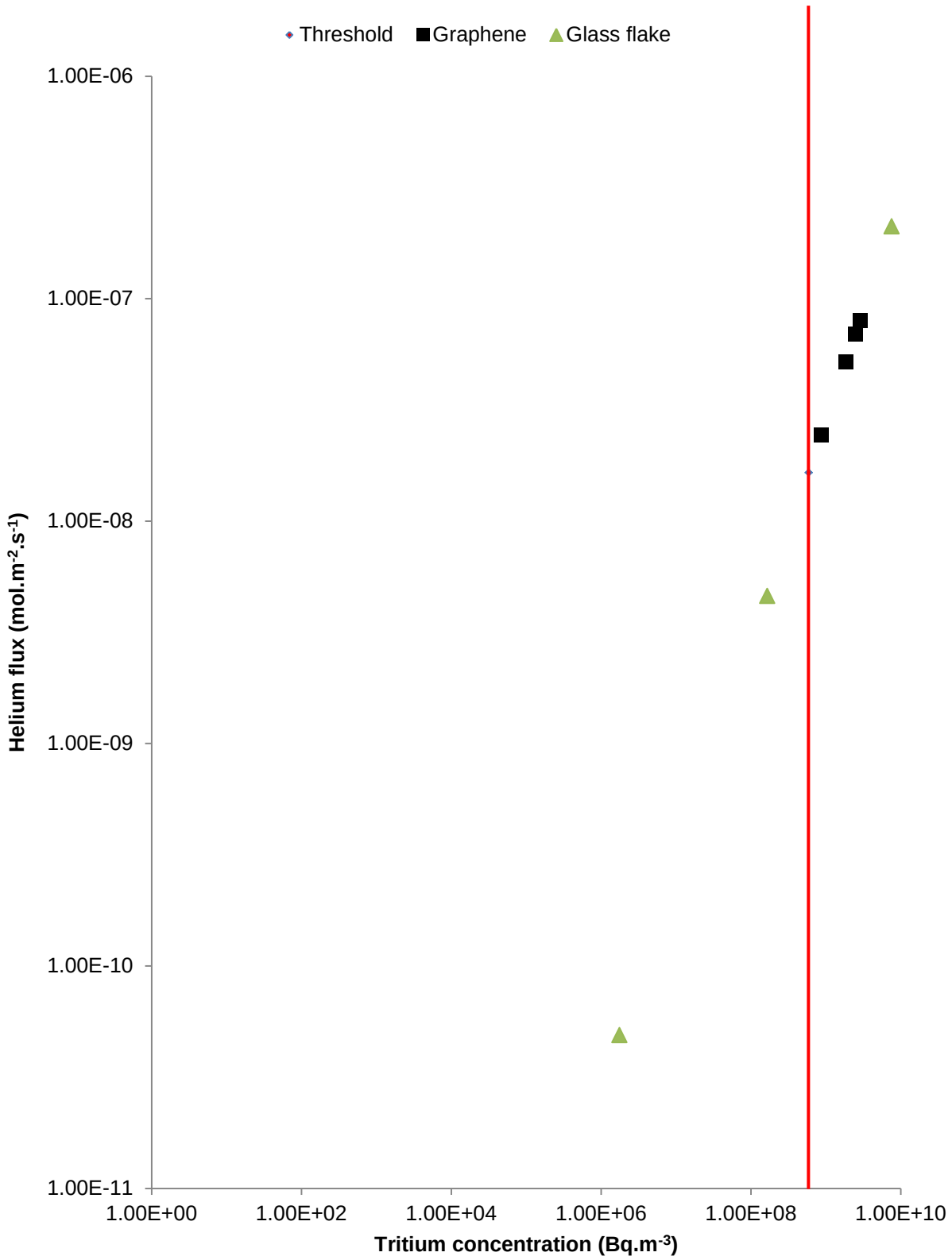

Figure 5.42 DAC results for moulded discs (Scenario 2)

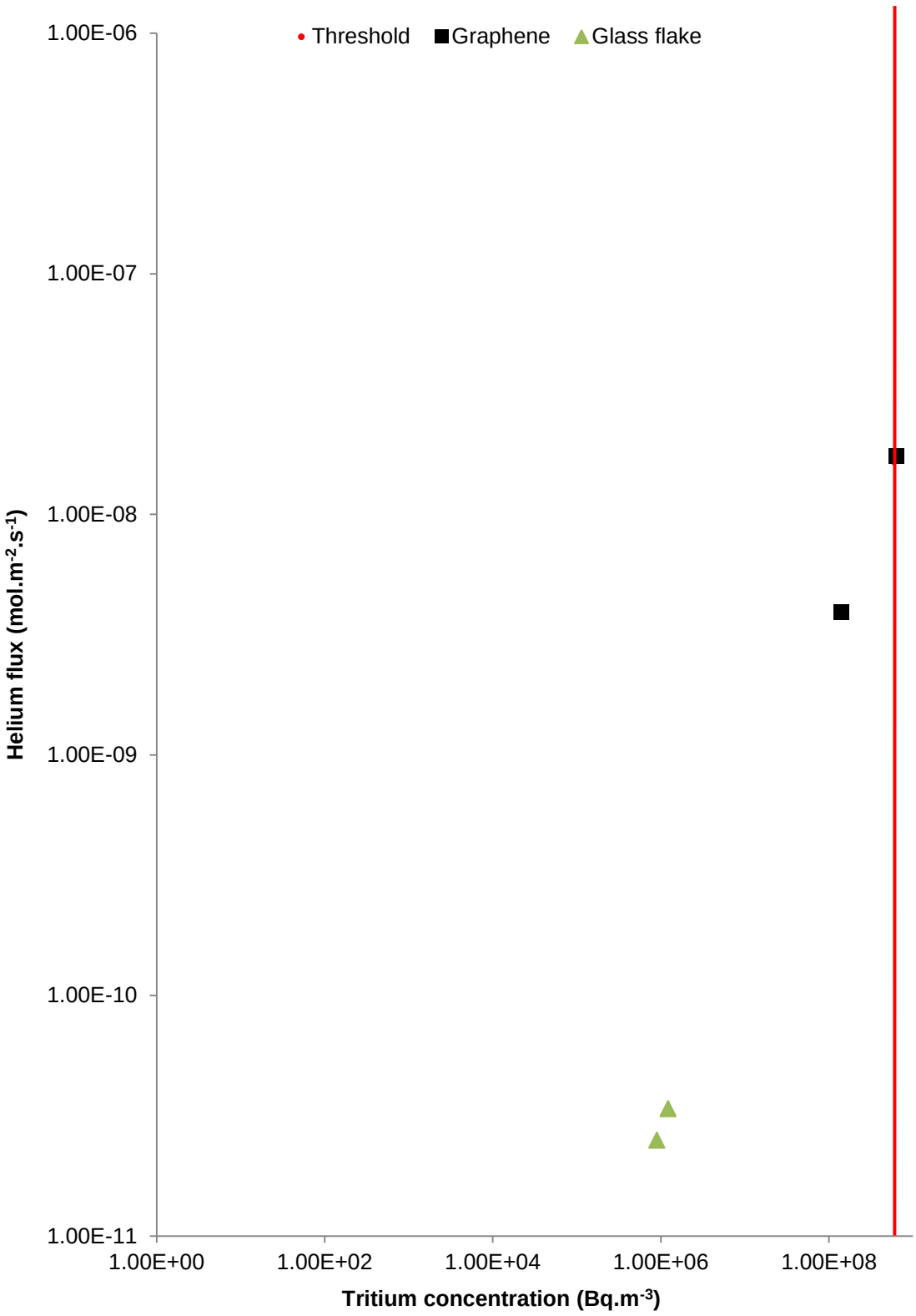

Figure 5.43 DAC results for multilayer sheets (Scenario 2)

The simulated results indicated that the glass flakes outperformed the graphene filled samples in reducing the tritium leak rate for both Scenario 1 and 2 below the required regulatory threshold. With the specified conditions, the glass flake filled epoxy coating applied in multiple layers appeared to be the best composite coating that may be considered as an effective gas barrier for gases containing radionuclides.

The predictions of tritium gas that might be released into the working environment of the two scenarios indicated the dependence of the concentration of tritium that would mix with the air in the repository. It must also be noted that the release of radioactive gases, especially tritium, from the graphite waste would be dependent on the porosity of the graphite and the content of radionuclides contained in the graphite. The amount of tritium contained in the irradiated graphite is very low and the leak rate will not be as high as in the case of the continual flow of helium for the measured samples. The radioactive half-life of the tritium gas will also decrease over time which will also change the radiation dosage.

5.5 ADHESION TO GRAPHITE

For the coating to be an effective barrier for gases, the coating must adhere well with the graphite surface. Graphite surfaces are known to generate dust which is caused by abrasion. The graphite waste from decommissioned reactors will most likely be highly degraded from radiation and biological degradation which would generate a lot of graphite dust. This graphite dust can hinder the adhesion of the epoxy coating during application which can cause delamination of the coating from the graphite surface. Therefore, the graphite sourced as the applicable substrate was graphite which was machined into smaller blocks. This machining caused a lot of dust to be generated on the graphite surface (**Figure 5.44**) which would resemble the expected graphite from a decommissioned reactor.

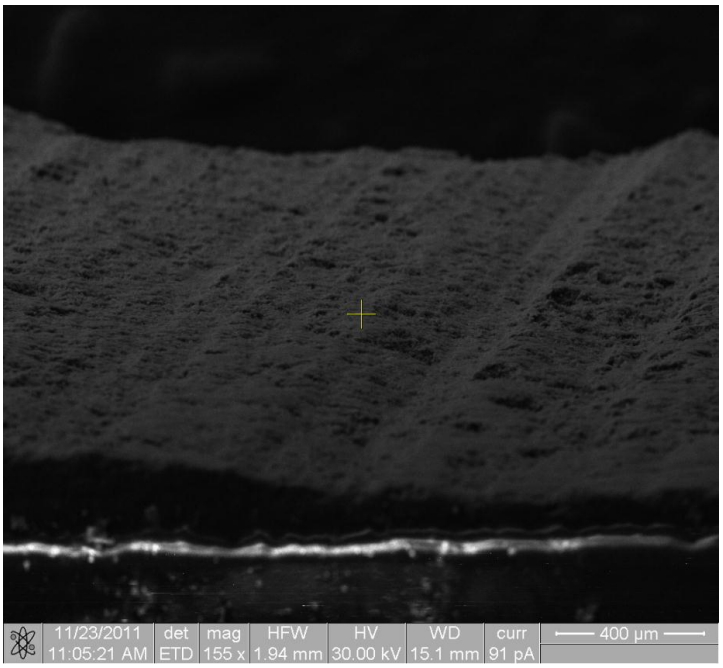

Figure 5.44 SEM image of machined graphite surface before coating with epoxy

The degree of adhesion was determined by the cross hatch test method according to the ASTM standard D 3359. The standard describes a method A and B, the latter method is recommended for laboratory evaluation. A thin layer of the epoxy resin was coated onto a graphite block and polyethylene block, the reason for coating onto a polyethylene surface was to display the weak adhesion of epoxy resin on polyethylene for comparison reasons. Polyethylene is known to exhibit poor adhesion due to the low surface energy and the non-polar properties of polyethylene (Berg, 2009, p.265). Six incisions were cut in the cured coating to produce a lattice pattern with a razor blade. The adhesive tape was firmly applied and peeled off to display the degree of flaking of the epoxy coating.

The cross-hatch testing of the epoxy resin produced results which were very promising with the application of the epoxy resin on graphite surfaces. The cross-hatch cutting showed very little flaking where the cuts met (**Figure 5.45 a**). On the adhesive tape, the

grading was 4B according to the ASTM standard (ASTM, 2009b, pp.400–406) which is less than 5% removal of coating from the graphite substrate. The polyethylene surfaces flaked and peeled as the blade cut into the epoxy resin producing a grade of 0B which indicates more than 65% removal of the epoxy resin. SEM investigation of the cross cuts of the coating on the graphite (**Figure 5.45b**) showed that the cuts still stayed in contact with the graphite surface while the coating on the polyethylene substrate (**Figure 5.46**) shows definite chunks being removed from the cut region. The SEM investigation of the graphite edges (**Figure 5.47**) coated with the resin indicated that the epoxy resin bonded well with the graphite surface by filling the pores of the graphite.

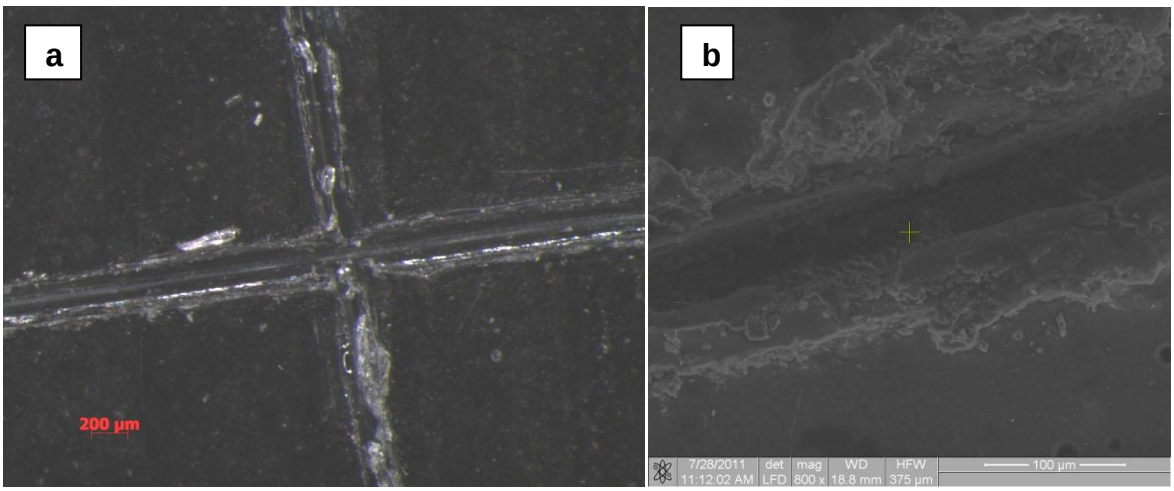

Figure 5.45 Microscopic images of cross hatch lattice taken with a a) stereomicroscope and b) SEM

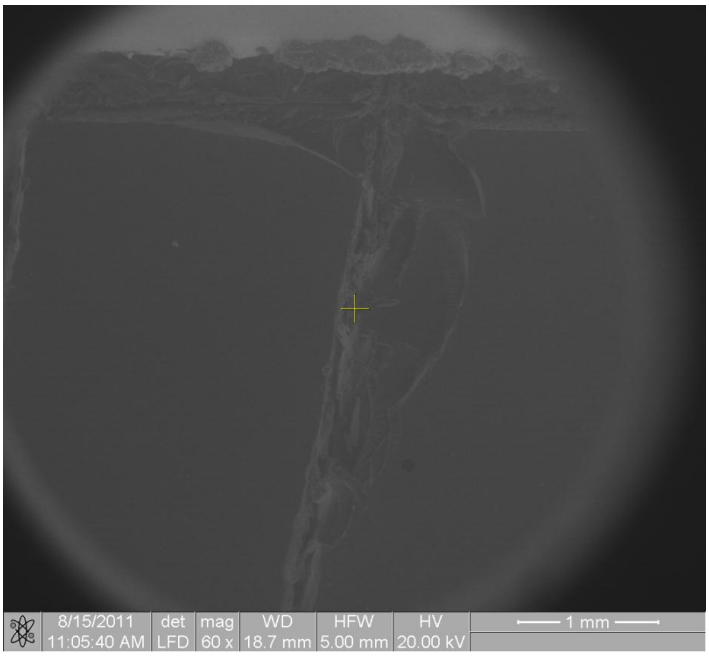

Figure 5.46 SEM image of cross hatch lattice of coated polyethylene

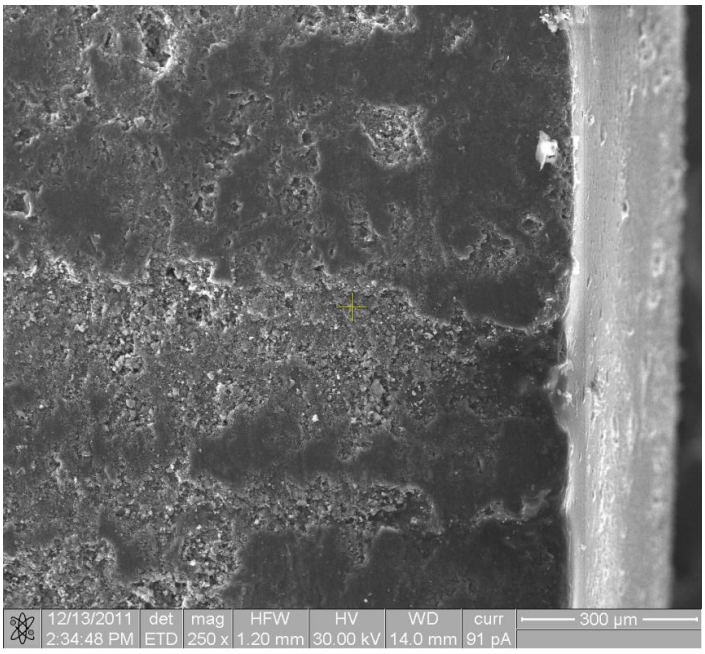

Figure 5.47 SEM image of graphite coated with epoxy resin

The generated dust could be seen to mix with the epoxy coating and discoloured the resin to an extent. Hence, the concern that the epoxy resin may peel (delaminate) from the graphite surface. Yet, a disc of graphite coated with a 4 mm layer of epoxy resin adhered

extremely well to the graphite surface that not even a screwdriver could lift the coating and peel it off. Also, the coating showed no indication of delamination after 2 months. This good adhesion with the graphite surface would make the epoxy resin ideal to immobilize reactor graphite waste.

6 CONCLUSION

6.1 SUMMARY OF OBJECTIVES

The main objective of this research project was to develop a composite coating from epoxy resin for irradiated graphite waste that could limit or prevent the release of radioactive gases like tritium, carbon-14 (released as carbon dioxide and methane), and chlorine-36. Tritium was the radionuclide that was focused on because the molecular size and mass of tritium is smaller than that of other radionuclides. Thus, tritium should diffuse out of the graphite structure at a faster rate. Therefore, if the cladding material could contain or limit the release of the tritium, then it should be able to limit heavier elements as well. It must be noted that helium gas was used as a substitute gas due the molecules being almost similar in size. To attain this goal, certain steps were followed to develop the cladding material (see section 1.3).

A suitable epoxy resin (Araldite LY 5082 epoxy resin and HY 5083 hardener) was sourced which exhibited a low viscosity and 2 to 3 h workable pot life which could coat large areas of irradiated graphite. The epoxy resin was also suitable for the incorporation of graphene nanoplatelets and glass flakes using various mixing techniques. The graphene and glass flake composite resin samples were prepared as sheets and moulds by three different methods to improve the orientation of the fillers in the resin,

- Doctor blade coating
- Moulding in plastic discs
- Coating thin layers on top of another with a brush (multilayer sheet)

Out of the three samples the multilayered samples showed to be the best technique to orientate and disperse the fillers in the resin. The morphology of the composite samples was successfully characterised with the aid of microscopic imaging techniques like SEM.

The helium gas barrier properties were successfully measured and the measured helium leak rates of the samples were fitted according to the model which is derived from Fick's law of diffusion to determine the helium permeability of the sheets and help predict the release of tritium from graphite waste.

The epoxy resin also showed good adhesion to the graphite surface it was applied to.

6.2 EFFECT OF MIXING TECHNIQUES AND SAMPLE FABRICATION ON THE DISPERSION OF THE FILLERS

Graphene nanoplatelets and glass flakes were identified as suitable fillers to improve the gas barrier properties of the epoxy resin. The fillers were incorporated into the resin with increasing loadings (wt%) using mechanical, manual, and ultrasonic mixing techniques.

The graphene platelets were the most difficult to disperse in the epoxy resin. Because of the low bulk density of the graphene platelets, the maximum loading was found to be 2 wt%. This loading appeared to be the weight fraction threshold of the graphene platelets because higher loadings increased the helium leak rate. At higher loadings, the platelets clumped and were difficult to separate and disperse in the epoxy resin. The use of solvents like DMF was thought to disperse the graphene platelets properly at higher loadings, but instead had an adverse effect by becoming entrapped in the epoxy resin structure. Therefore, the resin never cured properly and remained tacky. The use of mechanical shear

and ultrasonic techniques to disperse the graphene platelets proved to be the most effective at dispersing the graphene platelets in the resin matrix.

The glass flakes were found to disperse easier in the epoxy resin due to the higher bulk density and better separation of the flakes. Therefore, higher glass flake loadings, up to 30 wt%, could be incorporated into the epoxy resin. The glass flakes showed less of a tendency to agglomerate with other flakes and dispersed better in the epoxy resin than the graphene platelets.

6.3 EFFECT OF THE FILLERS ON THE HELIUM BARRIER PROPERTIES

The gas permeability of the graphene and glass flake filled composite samples was successfully measured using a specially designed permeation cell which was attached to a helium leak detector. The glass flakes showed a major improvement of a 100 to a 1000 times in the helium gas barrier properties when compared to the reference samples, as the glass flake loadings were increased from 1 to 30 wt%. The graphene filled samples (effective loadings up to 2 wt%) only improved the helium gas barrier properties about 10 times. The SEM characterization of the composite structures confirmed that the multilayer samples formed by brushing, improved the orientation and dispersion of the glass flakes and graphene platelets as could be seen with the multilayer 30 wt% glass flake filled samples which showed a typical tortuous path.

6.4 FIT TO FICK'S LAW AND PREDICTION OF THE POTENTIAL RELEASE OF TRITIUM GAS

The mathematical model derived from Fick's second law of diffusion was successfully used to determine the steady state flux. This was in turn used to determine the helium permeability and to predict the amount of tritium that could leak from graphite waste with an assumed inventory of unlimited tritium radioisotopes. Two 'worst-case' scenarios were created to calculate the concentration of tritium gas released into the environment of hypothetical underground repositories.

The predictions of the tritium gas released from the graphite waste stored in these underground repositories were successfully calculated using the specific assumptions regarding the release behaviour of the tritium gas and the repository conditions. The derived air concentration was determined from the steady state helium flux by calculating the amount of helium leaked and determining the radioactivity. The regulatory limit threshold 6×10^{8} $Bq.m^{-3}$ was used to determine if the helium leak rates were acceptable and fell below this limit. The samples filled with 30 wt% glass flake reduced the helium leak rate below the required regulatory limits. The multilayered graphene sample at 4 mm reduced the helium leak rate sufficiently to be considered for application with Scenario 2.

6.5 ADHESIVE PROPERTIES OF EPOXY RESIN TO GRAPHITE

The adhesion of the epoxy resin to the graphite surface was sufficient to be used as a coating. The inspection of the cross-hatch cuts showed that the cuts were smoothly cut through to the substrate surface with very little flaking. The SEM investigation showed that the epoxy resin fills the pores of the graphite sample and therefore would be considered

suitable to apply to other graphite surfaces. Actual graphite samples from decommissioned reactors still need to be assessed.

6.6 EVALUATION OF THE GRAPHENE AND GLASS FLAKE EPOXY RESIN COMPOSITES

Both the fillers improved the helium gas barrier properties. The results obtained from the helium leak rate measurements and the modelling showed that the glass flake composite resin outperformed the graphene filled samples by improving the helium gas barrier properties. The only graphene filled sample that showed a significant improvement was the multilayer sample at a thickness of 4 mm. Even then, the helium leak rate measurement showed that the helium was still busy leaking after 28 000 s and no steady state flux was reached. The agglomeration of the graphene was most likely the factor which limited the performance of the platelets. The glass flake filled multilayer samples displayed the best reduction of the helium leak rate and therefore could be used as a suitable coating to apply to the irradiated graphite waste to limit the release of radioactive gases, thereby achieving the objectives set out at the start of this research project.

6.7 RECOMMENDATIONS FOR FUTURE WORK

The following areas must still be evaluated to determine and improve the effectiveness of the composite coatings for actual application for irradiated graphite waste,

- Use of larger graphene flakes may improve the helium barrier properties.
- Radiation resistance.
- Actual tritium permeation measurements need to be performed on the composite epoxy resin coatings.

- Carbon dioxide and methane gas permeation measurements to show the leak rates of gases containing ^{14}C radionuclides.
- Chlorine gas permeation measurements to show the release of gases containing ^{36}Cl radionuclides from graphite waste.

REFERENCES

Aegerter, M.A. & Mennig, M. (2004) *Sol-gel technologies for glass producers and users*. Springer. Available from: <http://books.google.co.za/books/about/Sol_gel_technologies_for_glass_producers.html?id=ONBNBdPyuzAC&redir_esc=y> [Accessed 9 February 2012].

Aiello, A., Ciampichetti, A. & Benamati, G. (2004) An overview on tritium permeation barrier development for WCLL blanket concept. *Journal of Nuclear Materials*, 329–333, Part B (0), pp.1398-1402.

Amanat, N., Nicoll, A.F., Ruys, A.J., McKenzie, D.R. & James, N.L. (2011) Gas permeability reduction in PEEK film: Comparison of tetrahedral amorphous carbon and titanium nanofilm coatings. *Journal of Membrane Science*, 378 (1–2), pp.265-271.

Arepalli, S., Freiman, S.W., Hooker, S.A. & Migler, K.D. (2008) Measurement Issues in Single-Wall Carbon Nanotubes. *NIST SP*, 0 (960.19), p.78.

ASTM (2009a) Section fifteen: General products, Chemical specialties, andend use products. In: *Annual book of ASTM standards*. ASTM International Standards Worldwide.

ASTM (2009b) Section six: Paints, Related coatings and aromatics. In: *Annual book of ASTM standards*. ASTM International Standards Worldwide.

Beeslaar, F. (2012) DAC for certain radionuclides. Personal correspondence, radiation protection officer,Necsa.

Benamati, G., Chabrol, C., Perujo, A., Rigal, E. & Glasbrenner, H. (1999) Development of tritium permeation barriers on Al base in Europe. *Journal of Nuclear Materials*, 271–272 (0), pp.391-395.

Berg, J.C. (2009) *An introduction to interfaces & colloids: the bridge to nanoscience*. World Scientific.

Bharadwaj, R.K. (2001) Modeling the Barrier Properties of Polymer-Layered Silicate Nanocomposites. *Macromolecules*, 34 (26), pp.9189-9192.

Bhattacharya, M., Biswas, S. & Bhowmick, A.K. (2011) Permeation characteristics and modeling of barrier properties of multifunctional rubber nanocomposites. *Polymer*, 52 (7), pp.1562-1576.

Black, R. (2006) 'Deep disposal' for nuclear waste. *BBC*. Available from: <http://news.bbc.co.uk/2/hi/science/nature/4949096.stm#map> [Accessed 27 January 2012].

Bucknall, D.G. (2004) Influence of interfaces on thin polymer film behaviour. *Progress in Materials Science*, 49 (5), pp.713-786.

Bushuev, A.V., Verzilov, Y.M., Zubarev, V.N., Kachanovskii, A.E., Matveev, O.V., Proshin, I.M., Bidulya, L.V., Ivanov, A.A. & Kalugin, A.K. (1992) Quantitative determination of the amount of3H and14C in reactor graphite. *Atomic Energy*, 73 (6), pp.959-962.

Causey, R.A. & Wampler, W.R. (1995) The use of silicon carbide as a tritium permeation barrier. *Journal of Nuclear Materials*, 220–222 (0), pp.823-826.

Choudalakis, G. & Gotsis, A.D. (2009) Permeability of polymer/clay nanocomposites: A review. *European Polymer Journal*, 45 (4), pp.967-984.

Ciba Geigy (1991) Provisional data sheet: Laminating resin LY 5082.

Clifford, J. (2010) Sellafield Ltd._Windscale Piles Decommissioning Project.

Costes, J.R., de Tassigny, C. & Vidal, H. (1990) Conditioning of graphite bricks from dismantled gas-cooled reactors for disposal. *Waste Management*, 10 (4), pp.297-302.

Cozmuta, I., Blanco, M. & Goddard, W.A. (2007) Gas Sorption and Barrier Properties of Polymeric Membranes from Molecular Dynamics and Monte Carlo Simulations. *J. Phys. Chem. B*, 111 (12), pp.3151-3166.

Davenas, J., Stevenson, I., Celette, N., Cambon, S., Gardette, J.L., Rivaton, A. & Vignoud, L. (2002) Stability of polymers under ionising radiation: The many faces of radiation interactions with polymers. *Nuclear Instruments and Methods in Physics Research Section B: Beam Interactions with Materials and Atoms*, 191 (1–4), pp.653-661.

Demange, D., Grivet, M., Pialot, H. & Chambaudet, A. (2002) Indirect Tritium Determination by an Original 3He Ingrowth Method Using a Standard Helium Leak Detector Mass Spectrometer. *Anal. Chem.*, 74 (13), pp.3183-3189.

DeRocher, J.P., Gettelfinger, B.T., Wang, J., Nuxoll, E.E. & Cussler, E.L. (2005) Barrier membranes with different sizes of aligned flakes. *Journal of Membrane Science*, 254 (1–2), pp.21-30.

Disdier, S., Rey, J.M., Pailler, P. & Bunsell, A.R. (1998) Helium permeation in composite materials for cryogenic application. *Cryogenics*, 38 (1), pp.135-142.

Duffó, G.S., Farina, S.B., Schulz, F.M. & Marotta, F. (2010) Corrosion susceptibility of steel drums containing cemented intermediate level nuclear wastes. *Journal of Nuclear Materials*, 405 (3), pp.274-279.

Dumont, M.-J., Reyna-Valencia, A., Emond, J.-P. & Bousmina, M. (2007) Barrier properties of polypropylene/organoclay nanocomposites. *Journal of Applied Polymer Science*, 103 (1), pp.618-625.

ElBaradei, M. (2003) Geological Repositories: The Last Nuclear Frontier [Internet]. Available from: <http://www.iaea.org/newscenter/statements/2003/ebsp2003n028.html> [Accessed 27 January 2012].

El-Hussein, A. (2005) A study on natural radiation exposure in different realistic living rooms. *Journal of Environmental Radioactivity*, 79 (3), pp.355-367.

Frounchi, M., Dadbin, S., Salehpour, Z. & Noferesti, M. (2006) Gas barrier properties of PP/EPDM blend nanocomposites. *Journal of Membrane Science*, 282 (1–2), pp.142-148.

George, S.C. & Thomas, S. (2001) Transport phenomena through polymeric systems. *Progress in Polymer Science*, 26 (6), pp.985-1017.

González-Guzmán, J., Santana, J.J., González, S. & Souto, R.M. (2010) Resistance of metallic substrates protected by an organic coating containing glass flakes. *Progress in Organic Coatings*, 68 (3), pp.240-243.

Grevoz, A. (2005) Disposal of Low Activity Radioactive Waste Proceedings of an International Symposium held in Cordoba, 13-17 December 2004. In: *International Atomic Energy Agency*. Cordoba, International Atomic Energy Agency, p.478. Available from: <http://www-pub.iaea.org/books/IAEABooks/7271/Disposal-of-Low-Activity-Radioactive-Waste-Proceedings-of-an-International-Symposium-held-in-Cordoba-13-17-December-2004> [Accessed 27 January 2012].

Guikai, Z., Ju, L., Chang'an, C., Sanping, D. & Guoping, L. (2011) Tritium permeation barrier-aluminized coating prepared by Al-plating and subsequent oxidation process. *Journal of Nuclear Materials*, 417 (1–3), pp.1245-1248.

Guo, J. & Barbari, T.A. (2009) Unified Dual Mode Description of Small Molecule Sorption and Desorption Kinetics in a Glassy Polymer. *Macromolecules*, 42 (15), pp.5700-5708.

Gupta, M., Lin, Y., Deans, T., Baer, E., Hiltner, A. & Schiraldi, D.A. (2010) Structure and Gas Barrier Properties of Poly(propylene-graft-maleic anhydride)/Phosphate Glass Composites Prepared by Microlayer Coextrusion. *Macromolecules*, 43 (9), pp.4230-4239.

Gupta, M., Lin, Y., Deans, T., Crosby, A., Baer, E., Hiltner, A. & Schiraldi, D.A. (2009) Biaxially oriented poly(propylene-g-maleic anhydride)/phosphate glass composite films for high gas barrier applications. *Polymer*, 50 (2), pp.598-604.

Hennessy, B.J., Stening, T.C., Mead, J.A. & Plastics Institute, L. (1966) *Permeability of Plastics Films, By B. J. Hennessy, J.A. Mead And T.C. Stening*. Available from: <http://books.google.co.za/books?id=BCTwcQAACAAJ>.

Herring, H.M. (2003) *Characterization of Thin Film Polymers Through Dynamic Mechanical Analysis and Permeation*. NASA. Available from: <http://ntrs.nasa.gov/search.jsp?R=20030063899&hterms=Characterization+Thin+Film+Polymers+Through+Dynamic+Mechanical+Analysis+Permeation&qs=Ntx%3Dmode%2520matchallpartial%2520%26Ntk%3DAll%26N%3D0%26Ntt%3DCharacterization%2520of%2520Thin%2520Film%2520Polymers%2520Through%2520Dynamic%2520Mechanical%2520Analysis%2520and%2520Permeation> [Accessed 25 January 2012].

Hoffman, E.N. & Skidmore, T.E. (2009) Radiation effects on epoxy/carbon-fiber composite. *Journal of Nuclear Materials*, 392 (2), pp.371-378.

Humpenöder, J. (1998) Gas permeation of fibre reinforced plastics. *Cryogenics*, 38 (1), pp.143-147.

IAEA (2006) Characterization, Treatment and Conditioning of Radioactive Graphite from Decommissioning of Nuclear Reactors. Available from: <http://www-pub.iaea.org/MTCD/publications/PubDetails.asp?pubId=7579>.

IAEA (2008) Disposal Aspects of Low and Intermediate Level Decommissioning Waste. Available from: <http://www-pub.iaea.org/books/IAEABooks/7778/Disposal-Aspects-of-Low-and-Intermediate-Level-Decommissioning-Waste> [Accessed 1 February 2012].

ICRP (1996) Age-dependent dose to members of the public from intake of radionuclides: Part 5 compilation of ingestion and inhalation dose coefficients. *Annals of the ICRP*, 26 (1), pp.1-91.

ICRP (1997) Discussion. *Annals of the ICRP*, 27 (3–4), pp.1-161.

Iwai, Y., Hayashi, T., Kobayashi, K. & Nishi, M. (2001) Simulation study of intentional tritium release experiments in the caisson assembly for tritium safety at the TPL/JAERI. *Fusion Engineering and Design*, 54 (3–4), pp.523-535.

Jana, S.C. & Jain, S. (2001) Dispersion of nanofillers in high performance polymers using reactive solvents as processing aids. *Polymer*, 42 (16), pp.6897-6905.

Kalaitzidou, K., Fukushima, H. & Drzal, L.T. (2007) Multifunctional polypropylene composites produced by incorporation of exfoliated graphite nanoplatelets. *Carbon*, 45 (7), pp.1446-1452.

Kim, H., Abdala, A.A. & Macosko, C.W. (2010) Graphene/Polymer Nanocomposites. *Macromolecules*, 43 (16), pp.6515-6530.

Kim, H. & Macosko, C.W. (2009) Processing-property relationships of polycarbonate/graphene composites. *Polymer*, 50 (15), pp.3797-3809.

Kim, H.M., Lee, J.K. & Lee, H.S. (2011) Transparent and high gas barrier films based on poly(vinyl alcohol)/graphene oxide composites. *Thin Solid Films*, 519 (22), pp.7766-7771.

Kim, J.K. & Ma, P.C. (2011) *Carbon Nanotubes for Polymer Reinforcement*. Taylor & Francis. Available from: <http://books.google.co.za/books?id=Mw3dIJE7uJcC>.

Kotsilkova, R. & Pissis, P. (2007) *Thermoset Nanocomposites for Engineering Applications*. Smithers Rapra Technology. Available from: <http://books.google.co.za/books?id=uGyekcHA5AMC>.

Kotz, J.C., Treichel, P. & Harman, P. (2003) *Chemistry and chemical reactivity*. Thomson-Brooks/Cole. Available from: <http://books.google.co.za/books?id=pz1CAQAAIAAJ>.

Lape, N.K., Nuxoll, E.E. & Cussler, E.L. (2004) Polydisperse flakes in barrier films. *Journal of Membrane Science*, 236 (1–2), pp.29-37.

von Lenza, W. (2009) Carbowaste Home [Internet]. Available from: <http://www.carbowaste.eu//home> [Accessed 25 January 2012].

Lomax, M. (1980) Permeation of gases and vapours through polymer films and thin sheet—part I. *Polymer Testing*, 1 (2), pp.105-147.

Magielsen, A.J., Bakker, K., Chabrol, C., Conrad, R., van der Laan, J.G., Rigal, E. & Stijkel, M.P. (2002) In-pile performance of a double-walled tube and a tritium permeation barrier. *Journal of Nuclear Materials*, 307–311, Part 1 (0), pp.832-836.

McGann, O.J. & Ojovan, M.I. (2011) The synthesis of graphite–glass composites intended for the immobilisation of waste irradiated graphite. *Journal of Nuclear Materials*, 413 (1), pp.47-52.

Minelli, M., Baschetti, M.G. & Doghieri, F. (2011) A comprehensive model for mass transport properties in nanocomposites. *Journal of Membrane Science*, 381 (1–2), pp.10-20.

Molyneux, P. (2001) 'Transition-site' model for the permeation of gases and vapors through compact films of polymers. *Journal of Applied Polymer Science*, 79 (6), pp.981-1024.

Mortley, A., Bonin, H.W. & Bui, V.T. (2008) Radiation effects on polymers for coatings on copper canisters used for the containment of radioactive materials. *Journal of Nuclear Materials*, 376 (2), pp.192-200.

Muller, K., Botos, J., Bastian, M., Heidemeyer, P. & Hochrein, T. (2011) Faster Results. *Kunststoffe international*, pp.62-67.

Nematollahi, M., Heidarian, M., Peikari, M., Kassiriha, S.M., Arianpouya, N. & Esmaeilpour, M. (2010) Comparison between the effect of nanoglass flake and montmorillonite organoclay on corrosion performance of epoxy coating. *Corrosion Science*, 52 (5), pp.1809-1817.

Nielsen, K.L.C., Hill, D.J.T., Watson, K.A., Connell, J.W., Ikeda, S., Kudo, H. & Whittaker, A.K. (2008) The radiation degradation of a nanotube–polyimide nanocomposite. *Polymer Degradation and Stability*, 93 (1), pp.169-175.

O'Neill, A., Khan, U., Nirmalraj, P.N., Boland, J. & Coleman, J.N. (2011) Graphene Dispersion and Exfoliation in Low Boiling Point Solvents. *J. Phys. Chem. C*, 115 (13), pp.5422-5428.

Ogasawara, T., Ishida, Y., Ishikawa, T., Aoki, T. & Ogura, T. (2006) Helium gas permeability of montmorillonite/epoxy nanocomposites. *Composites Part A: Applied Science and Manufacturing*, 37 (12), pp.2236-2240.

Padinger, F., Brabec, C., Fromherz, T., Hummelen, J. & Sariciftci, N. (2000) Fabrication of large area photovoltaic devices containing various blends of polymer and fullerene derivatives by using the doctor blade technique. *Optoelectronics review*, (4), pp.280–283.

Park, S., An, J., Jung, I., Piner, R.D., An, S.J., Li, X., Velamakanni, A. & Ruoff, R.S. (2009) Colloidal Suspensions of Highly Reduced Graphene Oxide in a Wide Variety of Organic Solvents. *Nano Lett.*, 9 (4), pp.1593-1597.

Petrie, E.M. (2006) *Epoxy adhesive formulations*. McGraw-Hill Prof Med/Tech. Available from: <http://books.google.co.za/books?id=738MPfO5FEkC&printsec=frontcover&dq=epoxy+adhesive+formulations+by+Edward+Petrie&hl=en&sa=X&ei=RfgiT-W7LYuF-wb2j63VCA&ved=0CEAQ6AEwAA#v=onepage&q=epoxy%20adhesive%20formulations%20by%20Edward%20Petrie&f=false>.

Philibert, J. (2006) One and a half century of diffusion: Fick, Einstein, before and beyond. *Diffusion Fundamentals: Basic Principles of Theory, Experiment and Application - Online Journal*, 4 (6.1-6.19). Available from: <www.uni-leipzig.de/diffusion/pdf/volume4/diff_fund_4(2006)6.pdf> [Accessed 28 January 2012].

Potts, J.R., Dreyer, D.R., Bielawski, C.W. & Ruoff, R.S. (2011) Graphene-based polymer nanocomposites. *Polymer*, 52 (1), pp.5-25.

Qian, G., Cho, J.W. & Lan, T. (2001) Nanocor | Technical Papers | Preparation and Properties of Polyolefin Nanocomposites [Internet]. Available from: <http://www.nanocor.com/tech_papers/properties_polyolefin.asp> [Accessed 28 January 2012].

Rice, P. Charging effects on SEM images [Internet]. Available from: <ncf.colorado.edu/instdocs/quickguides/SEM-ChargingEffects.pdf> [Accessed 7 February 2012].

Rogers, W.A., Buritz, R.S. & Alpert, D. (1954) Diffusion Coefficient, Solubility, and Permeability for Helium in Glass. *Journal of Applied Physics*, 25 (7), pp.868-875.

dos Santos, J.M.F. (2005) Simple vacuum experiments for undergraduate student laboratories. *Vacuum*, 80 (1–3), pp.258-263.

Schultheiß, D. (2007) Permeation Barrier for Lightweight Liquid Hydrogen Tanks. University of Augsburg. Available from: <http://opus.bibliothek.uni-augsburg.de/volltexte/2007/683/> [Accessed 25 January 2012].

Singh, V., Joung, D., Zhai, L., Das, S., Khondaker, S.I. & Seal, S. (2011) Graphene based materials: Past, present and future. *Progress in Materials Science*, 56 (8), pp.1178-1271.

Spitsyn, A., Pisarev, A., Skovoroda, A., Gureev, V. & Martynenko, Y. (2007) Permeation of hydrogen through MPG-8 graphite. *Journal of Nuclear Materials*, 363–365 (0), pp.833-838.

Stankovich, S., Dikin, D.A., Dommett, G.H.B., Kohlhaas, K.M., Zimney, E.J., Stach, E.A., Piner, R.D., Nguyen, S.T. & Ruoff, R.S. (2006) Graphene-based composite materials. *Nature*, 442 (7100), pp.282-286.

Struers Struers [Internet]. Available from: <http://www.struers.com/modules/emetalog/login.asp> [Accessed 28 January 2012].

Takahashi, S., Goldberg, H.A., Feeney, C.A., Karim, D.P., Farrell, M., O'Leary, K. & Paul, D.R. (2006) Gas barrier properties of butyl rubber/vermiculite nanocomposite coatings. *Polymer*, 47 (9), pp.3083-3093.

UK Nirex Limited (2005) WPS/901 Guidance Note on the Use of Organic Polymers for the Encapsulation of Intermediate Level Waste: Review of Candidate Materials. Available from: <http://www.nda.gov.uk/documents/biblio/detail.cfm?fuseaction=search.view_doc&doc_id=5337> [Accessed 27 January 2012].

University of Manchester Waste Management: Dalton Nuclear Institute [Internet]. Available from: <http://www.dalton.manchester.ac.uk/our-research/waste-management/> [Accessed 27 January 2012].

Varian Vacuum Products (1995) Introduction to Helium mass spectrometer leak detection. Available from: <http://www.chem.agilent.com/Library/training/Public/Introduction_to_Helium_Mass_Spectrometer_Leak_Detection.pdf> [Accessed 27 January 2012].

Vemulapalli, G.K. & Vemulapalli, K.G. (1993) *Physical Chemistry*. Prentice Hall. Available from: <http://books.google.co.za/books?id=cuniAQAACAAJ>.

Vignoud, Lionel, David, L., Sixou, B., Vigier, G. & Stevenson, Isabelle (2001) Effect of electron irradiation on the mechanical properties of DGEBA/DDM epoxy resins. *Nuclear Instruments and Methods in Physics Research Section B: Beam Interactions with Materials and Atoms*, 185 (1–4), pp.336-340.

Wikipedia (2007) File:Magnox reactor schematic.svg - Wikipedia, the free encyclopedia [Internet]. Available from: <http://en.wikipedia.org/wiki/File:Magnox_reactor_schematic.svg> [Accessed 3 February 2012].

Wikipedia (2008) File:RBMK reactor schematic.svg - Wikipedia, the free encyclopedia [Internet]. Available from: <http://en.wikipedia.org/wiki/File:RBMK_reactor_schematic.svg> [Accessed 3 February 2012].

Wu, H. & Drzal, L.T. (2012) Graphene nanoplatelet paper as a light-weight composite with excellent electrical and thermal conductivity and good gas barrier properties. *Carbon*, 50 (3), pp.1135-1145.

Wu, Z.X., Zhang, H., Yang, H.H., Chu, X.X. & Li, L.F. (2010) Novel radiation-resistant glass fiber/epoxy composite for cryogenic insulation system. *Journal of Nuclear Materials*, 403 (1–3), pp.117-120.

Yamaguchi, K., Suzuki, Y., Tanaka, S. & Yamawaki, M. (1991) Effect of coatings on the hydrogen permeability of graphite. *Journal of Nuclear Materials*, 179–181, Part 1 (0), pp.242-245.

Yamanishi, T., Hayashi, Takumi, Kawamura, Y., Nakamura, H., Iwai, Yasunori, Kobayashi, Kazuhiro, Isobe, K., Suzuki, T. & Yamada, M. (2010) Recent activities on tritium technologies of BA DEMO-R&D program in JAEA. *Fusion Engineering and Design*, 85 (7–9), pp.1002-1006.

Yang, H.G., Zhan, Q., Zhao, W.W., Yuan, X.M., Hu, Y. & Han, Z.B. (2011) Study of an iron-aluminide and alumina tritium barrier coating. *Journal of Nuclear Materials*, 417 (1–3), pp.1237-1240.

Yao, X.F., Lei, Y.M., Xiong, C., Wang, X.Q. & Wang, Y.Q. (2010) Experimental Study on Damage-induced Helium Leakage in Flexible Composites. *Journal of Reinforced Plastics and Composites*, 29 (19), pp.2936 -2945.

Yasmin, A., Luo, J.-J. & Daniel, I.M. (2006) Processing of expanded graphite reinforced polymer nanocomposites. *Composites Science and Technology*, 66 (9), pp.1182-1189.

Yokozeki, T., Aoki, T. & Ishikawa, T. (2004) The effect of matrix cracks on gas permeability through CFRP laminates. *Advanced Composite Materials*, 13 (3), pp.227-236.

Yokozeki, T., Ogasawara, T., Aoki, T. & Ishikawa, T. (2009) Experimental evaluation of gas permeability through damaged composite laminates for cryogenic tank. *Composites Science and Technology*, 69 (9), pp.1334-1340.

Yokozeki, T., Ogasawara, T. & Ishikawa, T. (2006) Evaluation of gas leakage through composite laminates with multilayer matrix cracks: Cracking angle effects. *Composites Science and Technology*, 66 (15), pp.2815-2824.

Zhang, K. & Hatano, Y. (2011) Sealing of pores in sol–gel-derived tritium permeation barrier coating by electrochemical technique. *Journal of Nuclear Materials*, 417 (1–3), pp.1229-1232.

ANNEXURE A: MODEL FIT OF REFERENCE SAMPLES

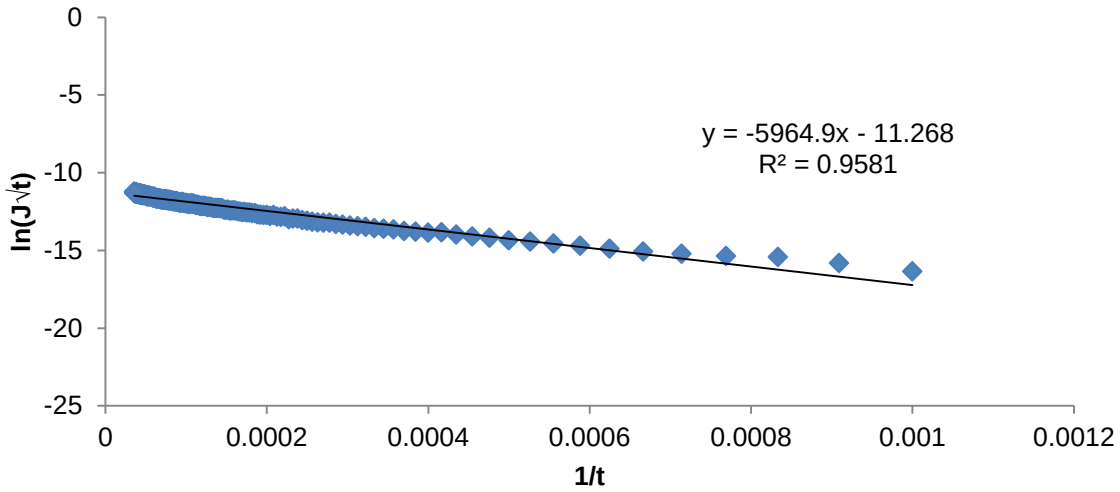

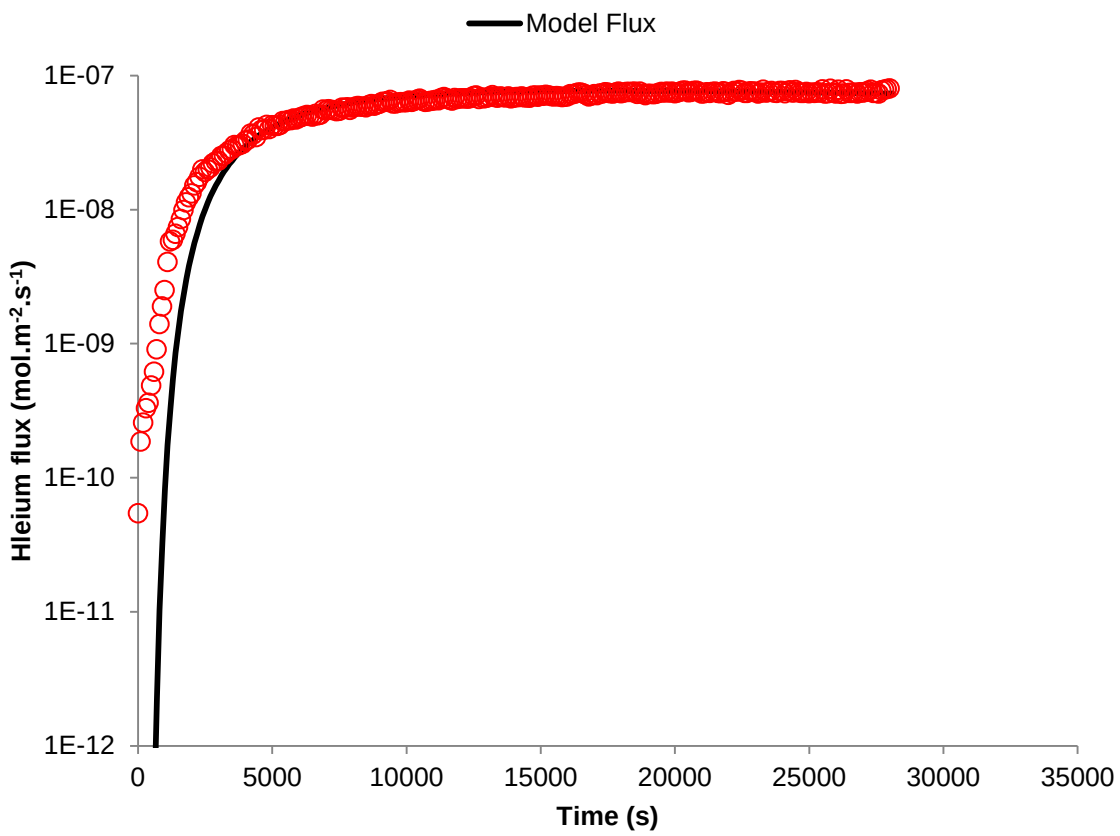

Figure A 1 Linear fit of trend line and measured flux vs. the theoretical model flux of the Araldite 01 reference sample

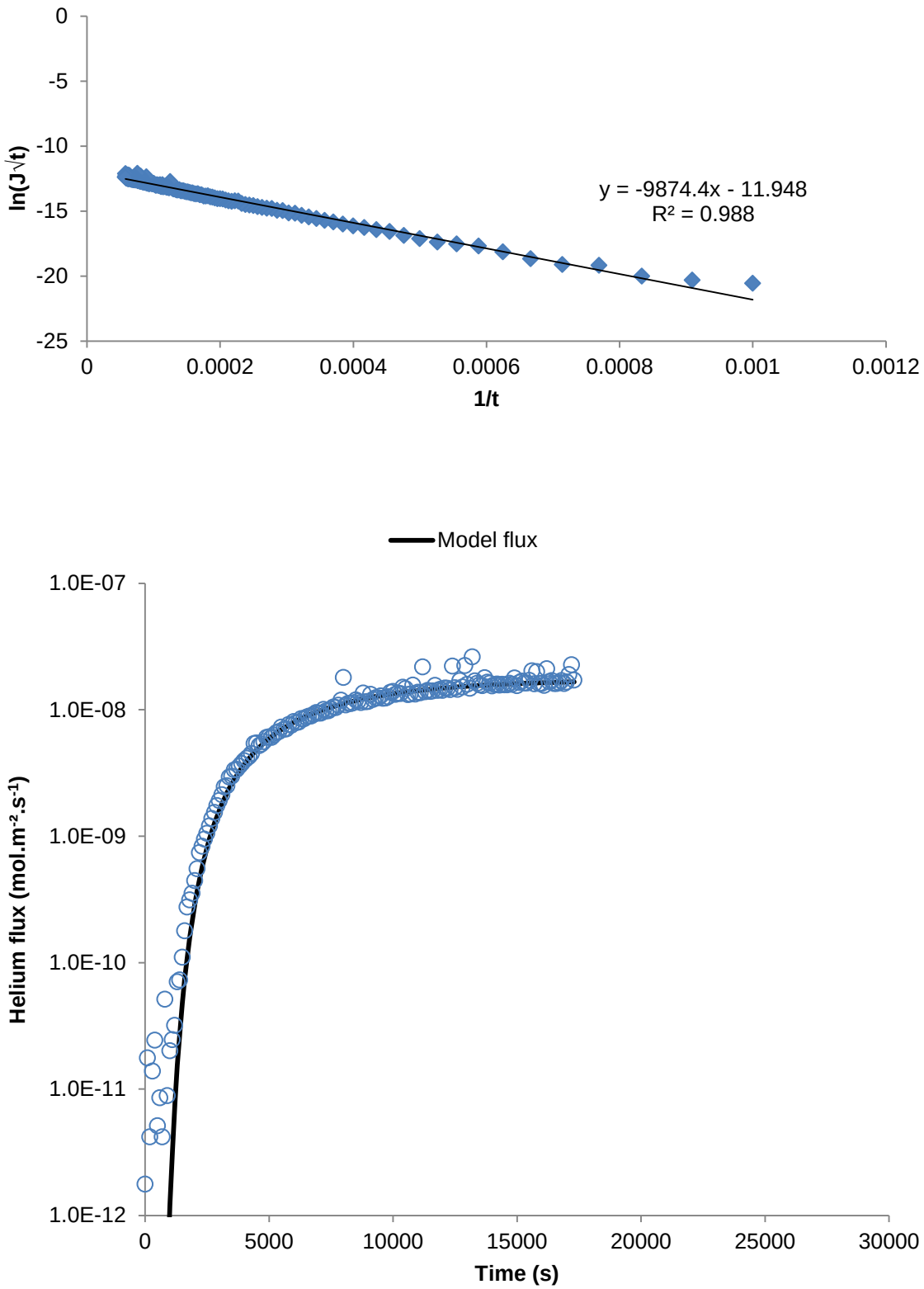

Figure A 2 Linear fit of trend line and measured flux vs. the theoretical model flux of the 0% Araldite reference sample

ANNEXURE B: MODEL FIT OF DOCTOR BLADE SHEET SAMPLES

B1 Graphene filled sheets

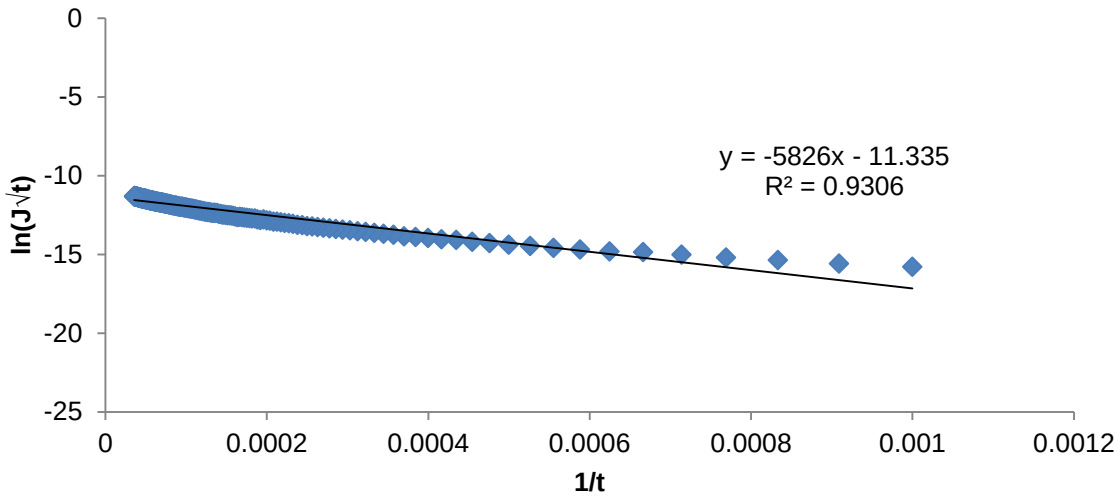

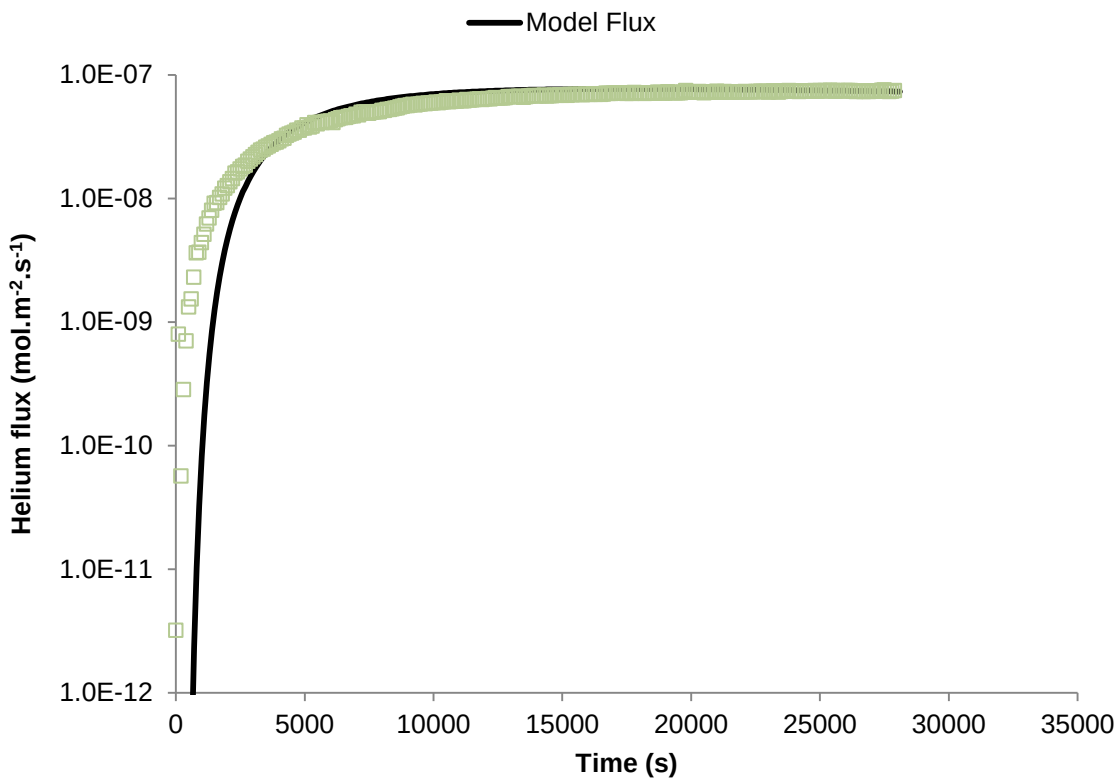

Figure B 1 Linear fit of trend line and measured flux vs. the theoretical model flux of the sample mixed in the ultrasonic bath with 1 wt% graphene

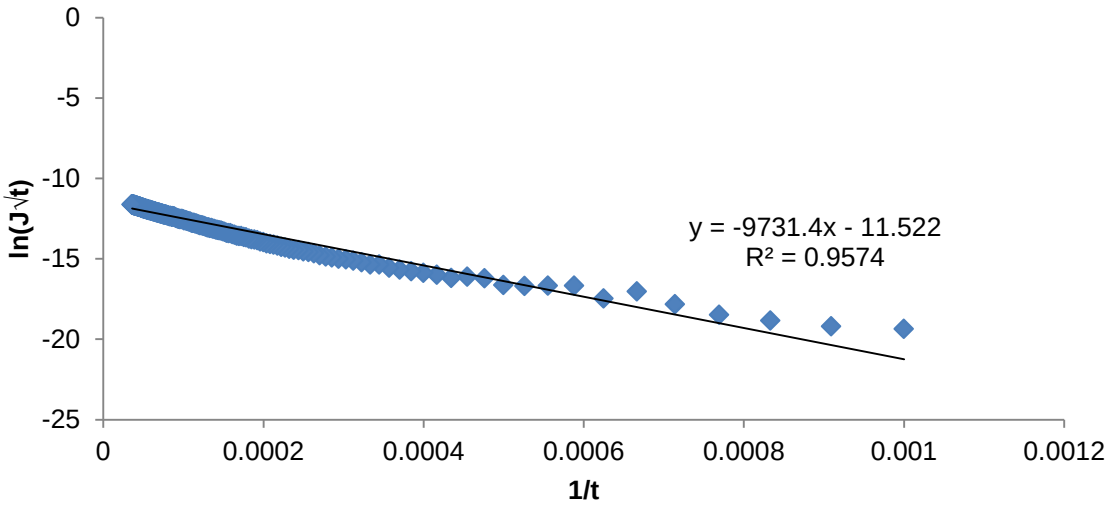

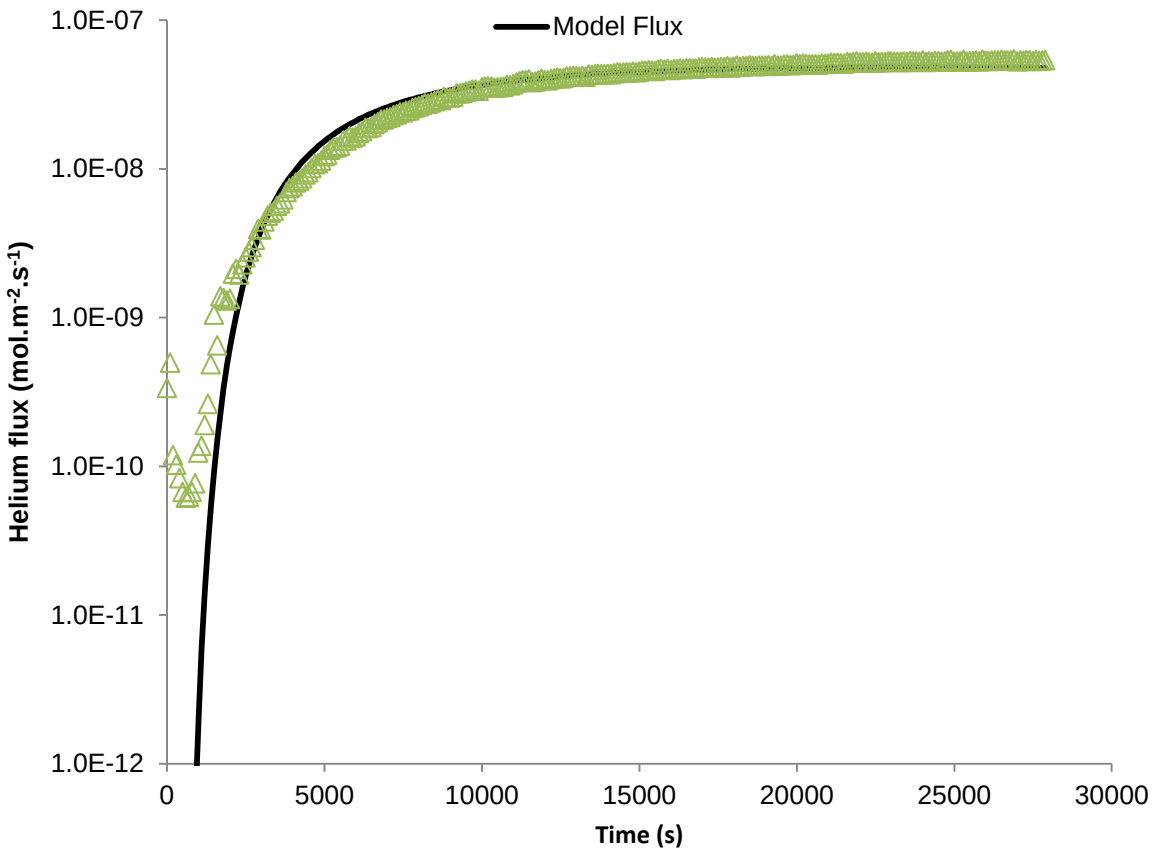

Figure B 2 Linear fit of trend line and measured flux vs. the theoretical model flux sample mixed by hand with 1 wt% graphene

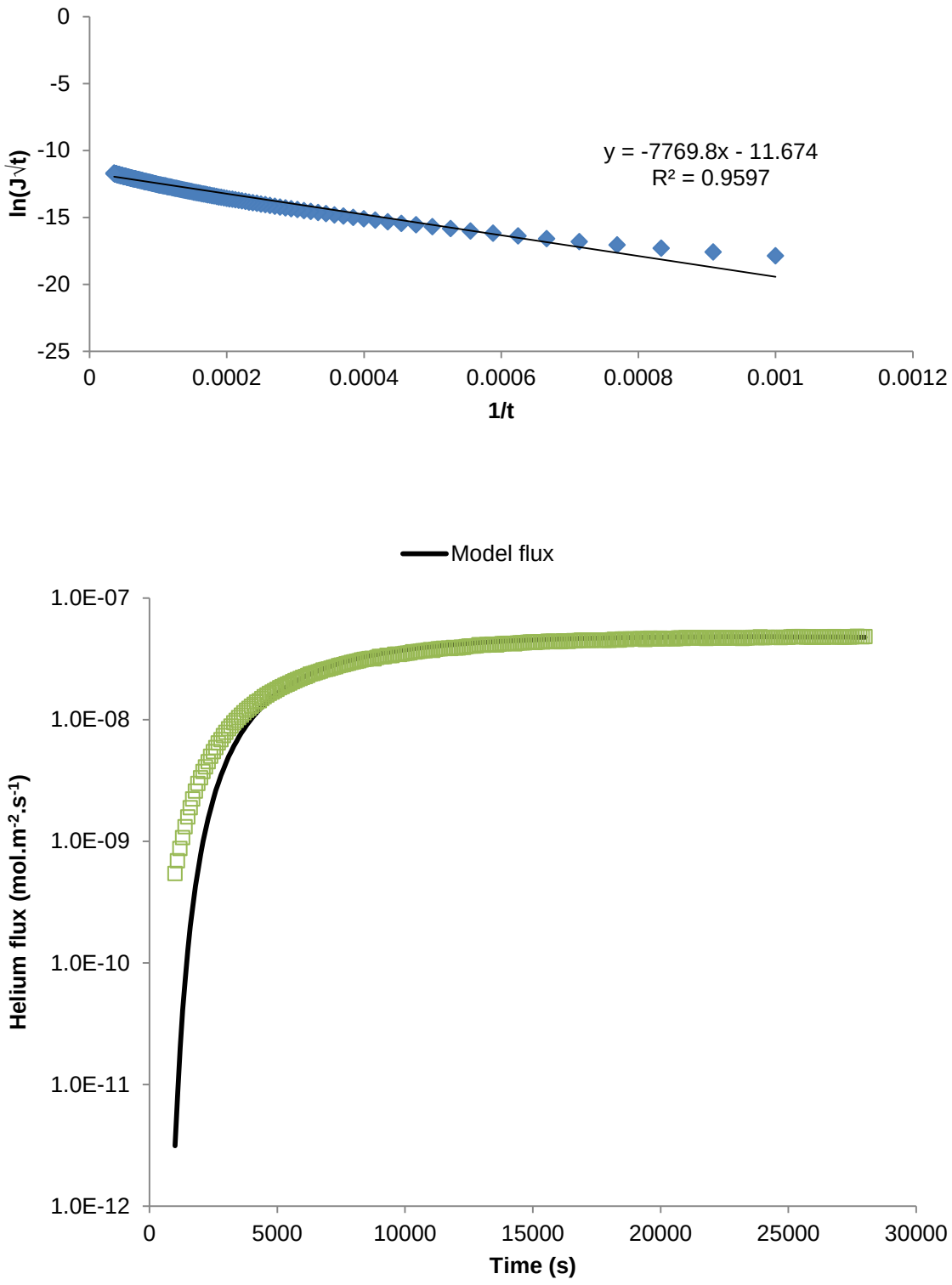

Figure B 3 Linear fit of trend line and measured flux vs. the theoretical model flux of the sample mixed with the blender with 1 wt% graphene

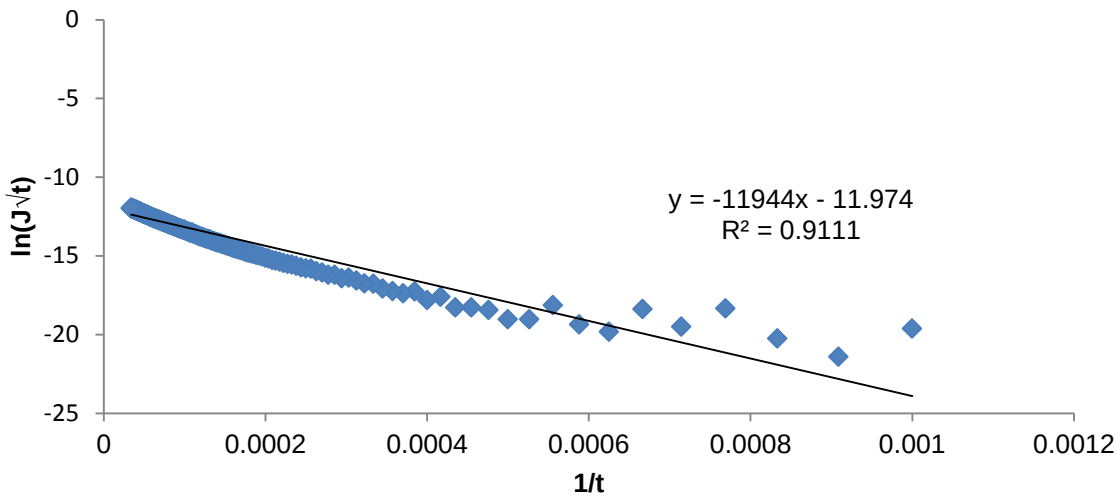

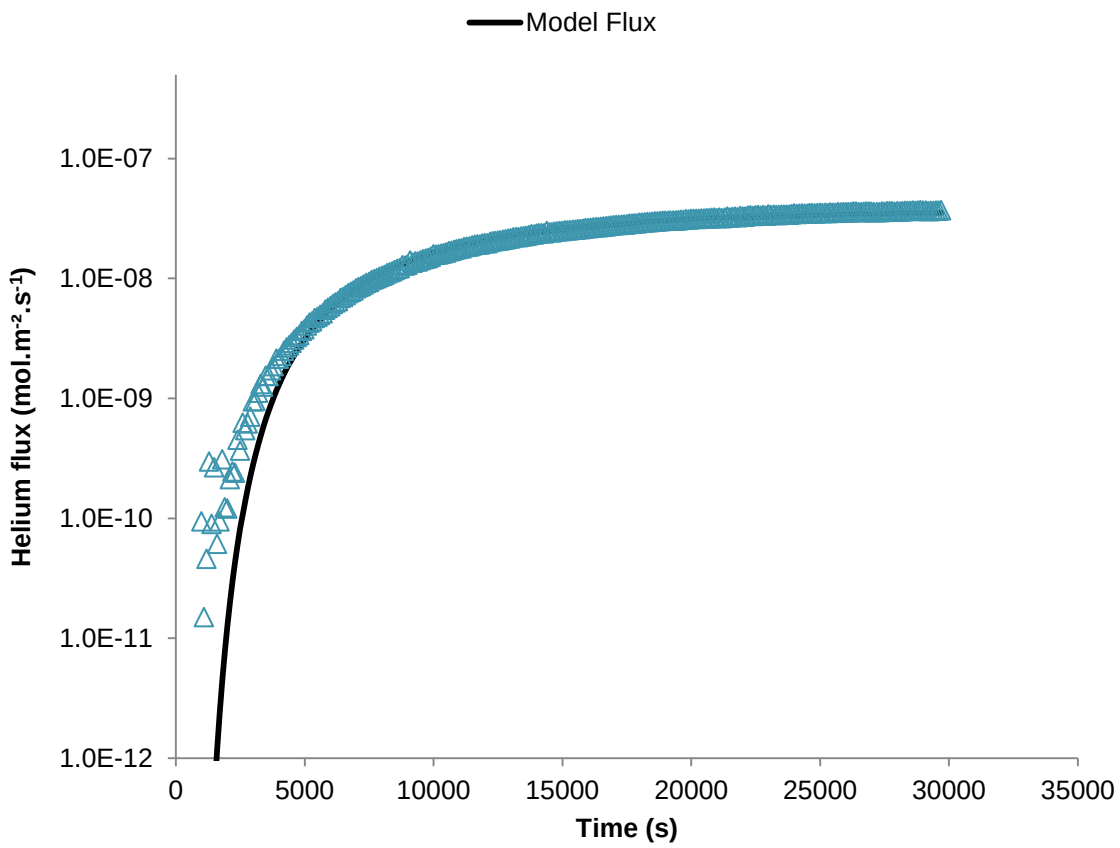

Figure B 4 Linear fit of trend line and measured flux vs. the theoretical model flux of the sample mixed with the blender with 2 wt% graphene

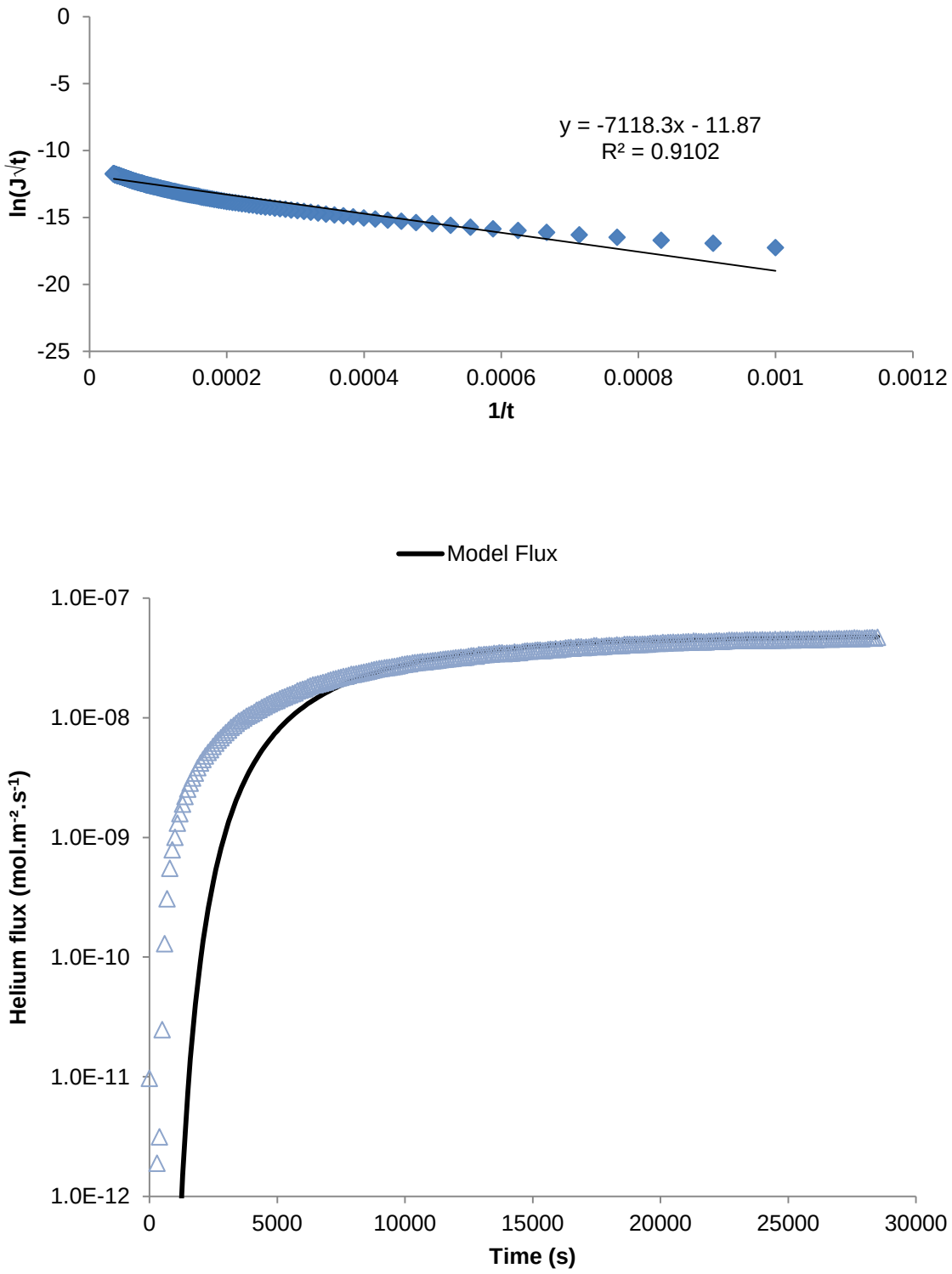

Figure B 5 Linear fit of trend line and measured flux vs. the theoretical model flux of the sample mixed with the blender with 3 wt% graphene

B.2 Glass Flake filled sheets

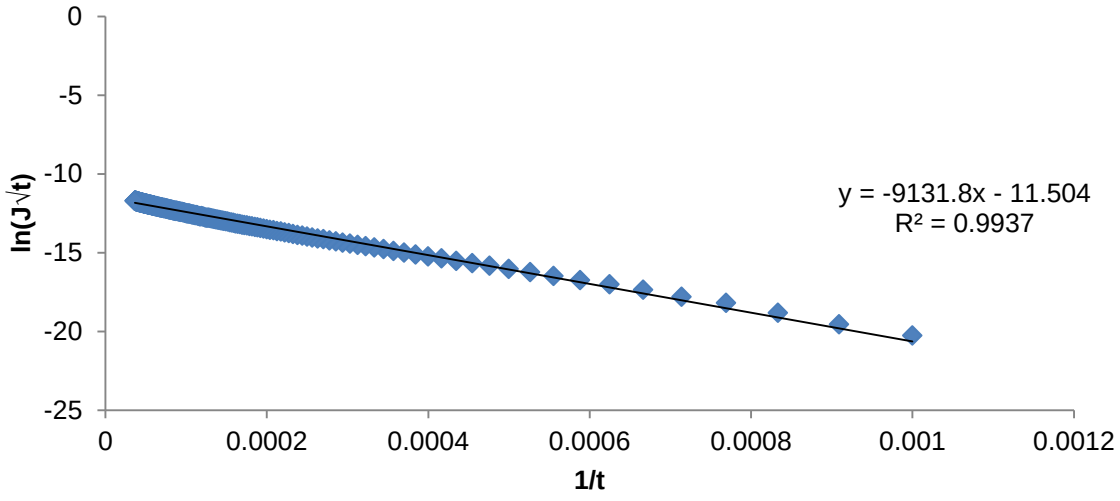

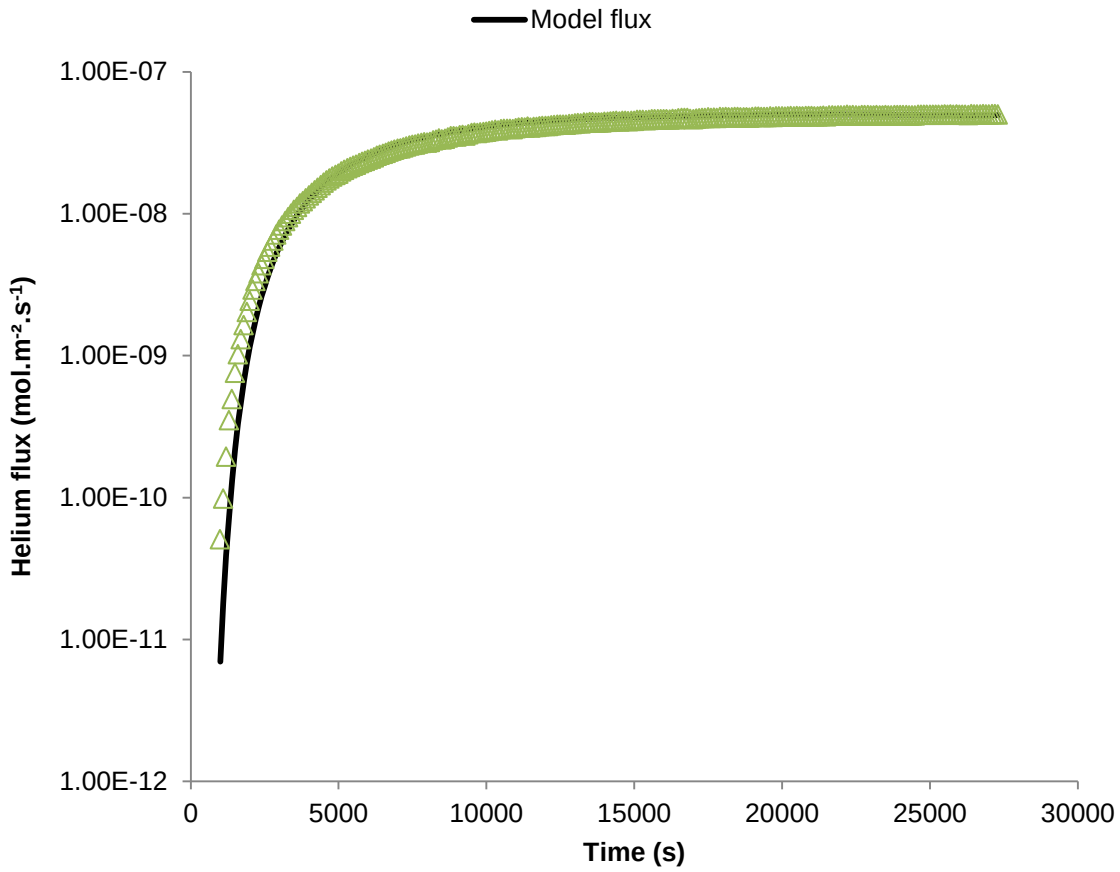

Figure B 6 Linear fit of trend line and measured flux vs. the theoretical model flux of the glass flake 1 wt%

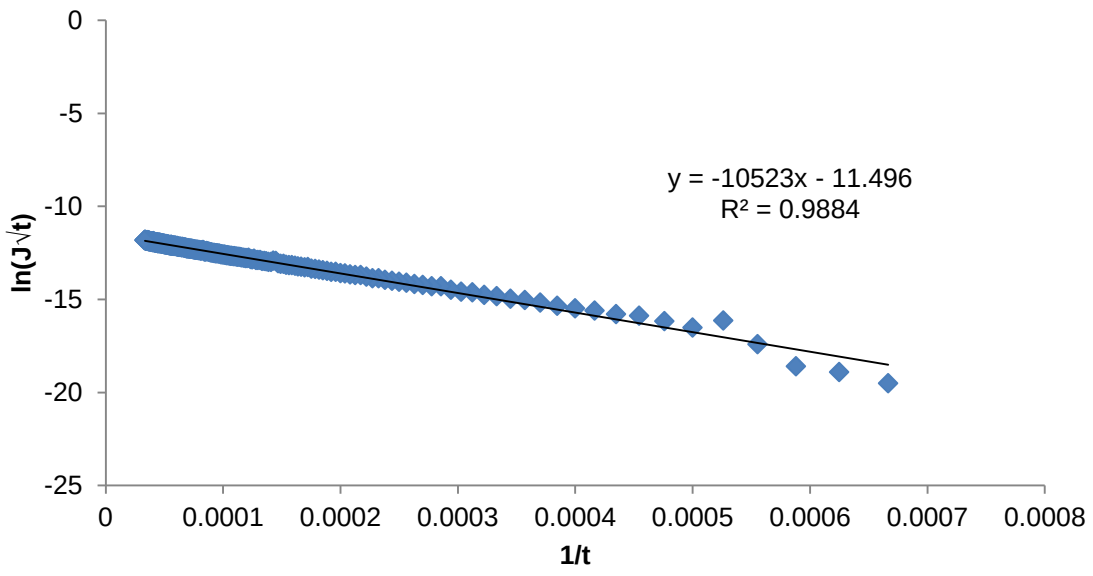

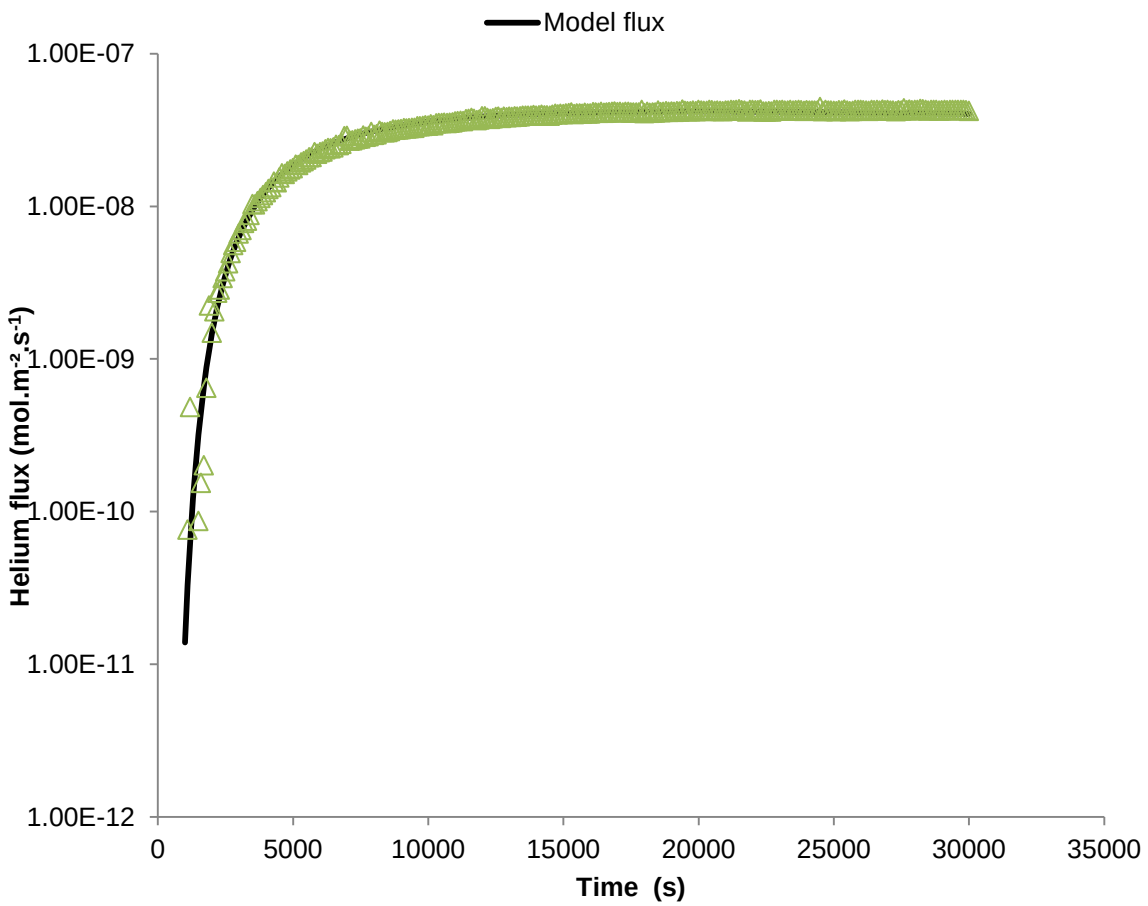

Figure B 7 Linear fit of trend line and measured flux vs. the theoretical model flux of the glass flake 3 wt% sheet

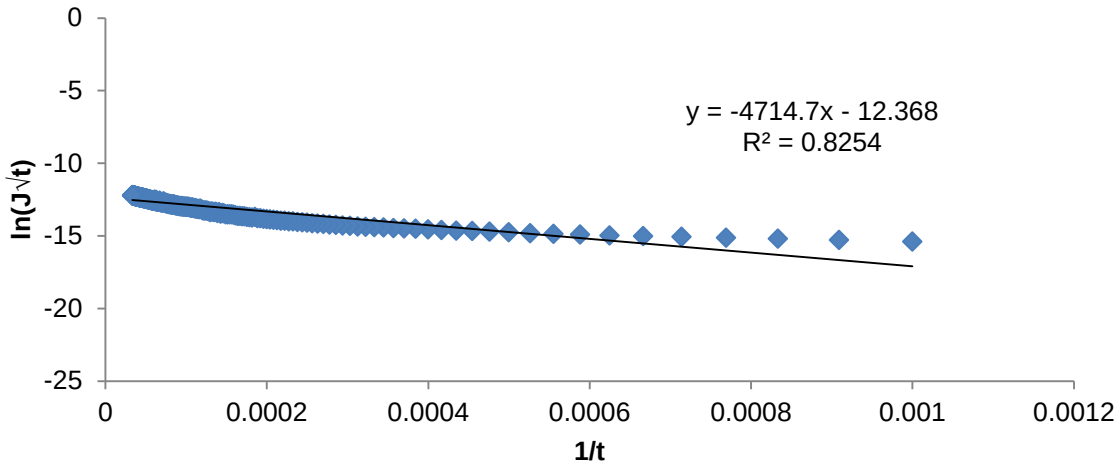

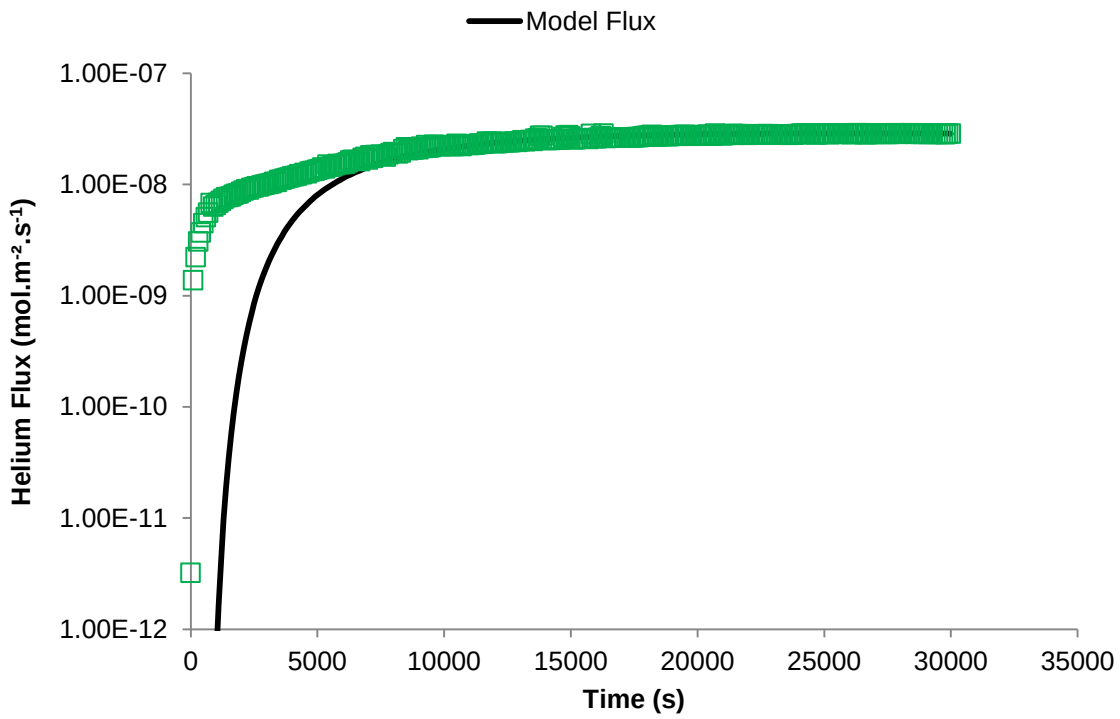

Figure B 8 Linear fit of trend line and measured flux vs. the theoretical model flux of the glass flake 6 wt% sheet

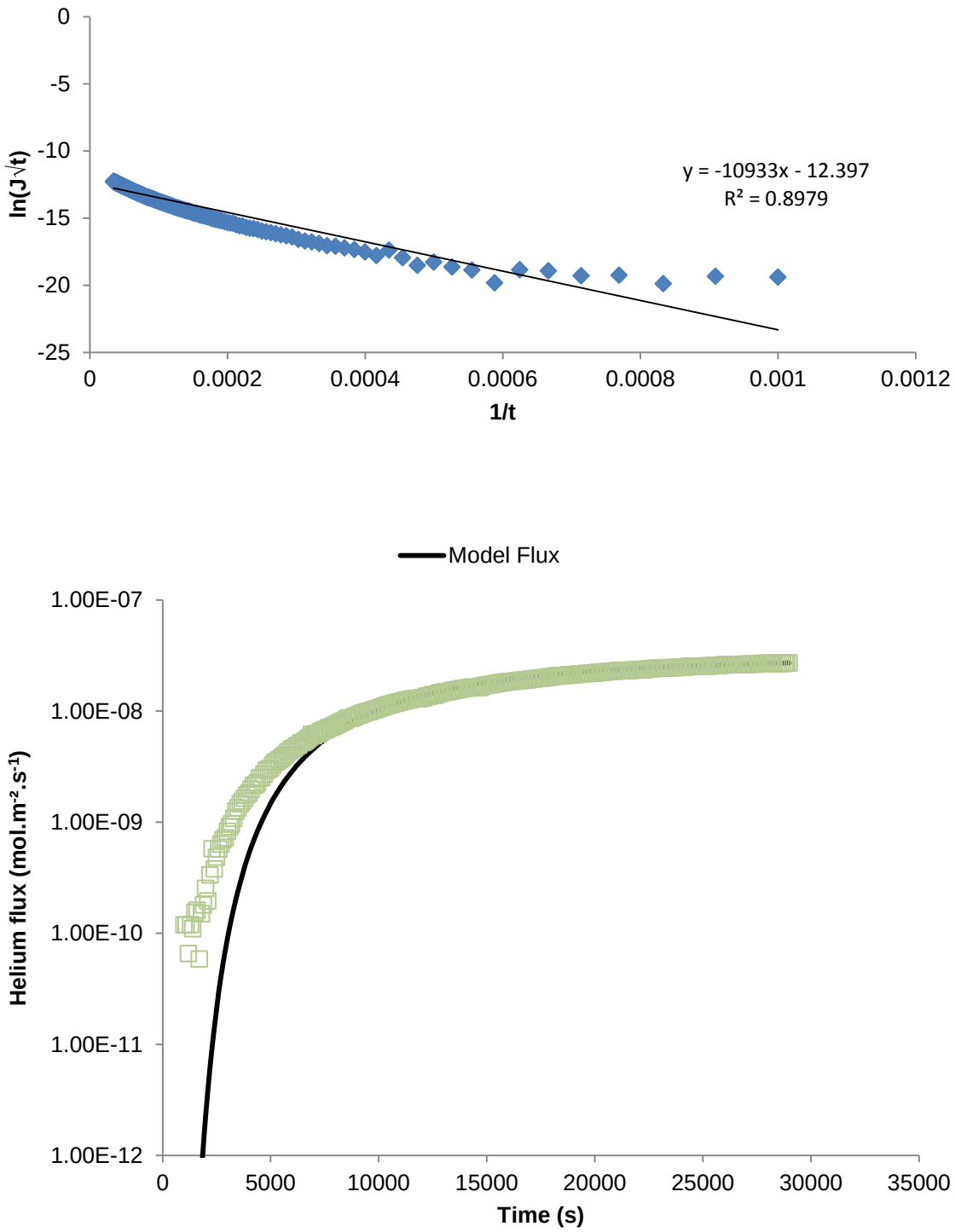

Figure B 9 Linear fit of trend line and measured flux vs. the theoretical model flux of the glass flake 10 wt% sheet

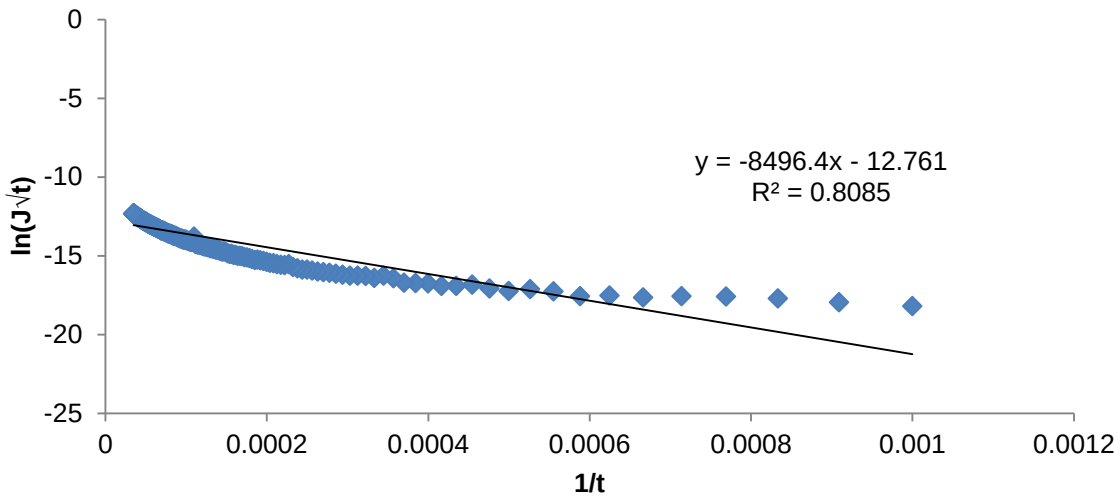

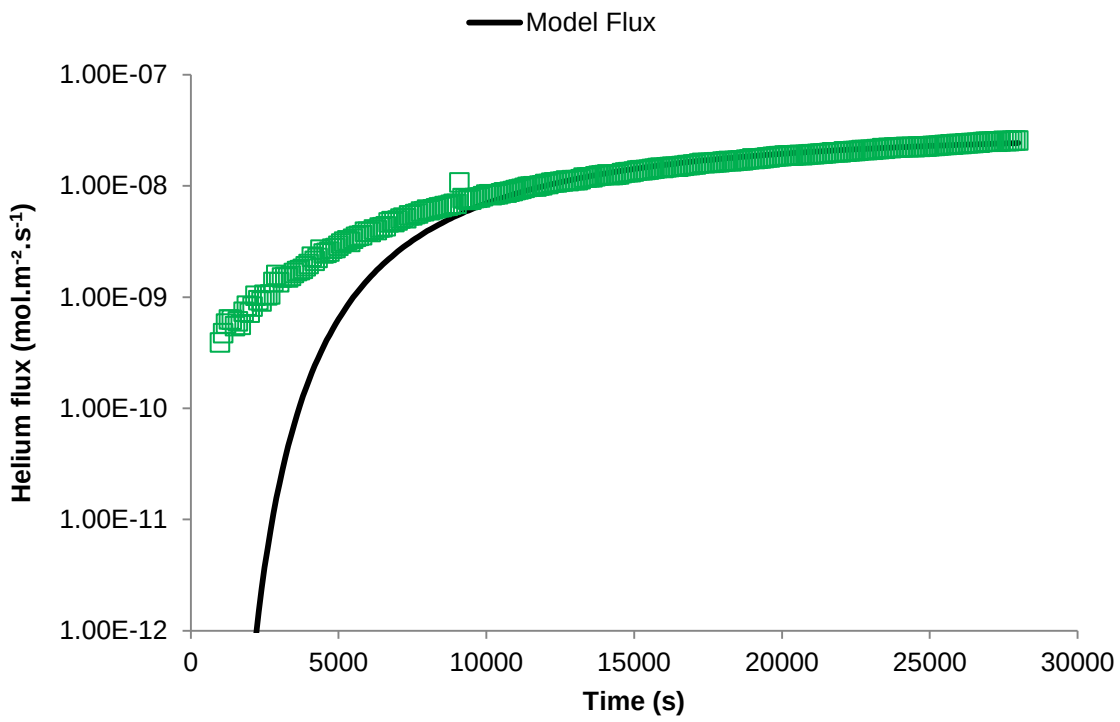

Figure B 10 Linear fit of trend line and measured flux vs. the theoretical model flux of the glass flake 15 wt% sheet

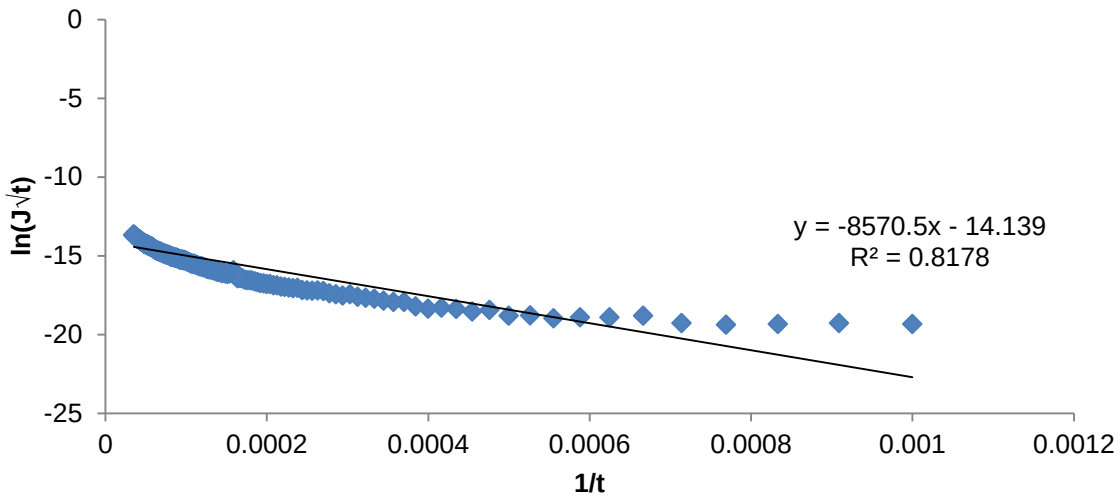

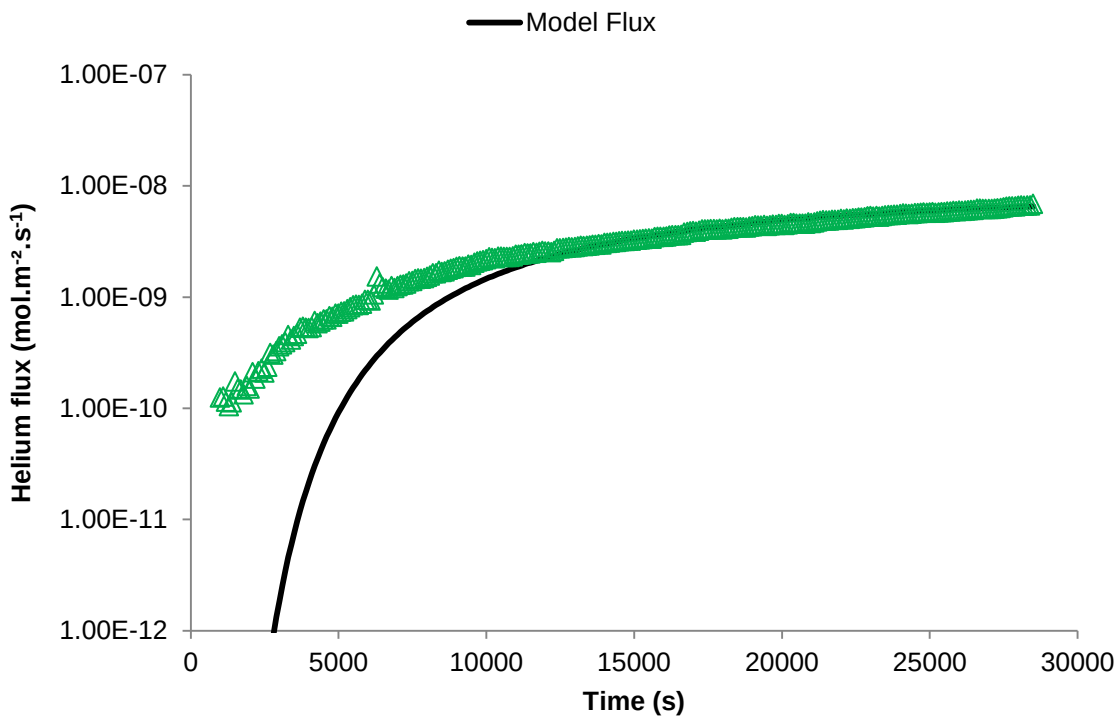

Figure B 11 Linear fit of trend line and measured flux vs. the theoretical model flux of glass flake 20 wt% sheet

ANNEXURE C: MODEL FIT OF MOULDED DISC SAMPLES

C.1 Graphene filled discs

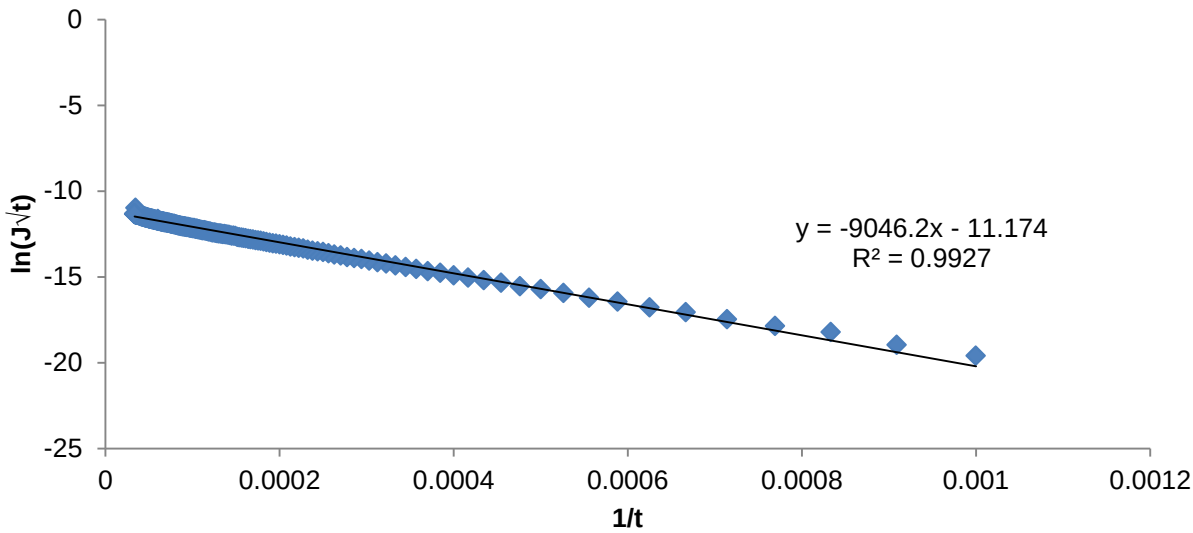

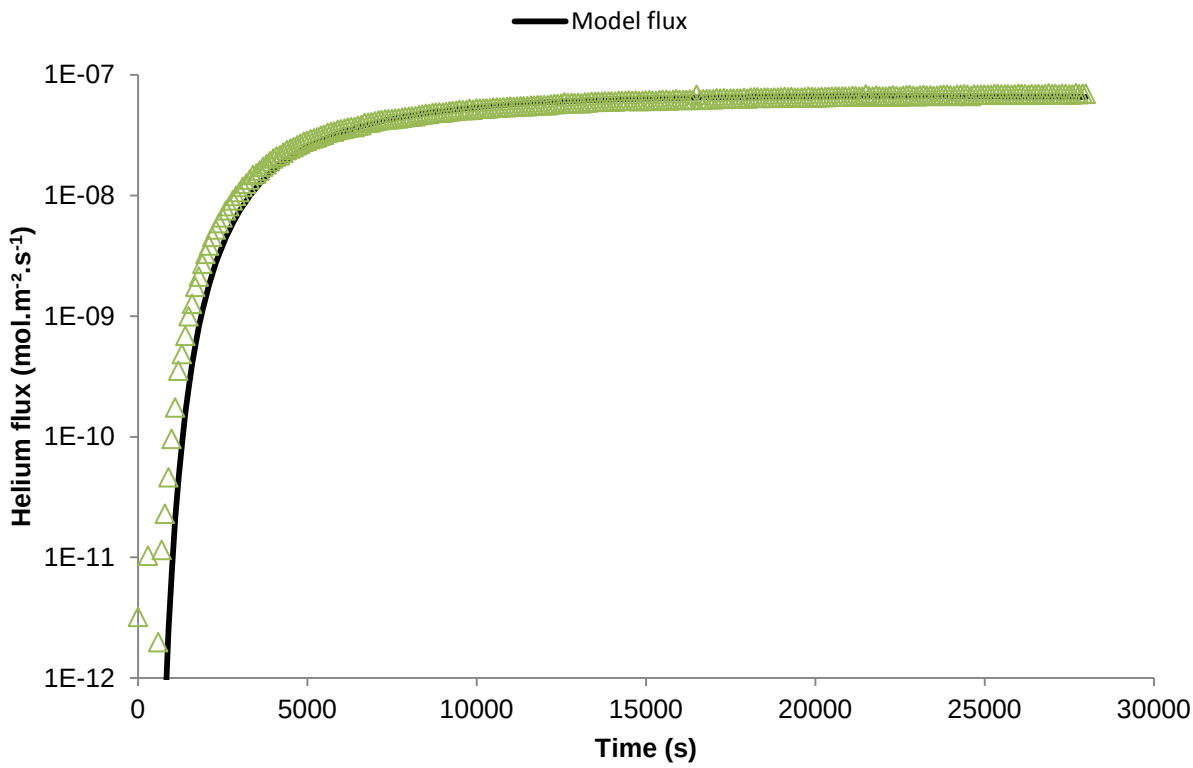

Figure C1 Linear fit of trend line and measured flux vs. the theoretical model flux of the DCM 2 wt% moulded disc

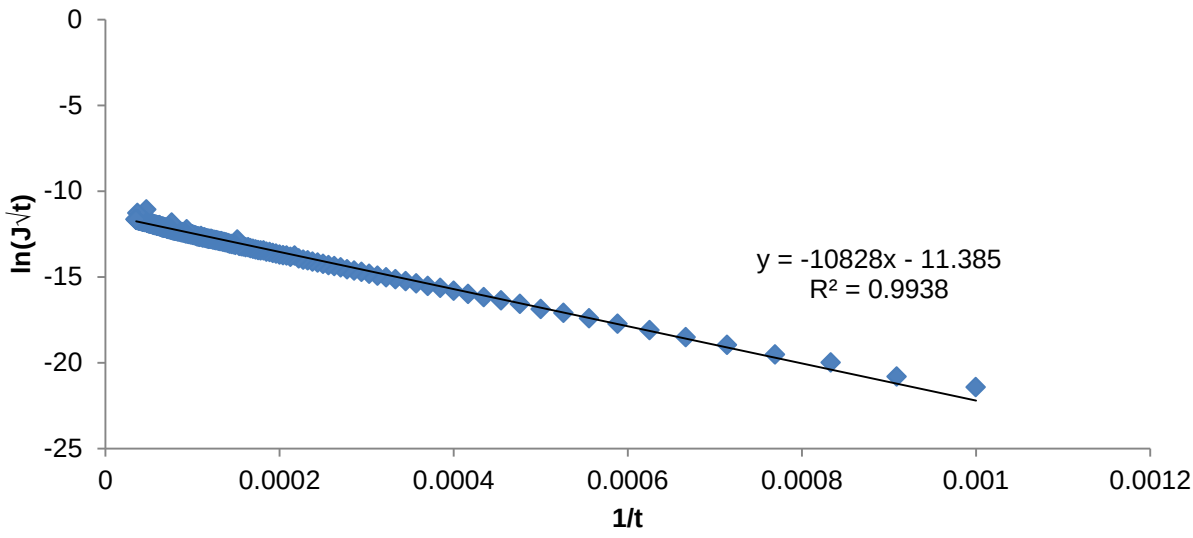

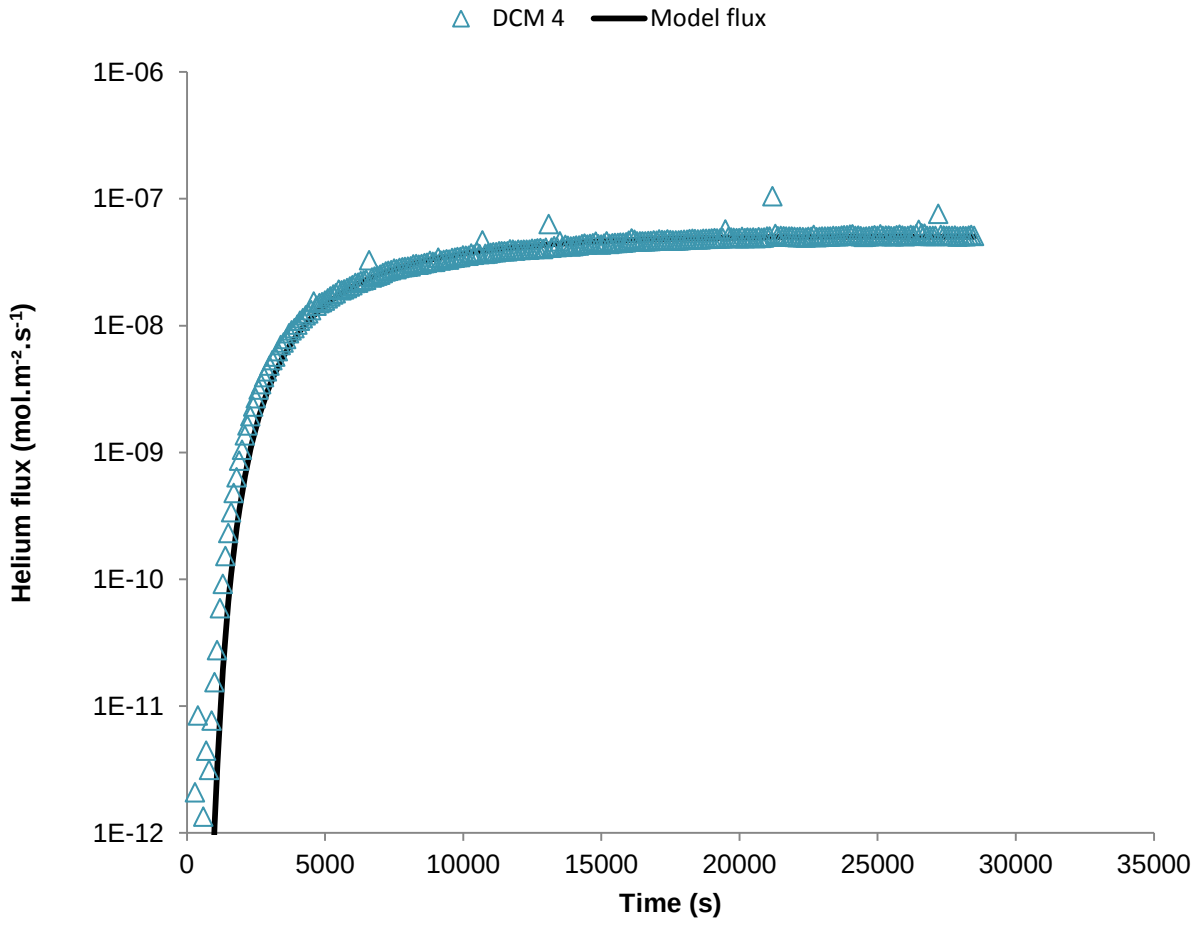

Figure C 2 Linear fit of trend line and measured flux vs. the theoretical model flux of the DCM 4 wt% moulded disc

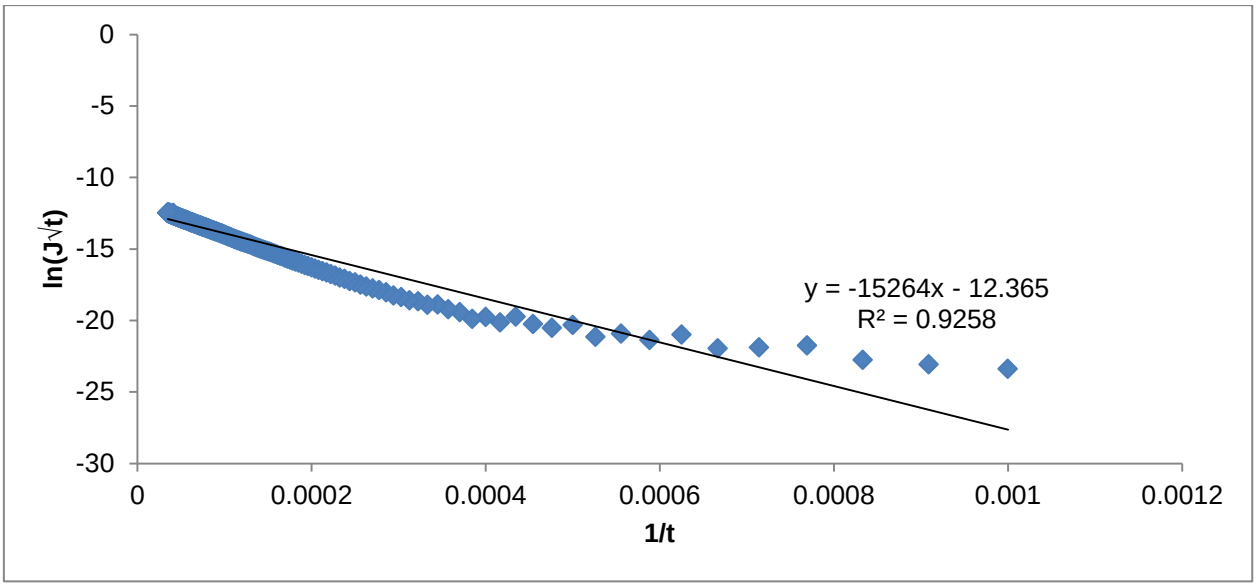

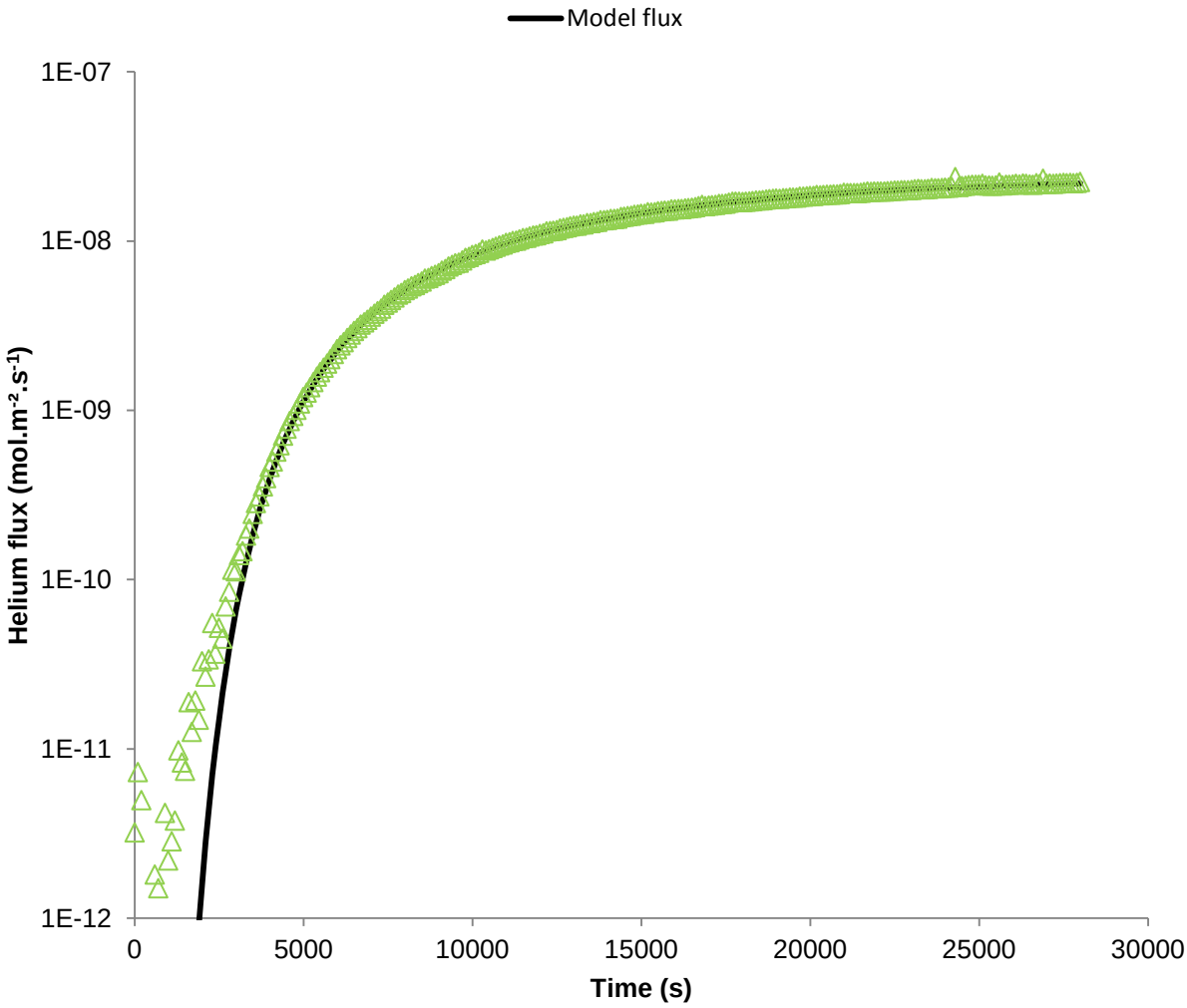

Figure C3 Linear fit of trend line and measured flux vs. the theoretical model flux of the DMF 4 wt% moulded disc

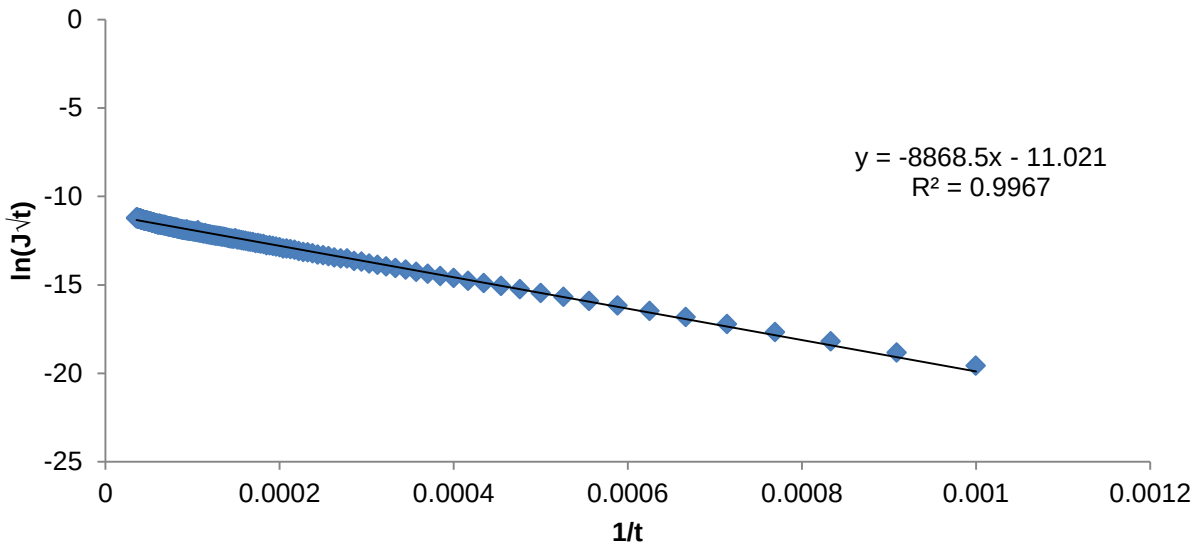

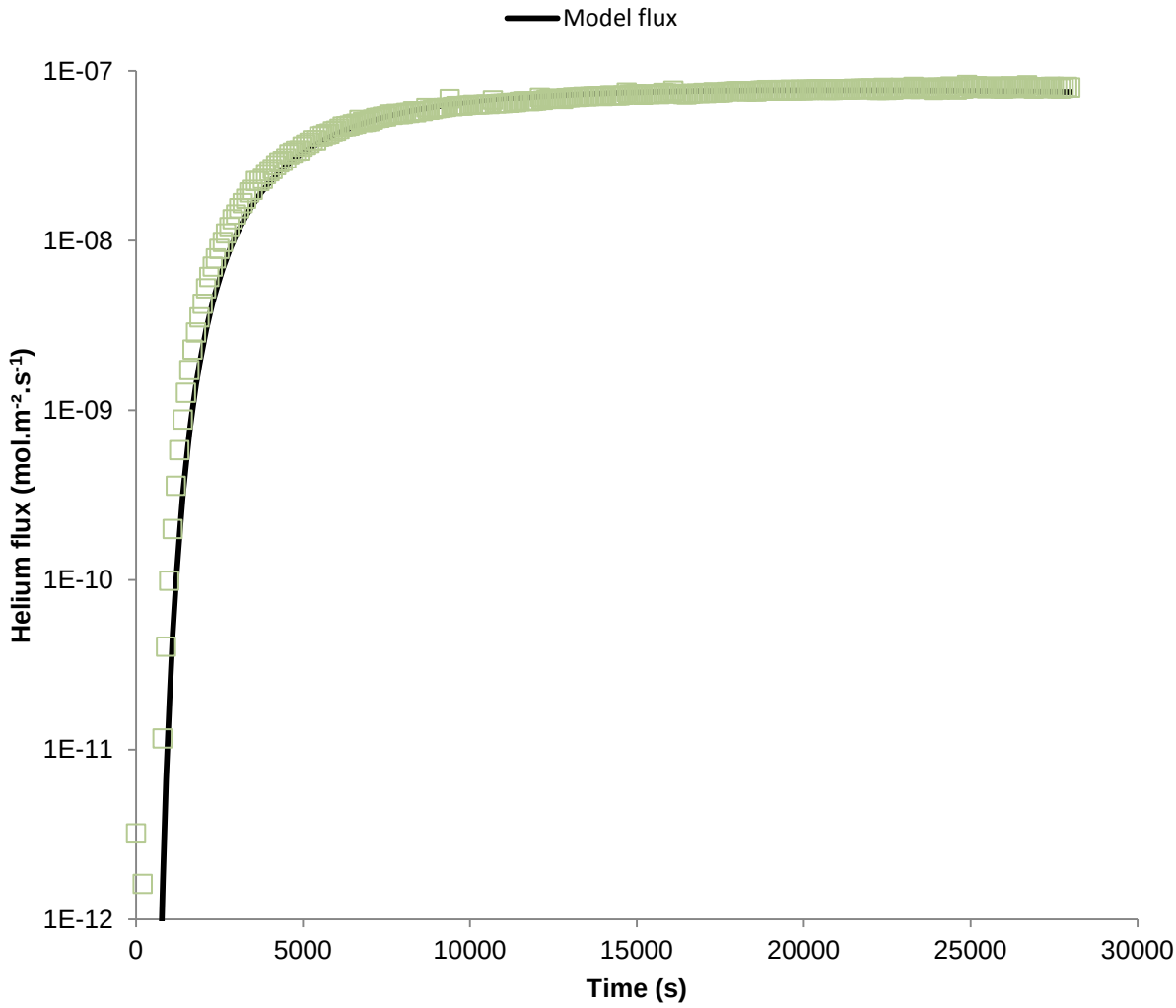

Figure C4 Linear fit of trend line and measured flux vs. the theoretical model flux of the THF 4 wt% moulded disc

C.2 Glass flake filled discs

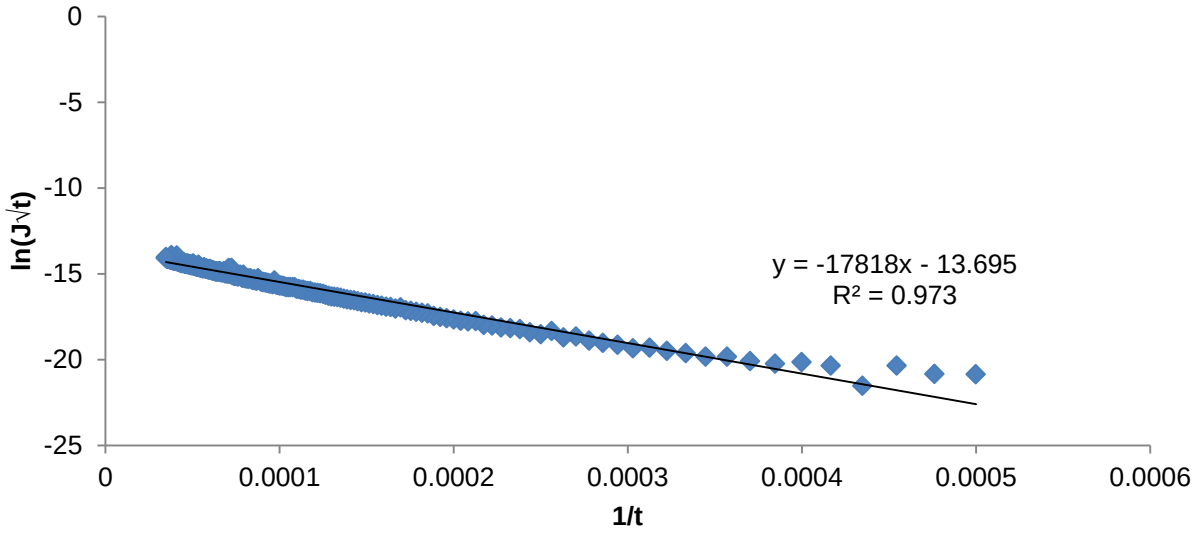

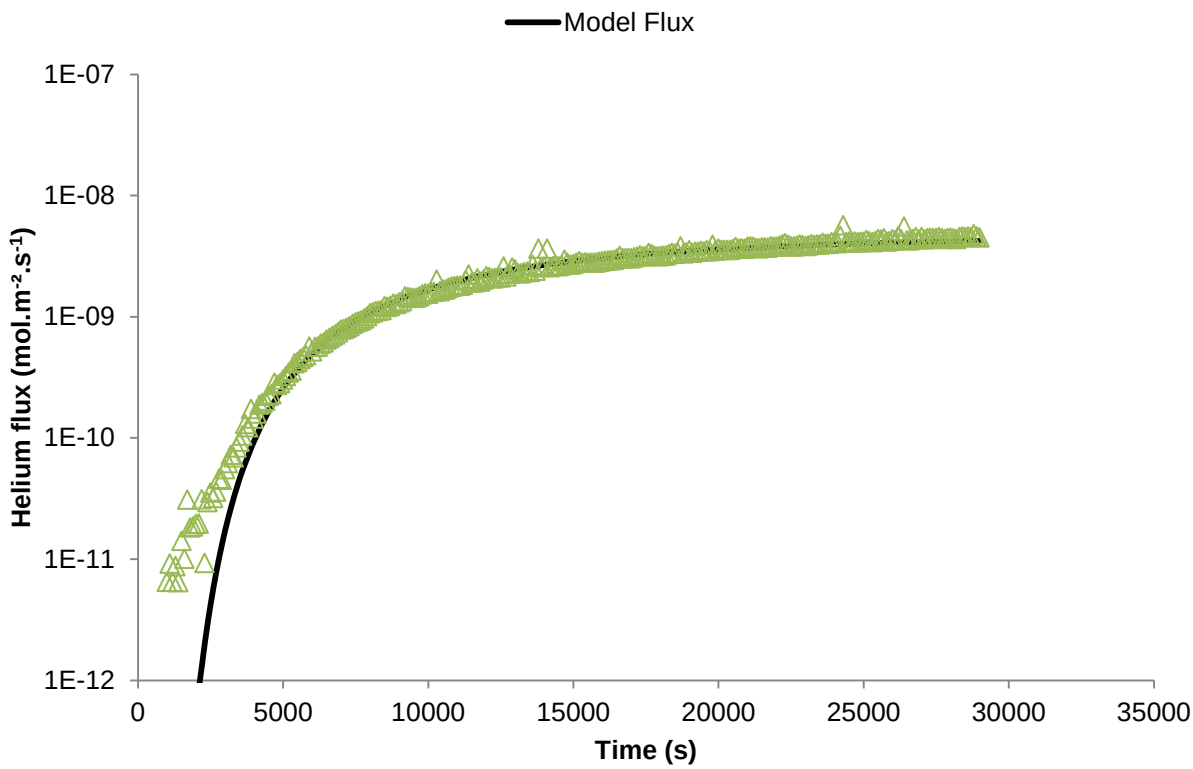

Figure C 5 Linear fit of trend line and measured flux vs. the theoretical model flux of the glass flake 25 wt% moulded disc

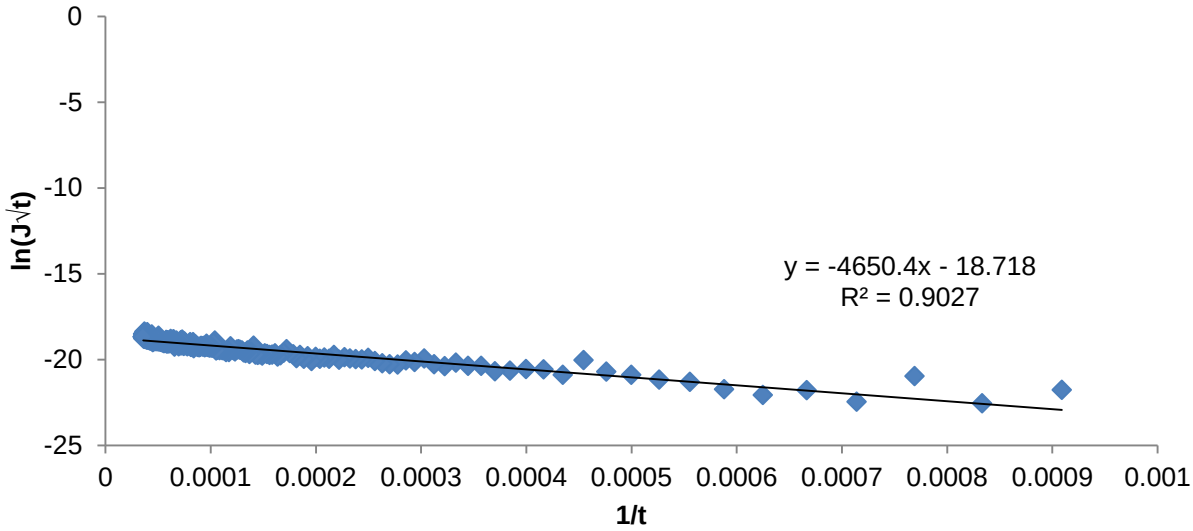

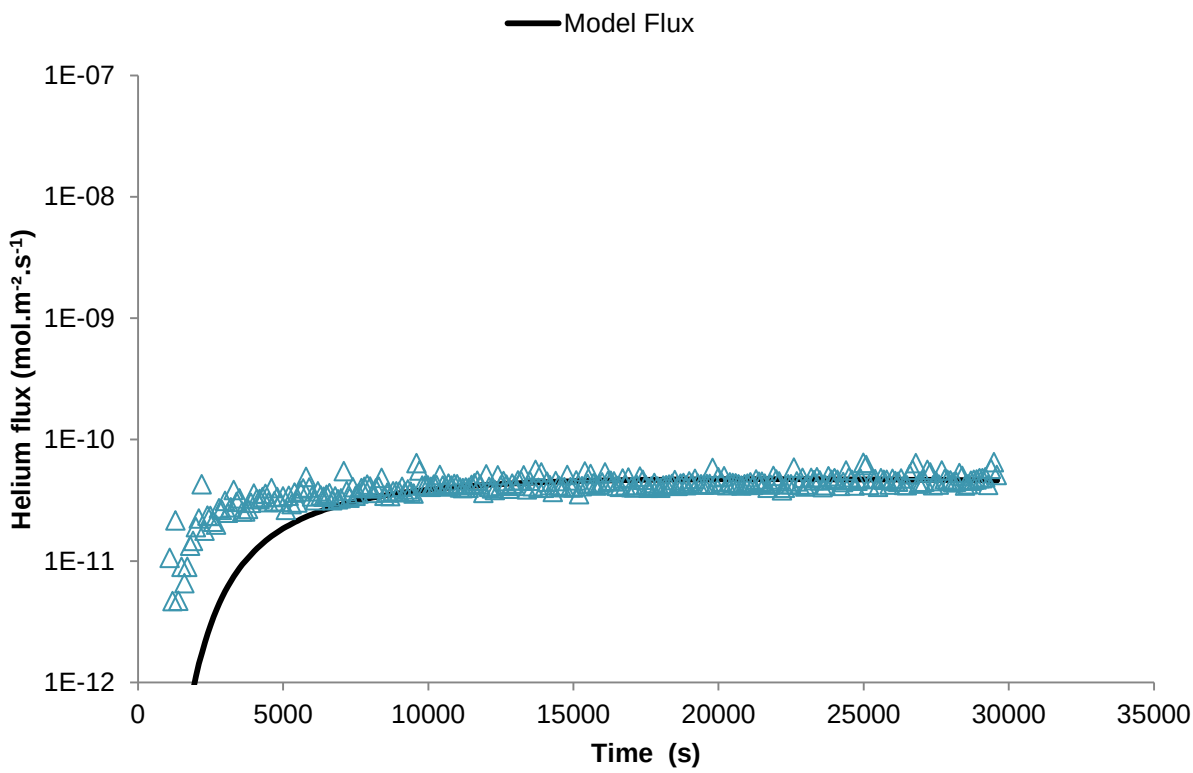

Figure C 6 Linear fit of trend line and measured flux vs. the theoretical model flux of the glass flake 30 wt% moulded disc

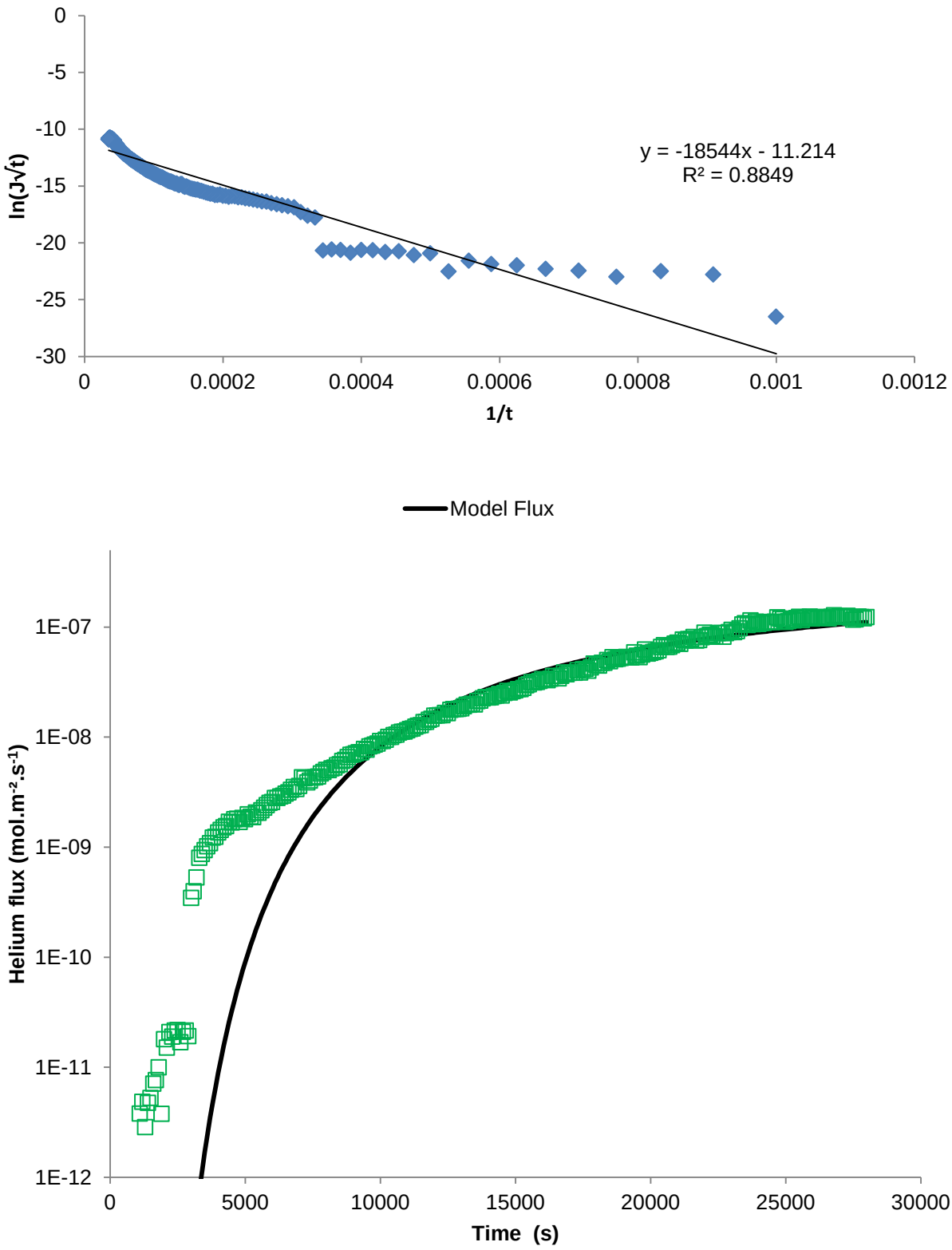

Figure C 7 Linear fit of trend line and measured flux vs. the theoretical model flux of the glass flake 35 wt% moulded disc

ANNEXURE D: MODEL FIT OF MULTILAYER SHEETS

D.1 Graphene

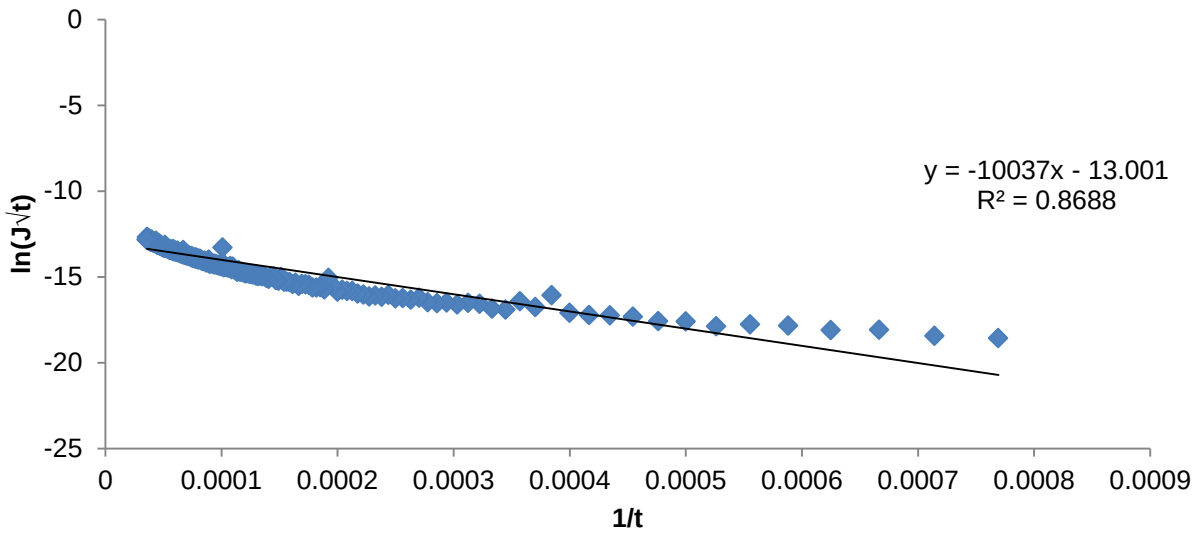

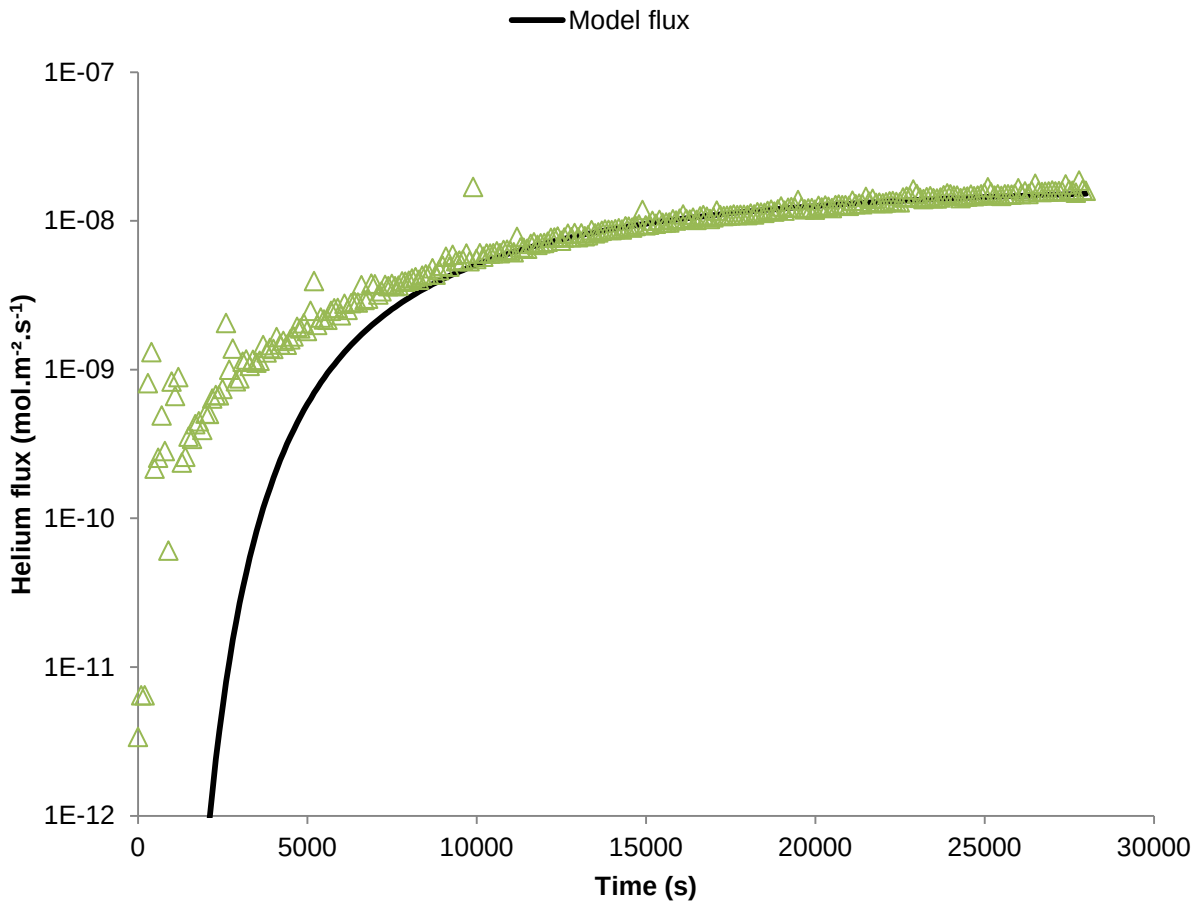

Figure D1 Linear fit of trend line and measured flux vs. the theoretical model flux of the graphene 2 wt% 3 mm multilayer sheet

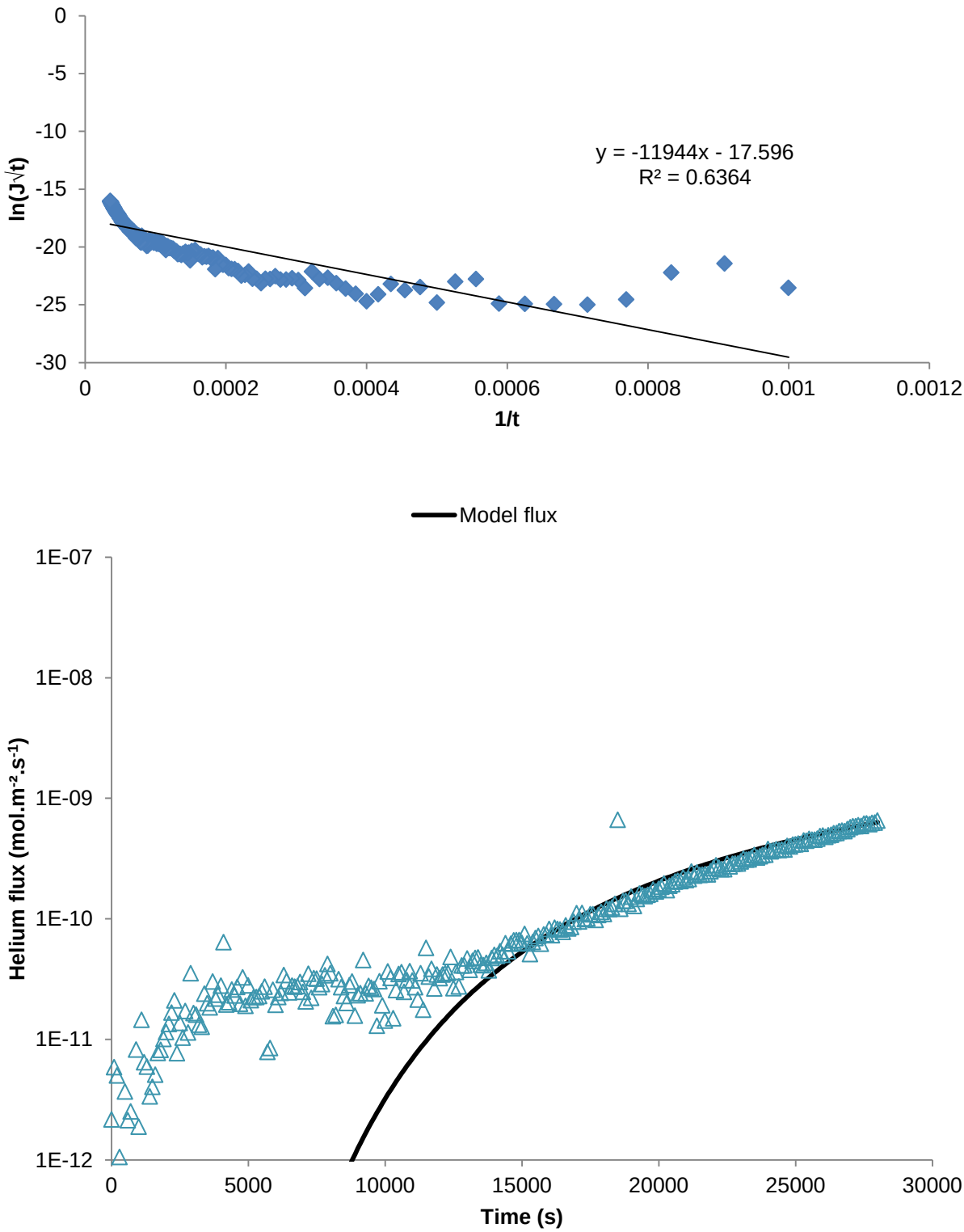

Figure D2 Linear fit of trend line and measured flux vs. the theoretical model flux of the graphene 2 wt% 4 mm multilayer sheet

D.2 Glass flake

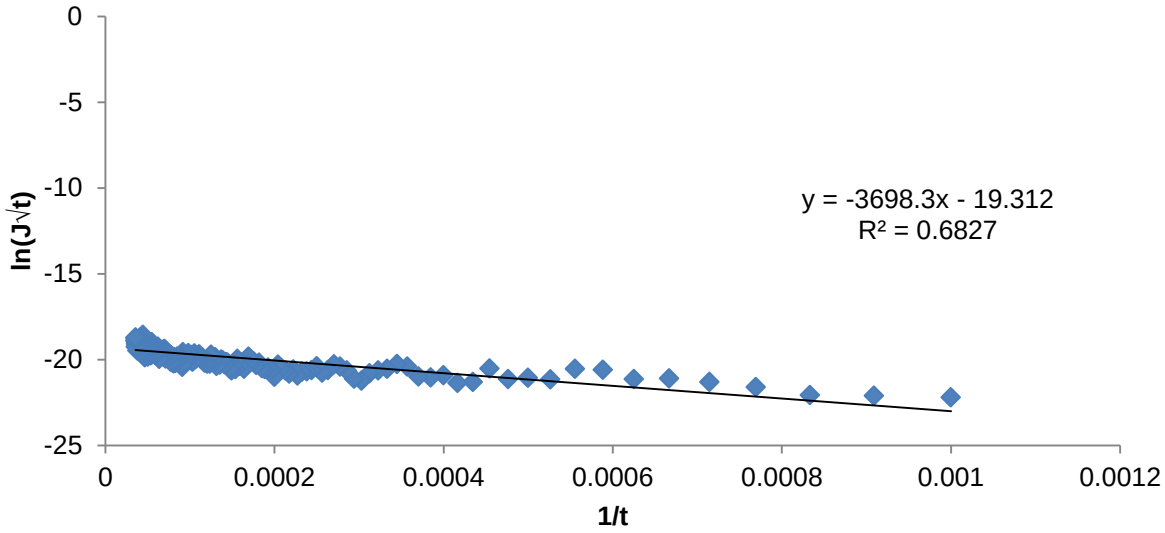

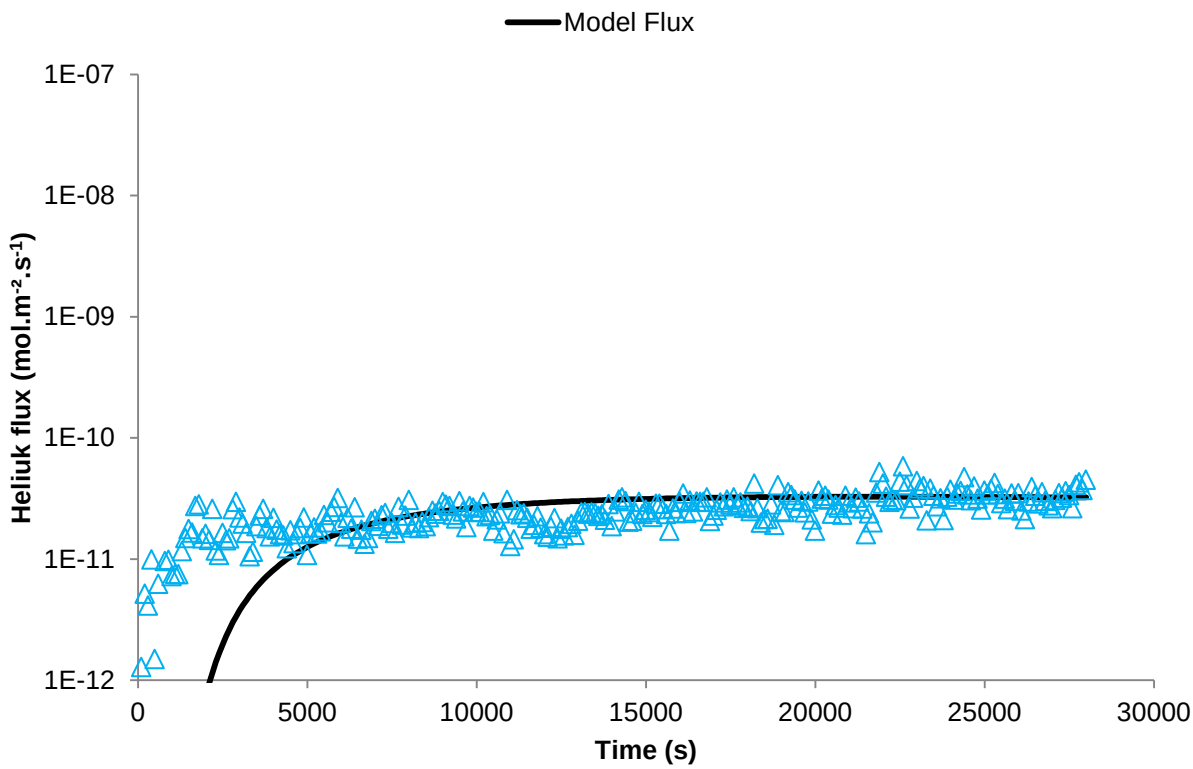

Figure D 3 Linear fit of trend line and measured flux vs. the theoretical model flux of the glass flake 30 wt% 3 mm multilayer sheet

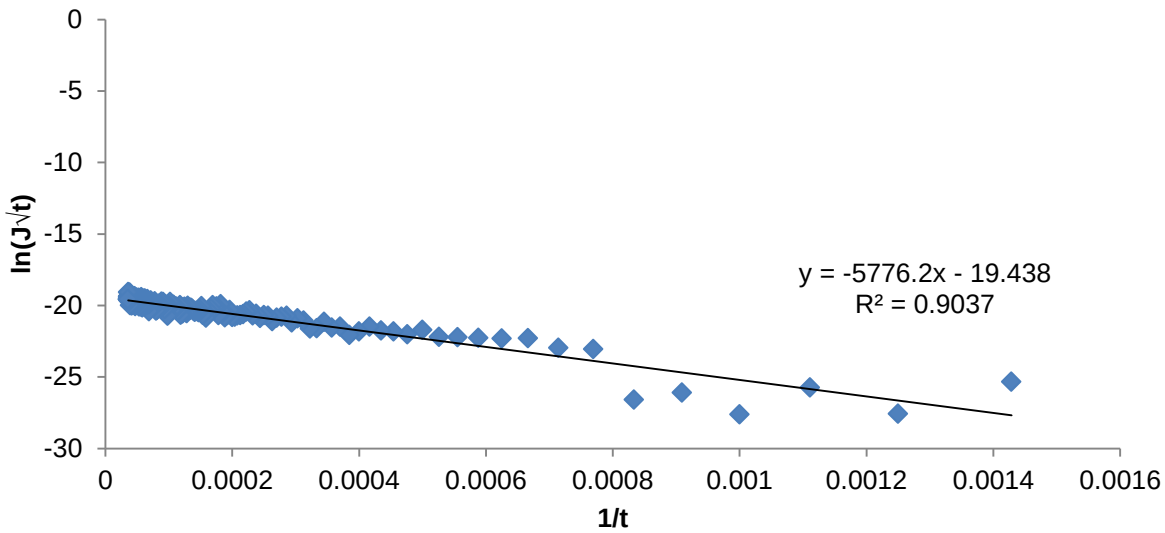

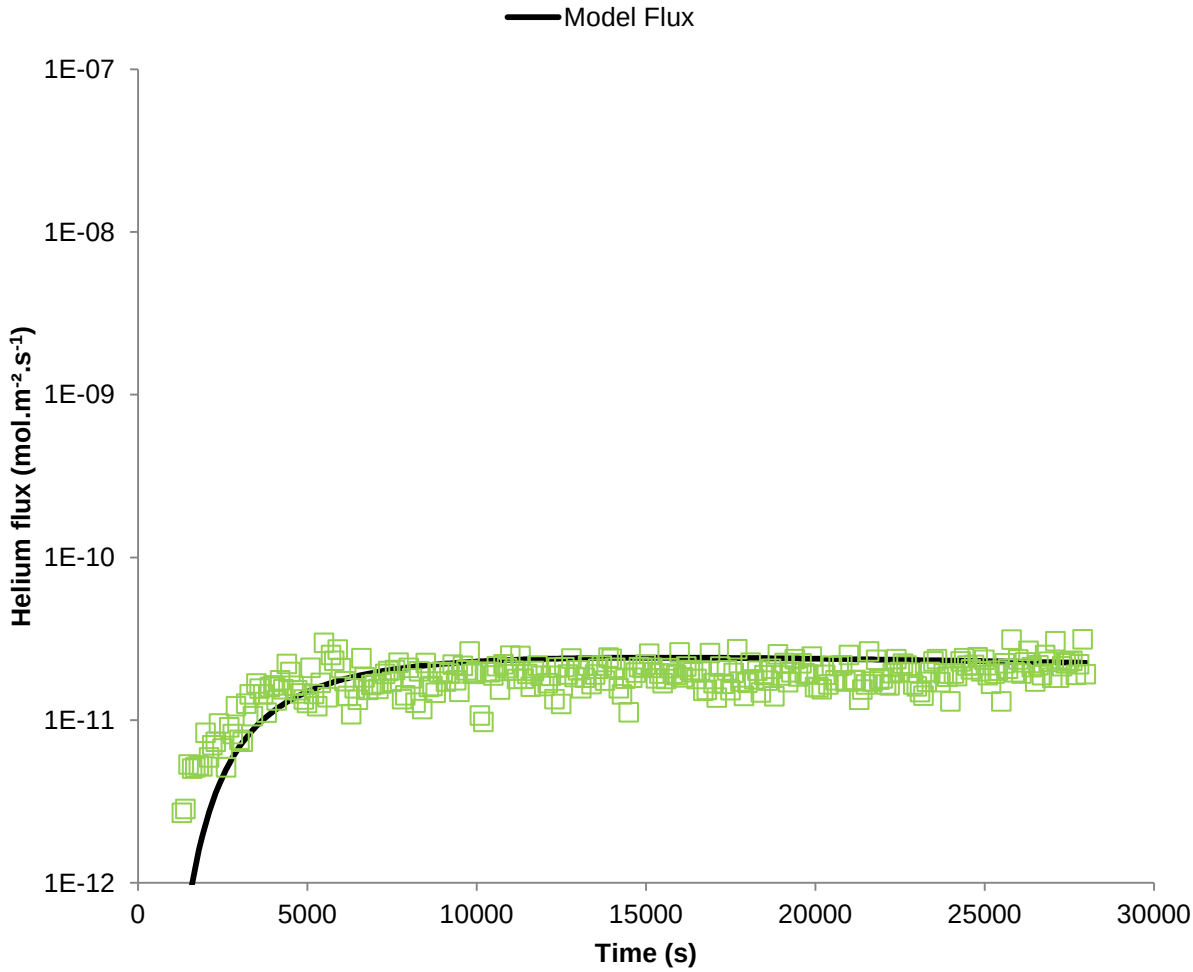

Figure D4 Linear fit of trend line and measured flux vs. the theoretical model flux of the glass flake 30 wt% 4 mm multilayer sheet